THESIS

POTENTIAL INDIRECT EFFECTS OF AEROSOL ON TROPICAL CYCLONE DEVELOPMENT

Submitted by

Geoffrey Krall

Department of Atmospheric Science

In partial fulfillment of the requirements

For the Degree of Master of Science

Colorado State University

Fort Collins, Colorado

Fall 2010

Master's Committee:

Department Chair: Richard Johnson
Advisor: William Cotton
Sue van den Heever
Richard Eykholt

ABSTRACT

POTENTIAL INDIRECT EFFECTS OF AEROSOL ON TROPICAL CYCLONE DEVELOPMENT

Observational and model evidence suggest that a 2008 Western Pacific typhoon (NURI) came into contact with and ingested elevated concentrations of aerosol as it neared the Chinese coast. This study uses a regional model with two-moment bin emulating microphysics to simulate the typhoon as it enters the field of elevated aerosol concentration. A continental field of cloud condensation nuclei (CCN) was prescribed based on satellite and global aerosol model output, then increased for further sensitivity tests. The typhoon was simulated for 96 hours beginning 17 August 2008, the final 60 of which were under varying CCN concentrations as it neared the Philippines and coastal China. The model was initialized with both global reanalysis model data and irregularly spaced dropsonde data from a 2008 observational campaign using an objective analysis routine. At 36 hours, the internal nudging of the model was switched off and allowed to evolve on its own.

As the typhoon entered the field of elevated CCN in the sensitivity tests, the presence of additional CCN resulted in a significant perturbation of windspeed, convective fluxes, and hydrometeor species behavior. Initially ingested in the outer rainbands of the storm, the additional CCN resulted in an initial damping and subsequent invigoration of convection. The increase in convective fluxes strongly lag-correlates with increased amounts of supercooled

liquid water within the storm domain. As the convection intensified in the outer rainbands the storm drifted over the developing cold-pools, affecting the inflow of air into the convective towers of the typhoon. Changes in the timing and amount of rain produced in each simulation resulted in differing cold-pool strengths and size. The presence of additional CCN increased resulted in an amplification of convection within the storm, except for the extremely high CCN concentration simulation, which showed a damped convection due to the advection of pristine ice away from the storm. This study examines the physical mechanisms that could potentially alter a tropical cyclone (TC) in intensity and dynamics upon ingesting elevated levels of CCN.

TABLE OF CONTENTS

Abstract ii

Table of Contents iv

Acknowledgements vi

Chapter 1 - Introduction

1.1 Aerosol Theory and Droplet Growth 1
1.2 Aerosol Sources and Spatial Distribution in and Around China 4
1.3 TCs and TC Formation Theory 7
1.4 TC-Aerosol Interaction 9
1.5 Objective of Research 12
1.6 DoD Relevance 13
1.7 Chapter 1 Figures 15

Chapter 2 – The RAMS Model

2.1 RAMS 4.3: The Microphysical Scheme 16
2.2 ISAN (ISentropic ANalysis) Processing and the Barnes Scheme 19
2.3 Past RAMS-TC Experiments 19

Chapter 3 – T-PARC and TC NURI

3.1 The T-PARC Campaign 23
3.2 Dropsonde Data 24
3.3 TC NURI 24
3.4 Chapter 3 Figures 27

Chapter 4 – Model Configuration and Control Simulation

4.1 Grid Configuration 29
4.2 Model Initialization 30
4.3 Aerosol Prescription 31
4.4 Discussion of Control Simulation Results 33
4.5 Chapter 4 Tables and Figures 35

Chapter 5 - Results

5.1 General Discussion 47
5.2 Precipitation Modulation and Convective Activity 49
5.3 Downward Flux 52
5.4 Cold-pool Parameters 56
5.5 Response of Hydrometeors 60
5.6 Chapter 5 Figures 65

Chapter 6 - Conclusions

6.1 Summary of Study 97
6.2 TC Windspeed and Track 98
6.3 Droplet size, SCLW, and Convective Fluxes 98
6.4 Cold-pool Modulation 99
6.5 Two Potential Routes of CCN to Weaken a Storm 100
6.6 A Comment on the Importance of Microphysics in TC Forecasting and Predicting 101
6.7 Recommendations for Future Work 102
6.8 Chapter 6 Figures 104

References 105

ACKNOWLEDGEMENTS

There are too many persons who helped and supported me over the course of my Masters work at CSU to recount. Nevertheless I will try.

Particular thanks is reserved for my advisor and personal trainer Dr. William Cotton, who plucked me seemingly out of thin air and gave me an excuse to move from Texas to Colorado; for that I and my family are grateful. I am indebted to the entire Cotton group, past and present. Every single member offered encouragement, helped me troubleshoot, and helped me better understand how the atmosphere worked; in particular, Dan Ward, who was easily the best TA I had at CSU, Stephen Saleeby, who was my go-to guy for any questions I had about anything, and Gustavo Carrio – I hope my assistance with the English language made up for your assistance with the only slightly less understandable atmosphere. I would like to thank my committee member Dr. Sue van den Heever for continuing to give advice to a student, long after I completed AT540. I would also like to thank Professor Dr. Tom Vonder Haar, Andy Jones and the entire CG/AR community for their support - the annual review sessions and ongoing conversations helped hone my research and ability as a scientist. Thanks to Nick Guy and his beautiful family: it was crucial to find someone else who knows the trials and tribulations brought on by a lack of caffeine, rooting for terrible football teams, and obtaining an advanced degree

while rearing small children. I would like to thank Omar Little for his sage words of wisdom. I would also like to extend my deepest gratitude to my parents, Ed and Lee Krall, for their continued support in my ongoing endeavors and instilling in me a love for education and science.

My research could not have taken place without the selfless childcare provided by my mother-in-law, Natalie Kimble and her husband Donald. To my indefatigable daughter and son, Adeline and Jude, I can only hope that your lives have been made more adventurous by our move to Colorado. Thank you for always being excited to see me at the end of the day. Your unrelenting joy is a cool drink of water. And lastly, to my best friend and wife, Stephanie, thank you for simultaneously challenging me, encouraging me, and for continuing to make me laugh decade after decade.

This research was made possible by funding from CG/AR and the Department of Defense.

CHAPTER 1 – INTRODUCTION

1.1: Aerosol Theory and Droplet Growth

Aerosols are tiny particles that exist or are emitted into the atmosphere through natural and anthropogenic processes. These particles have the potential to alter both weather and climate patterns through modulating the earth's radiation budget and by perturbing the water cycle upon their interaction with water vapor. These processes are among the most difficult to quantify on a global scale as the sources, species, quantity, and effect of aerosols vary wildly throughout the globe; they are difficult to track with certainty. However, due to their weather and climate altering potential, research into aerosol effects has expanded in recent years.

When a particle travels through air with a certain amount of water vapor, the particle may have the ability to develop tiny water drops on its surface. Absent the introduction of aerosols, water vapor may only convert into water droplets by homogeneous nucleation, which requires very low temperatures and/or unrealistic levels of supersaturation. The introduction of aerosol acts to facilitate the development of the initial droplet in air. The aerosol at this point acts as cloud condensation nuclei (CCN) and allows liquid water to form from water vapor at lower values of supersaturation and higher temperatures. The ability of an aerosol particle to act as CCN is a

function of both its size and chemical species. These variables work to control the hydroscopicity which determines the particle's ability to take on water, although Dusek et al. (2006) provided evidence that a particle's ability to nucleate droplets was more affected by size: the larger the particle, the greater the ability to activate cloud droplets.

At this point, the microscopic water molecule may grow. Kohler (1926) determined the equilibrium vapor pressure above small droplets. This allowed him to develop what are now known as the Kohler curves. They yield a size threshold of droplet growth according to the supersaturation of the air with respect to water vapor. Given a water droplet and supersaturation, the droplet may either remain at its size as a stable water droplet if it does not pass that prescribed threshold or it may continue to grow once it surpasses a certain size and supersaturation. The droplet at this point will continue to grow indefinitely until it is rained out or broken up in some other manner. The droplet may also evaporate if forced in the opposite direction. This basic model of droplet initialization, growth, and fallout is the prevalent model of precipitation. Because these processes occur on the microscopic scale, atmospheric models are burdened with the challenge of representing this process in a dynamic system countless times without utilizing an unrealistic amount of computing power.

Howell (1949) was the first to discuss CCN quantitatively. He noted that the observed size spectra of water droplets were much broader than would be predicted theoretically. Twomey and Squires (1959) were among the first to attempt to obtain an observed concentration of CCN by measuring the spectrum of critical supersaturation of cloud nuclei (CN) in the air beneath a cumulus cloud as well as the droplet concentration within the cloud. Volkovitsky and Laktionov

(1969) utilized a 3000 m^3 cloud chamber to obtain a droplet spectrum according to various temperatures.

As global anthropogenic emission of aerosols have increased over the past several decades (Streets et al. 2000; Streets and Waldhoff 2000) aerosol effects are at the forefront of advertent and inadvertent weather modification research. As such, aerosol effects have been well-categorized. They have been shown to be direct scatterers of radiation (Charlson et al. 1992) and direct absorbers (Ramanathan and Vogelmann 1997). In addition, aerosols have been shown to affect precipitation. If water vapor is considered constant, the introduction of more CCN would imply that the nascent water droplets would be smaller and therefore inhibit the collision-coalescence process. While CCN are critical to the formation of droplets, in the presence of high concentrations of CCN, water droplets may be unable to grow large enough to precipitate out of a cloud. This phenomenon and its consequences have been documented as so-called indirect effects. The first indirect effect (Twomey 1991) suggests that given the same liquid water content (LWC) additional CCN may act to increase the number droplet concentration and increase cloud albedo. The second indirect effect (Albrecht 1989), or lifetime effect, suggests in the presence of heightened CCN concentration clouds will be less able to precipitate out their moisture, thereby lengthening the lifetime of the cloud. This effect is primarily attributed to stratocumulus clouds.

Aerosol induced precipitation changes do not generally have such a linear response. Modeling studies suggest that in certain types of precipitating regimes, in particular convectively driven systems, CCN may work to enhance precipitation intensity. While additional CCN may initially inhibit precipitation, over the course of a storm the smaller droplets, unable to rain out, are

lifted in an updraft; this causes the latent heat release due to freezing droplets in the atmosphere to significantly increase the vertical velocity and amplify the storm (van den Heever et al. 2006; Seifert and Beheng 2006). The nonlinear response of precipitation to aerosols provides a wealth of research opportunities.

1.2: Aerosol Sources and Spatial Distribution in and Around China

Providing a global survey of aerosol concentrations is challenging due to their small size, tendency to react chemically, and not being a purely surface emission process. In addition to being emitted at the surface, aerosol particles may form in the atmosphere itself via gas-to-particle (GTP) conversion. Taking chemical composition into account provides another level of complexity as aerosol particles may change chemically by interacting with other particles or solar radiation. For the purposes of this research, three general types of contributing aerosols are considered: soil and mineral dust, sea salt, and anthropogenic particles.

Among the most prevalent natural source of aerosols is soil and mineral dust (Duce 1995), sourced primarily from large, arid deserts. Tegen (2003) and Zender et al. (2004) well summarize the most recent research into estimates of soil and mineral dust concentrations globally. Dust is of particular interest due to its composition: often it is made up of soluble materials that render the dust particles highly suitable as CCN (Formenti et al. 2003) and ice nuclei (IN) (DeMott et al. 2003; Twohey et al. 2009). Strong winds blown over a dust source can quickly generate extremely high concentrations of dust near the surface (Cheng et al. 2004). Once the larger dust particles have been scavenged or sedimented out, the remaining smaller dust particles can travel thousands of kilometers horizontally and several kilometers vertically. Saharan dust regularly advects westward across the Atlantic ocean into the southeastern continental United

States. The Gobi desert meanwhile is under siege by westerly winds, carrying particles into and across the Pacific Ocean. The frequency and intensity of these major dust events is exacerbated under dry or drought conditions.

Sea salt is also a suitable CCN. Sea salt particles are emitted to the atmosphere when air bubbles rise to the ocean surface and burst during whitecap formation (Schulz et al. 2004). In maritime environments sea salt is often the dominant source of aerosols. Since the formation of sea salt particles is directly linked to whitecap formation, it stands to reason that there is a direct correlation between surface windspeed and sea salt aerosol concentration just as in dust aerosols. Sea salt can have a wide size distribution spectrum (from 0.05 to 10 microns in diameter; Leinert et al. 2003) and therefore has been implicated in affecting warm rain processes in marine environments (Jensen and Lee 2008).

While dust and sea salt particles dominate the natural influencing aerosols for the purposes of this study, anthropogenic aerosols in and around China are also strongly considered due to their potential for interaction with tropical storms (TSs). From 1980 to 1990, China saw a 60% increase in sulfur dioxide (Streets et al. 2000). This was a result of a sharp population increase, rapid economic growth, and an increased dependence on coal. Similarly, throughout the 1990's China's SO_2 emissions increased by an average of 3.6% a year (Streets and Waldhoff 2000). Satellite retrievals have suggested a decadal increase in aerosol optical depth (AOD) of about 17% over the China coastal plain (Massie et al. 2004). More recently - thanks to technological advances in energy production, a lessened emphasis on coal, and an emphasis on pollution capturing - Asian SO_2 emissions have declined from 38.5 Tg in 1995 to 34.4 Tg in 2000, a

decrease of 2.3% a year (Carmichael et al. 2002).

SO_2 is the dominant player for anthropogenic aerosol compounds in the region. Once aloft, SO_2 can oxidize into sulfate aerosol particles (Saxena and Seignuer 1987). Berglen et al. (2004) estimated between 51 and 56% of SO2 gets converted to sulfate into the atmosphere. Globally, sulfates dominate number load of anthropogenic aerosols for now and into the foreseeable future (Dentener et al. 2006).

The vertical distribution of aerosols in and around China is also considered. Observational studies have shown that dust, which dominates the coarse mode of aerosol exists throughout a vertical column while pollution generated aerosol, which dominate the accumulation mode of aerosol, are generally confined near the boundary layer (Anderson et al. 2003a; Chin et al. 2003). However, the dust aerosol advecting out of Asia over the ocean shows a tendency to contain layers of particles separated by layers of relatively clean atmosphere often 2-4 km above ground level (Redemann et al. 2003; Bahreini et al. 2003) .

These three types of aerosol are considered in this study as the dominant regional aerosol modes in China and the Western Pacific insofar as weather and climate modification. As noted by Dusek et al. (2006), the chemical makeup of the aerosol constituents is of secondary concern relative to number concentration and size. Unable to examine every aerosol species available, the primary aerosol focus of this study is on number concentration and size. Therefore, we utilize observational studies, in-situ measurements, and satellite retrievals that do not necessarily distinguish between aerosol species.

1.3: TCs and TC Formation Theory

Few weather events attract as much research as landfalling tropical cyclones (TCs) thanks to their high destructive potential, a life cycle that allows for intensification, deintensification, sudden track shifts, and the countless meteorological variables that may affect a particular storm. Characterized by a low-pressure system center, tropical depressions (TDs), tropical storms (TSs), and TCs are fueled by warm ocean water vapor and the associated deep convection latent heat release, distinguishing it from mid-latitude cyclones which are driven by a preexisting horizontal temperature gradient. The deep convection associated with a TS requires a constant supply of moisture and therefore deintensify rapidly upon reaching land. Still, a strong TC can still remain active thousands of kilometers inland, spawning tornadoes (Novlan and Gray 1974; Gentry 1983; McCaul 1991), thunderstorms, and flooding from rainfall and storm surges (Crawford 1979) for days after making landfall.

While TC forecasting has improved dramatically over the past several decades in terms of track and intensity (Willoughby et al. 1982; Emanuel 1986,1988; Willoughby 1990a, b, 1998, Powell 1990a, b; Gray 1995; Shapiro and Franklin 1999; Braun and Tao 2000; Wang 2002a; Zhu and Smith 2002; McFarquhar and Black 2004; Zhu and Zhang 2006; Rogers et al. 2007), there is still considerable uncertainty when it comes to TC genesis and TC response to anthropogenic forcing (Bender et al. 2010). Furthermore, while TC forecasts have improved significantly, there still remains enough uncertainty that improvements in track and intensity forecasting could greatly benefit regions of high TC landfalling activity, particularly regions close to sea level.

Tropical cyclogenesis has been a subject of great debate in the atmospheric science community for decades since Reihl and Malkus's (1958) pioneering work noting the role of convectively-

generated hot towers in TC formation. From this work came the most cited theory of tropical cyclone formation of the subsequent decades - conditional instability of the second kind, or CISK, as described by Ooyama (1964) and Charney and Elliasson (1964). CISK assumes a destabilization of the atmosphere driven by organized moist convection due to surface fluxes and radiation fluxes. A competing, though not mutually exclusive, alternative theory to TC formation began to emerge in the mid-1980s, introduced by Emanuel (1986) as air-sea interaction instability (ASII), subsequently renamed wind-induced surface heat exchange, or WISHE, instability (Emanuel et al. 1994). In the WISHE model, the convective instability is generated by a feedback mechanism from surface fluxes of heat and moisture dependent on windspeed derived from a preexisting vortex. The primary difference between the two theories can be seen as their dependence on convective available potential energy (CAPE). An implication of CISK theory is that TC genesis must be accompanied by a positive amount of CAPE, while according to WISHE, the atmosphere may be initially convectively neutral and therefore TC genesis may occur when CAPE is zero. Recent modeling studies (e.g. Craig and Gray 1996) have tended to support the potential for TC formation in a zero CAPE atmosphere. However, the CISK-WISHE debate was of paramount importance in our understanding of TC development in terms of convective fluxes.

Of particular value in the CISK-WISHE debate was the increased attention given to convectively-generated downdrafts in TC formation. Zipser (1977) described the importance of downdrafts in convective systems, while Simpson (1980) proposed these downdrafts could initiate future convection. Other studies (e.g. Thorpe et al. 1982; Rotunno et al. 1988) directly implicated surface-based cold pools as a crucial factor in organizing deep convection. Emanuel (1994) cited the lifting of the boundary layer (BL) at cold-pool front through its negatively buoyant

convective inhibition layer, allowing free convection to commence as a method to convection organization. Mapes (2000) extended this in a toy tropical model. Tompkins (2001) observed that new convective events were being initiated on the boundaries of cold-pools emanating from previous cumulus towers. Due to the intense convection in a TC, lightning has been used recently to link TC activity and latent heat release (Lyons and Keen 1994; Orville and Coyne 1999, Molinari et al 1999; Shao et al. 2005; Fierro et al. 2007, Price et al. 2009). Other factors in TC formation include vertical wind shear, assumed to have a negative impact on TC development (Rotunno et al. 1998; LeMone et al. 1998), gravity waves (Mapes 1993). Recently much attention has been focused on the bottom-up development of near-eye vortical hot towers (Montgomery and Enagonio 1998; Hendricks et al. 2004; Montgomery et al. 2006) as a potential route to cyclogenesis.

This study will focus much of its attention on the cold-pools generated within a TC due to latent heat release and convective fluxes.

1.4: TC-Aerosol Interaction

The origins of microphysical impacts on TC development stem from project STORMFURY from 1962 to 1983.During this lengthy campaign, TC rainbands were seeded with silver iodide. The hypothesis was that the silver iodide, also used in cloud seeding experiments during this time, would enhance thunderstorms along the outer rainbands of the storm, which would in turn compete with the eyewall by damping convergence (Simpson and Malkus, 1964). Despite some initially promising results, the success of STORMFURY came into question in the mid-1980s as it became apparent that it was impossible to distinguish the effects of the seeding with natural processes (Willoughby et al. 1985). At this time there was still a considerable lack of

understanding of microphysical processes involved in rain formation, droplet growth, and the resultant perturbation in latent heat release.

While the results of STORMFURY may have been questionable, the idea that microphysical processes could potentially alter and hopefully mitigate storm damage is gaining strength in the atmospheric modeling community (Khain et al. 2009; Carrio and Cotton 2010). With increased computing power and more intricate models that include a fuller microphysics scheme than previously possible, research on particle-TC interaction is experiencing a reinvigoration.

Of particular interest is the importance of CCN induced cold-pool activity. Wang (2002) concluded that downdrafts emanating from a TD's peripheral spiral rain bands acted to hinder BL convergence at the eyewall. The cold-pool downdraft front can potentially act to cut off the inflow of warm, near sea-surface air, requisite in maintaining the energetics of the system. Wang (2009) proposed a relatively linear association between outer rain band activity and TC intensity: heating the outer rainbands decreases TC intensity by breaking down the thermodynamic structure of the storm by inducing shear, while cooling the rainbands increases TC intensity. While it is hard to imagine the relationship being so simple, the impetus to conduct further modeling and observational studies relating rainband activity and TC intensity is evident.

Based on studies that have shown significant aerosol impacts on cold- pool downdrafts (e.g. van den Heever and Cotton 2007), the question may be posited: if increased aerosol concentration may strengthen the downdrafts in a convective storm, could increased aerosol concentration also amplify the downdrafts in the convective bands in a TC? Should the downdrafts prove to be strong enough, they could work to damp the BL inflow of warm, moist air which drives the TC.

Recent studies have addressed this question largely by examining Atlantic Hurricanes that entrain dust from the Saharan Desert. Saharan dust is prevalent during the Atlantic hurricane season, carried for thousands of kilometers on consistent easterly winds. As previously mentioned, desert dust may act as CCN, which would possibly affect the convection occurring in the outer rainbands of an existing TC. Zhang et al. (2007;2009) used an idealized simulation of a TC entraining CCN, showing that the increased aerosol concentration worked to damp the intensity of the hurricane while increasing its size, consistent with Wang (2009). The aerosols in such an instance are carried within the Saharan Air Layer (SAL), an exceptionally dry and stable layer of air which may be of as much importance in suppressing Atlantic TC activity as the aerosols themselves (Dunion and Velden 2004). It is also possible that the radiative properties of the dust within the SAL may perturb the atmospheric energy balance and work to weaken TSs (Evan et al. 2006). A schematic diagram of TC energetics being hindered by a CCN-induced cold-pool is shown for clarity in Figure 1.1.

Khain et al. (2009), using the Weather Research and Forecasting (WRF) model with spectral bin microphysics concluded that the entrainment of continental aerosols acted to weaken hurricane Katrina (2005) just before it made landfall. As noted in Fovell et al. (2009), the microphysics scheme used in the research model, along with the differences in particle fall speed and how various species of water vapor are handled, may greatly affect the results. Therefore, as research on aerosol induced changes in TC intensity is reinvigorated, there must be a wealth of both modeling and observational studies to corroborate any prevailing theory.

1.5: Objective of Research

The primary objective of this research is to determine the indirect effects of aerosols on TC development. As indicated in previously, there have been many studies examining the effects of aerosols on TCs, often in the context of dust particles contained within the SAL, which makes it difficult to distinguish between the aerosol effects and the effects of a dry, stable air layer being entrained within a TC as a means to deintensification. For this reason, this research will focus on TC development in the Western Pacific (WP), where aerosol contributions are significant and carried in an atmosphere similar to the large scale environment. As discussed earlier in this chapter, both natural and anthropogenic sources of aerosols are present in the WP. A TC case study was selected for both its wealth of observational data and its assumed interaction with aerosol particles emanating from the East Asian coast.

In order to best represent the microphysical processes potentially involved in TC modulation, a regional model with a bin emulating microphysics scheme was implemented. By running sensitivity tests with various aerosol concentrations, this research allows for a teasing out of the indirect effects that could potentially modulate and perhaps mitigate the intensity of TCs. Particular attention is given to the development and modulation of cold-pool activity. This is achieved by examining rainfall rates in the outer bands of the TC, buoyancy (Emmanuel 1994), perturbations in equivalent potential temperature (θ_e) and vertical velocity (w). Attention is also given to the variation in TC track, maximum and average windspeed, and perturbation pressure.

The final section in this chapter addresses the relevance to the Department of Defense (DoD), whose collaboration with the Center for Geosciences/Atmospheric Research (CG/AR) worked to fund this research. A description of the regional model with particular emphasis on the

development of the microphysical scheme of the model used is presented in chapter 2. A background of the TC case study selected and observational campaign used to assist the initialization of the model assess the quality of the model results is presented in chapter 3. Chapter 4 contains a detailed description of the model experiment and a discussion of the control results. Chapter 5 focuses on the subsequent sensitivity tests run assessing the aerosol induced perturbations on the TC. A summary of the research, along with pertinent conclusions and suggestions for future TC-aerosol research, is given in chapter 6.

Chapter 1.6: DoD Relevance

The United States Military continues to maintain a presence in the WP for reconnaissance, research, and relief purposes. The Naval Research Laboratory (NRL) has been particularly interested in improving the forecast of intensity, structure, and track of TCs (Reynolds et al. 2009) by improving the Coupled Ocean/Atmosphere Mesoscale Prediction System (COAMPS) and the Navy Operational Global Atmosphere Prediction System (NOGAPS). To do this, the NRL has collaborated with the Navy and US Air Force to conduct research field campaigns, most recently in the Western Pacific studying typhoons.

NRL has shown a commitment to atmospheric research for decades and helped to fund this work. Past DoD funded research has included the development and implementation of a more accurate CCN advection scheme within the regional model used in this study (Smith 2008). The DoD has also funded the inclusion of a direct radiative scheme within the regional model (Stokowski 2005).

The Navy continues to be active in providing relief in the form of food, supplies and labor in the aftermath of a WP typhoon. This research will potentially improve the forecasting of TCs by including microphysical effects in their predictions, thus giving communities more time to evacuate or prepare for storms.

1.7: Chapter 1 Figures

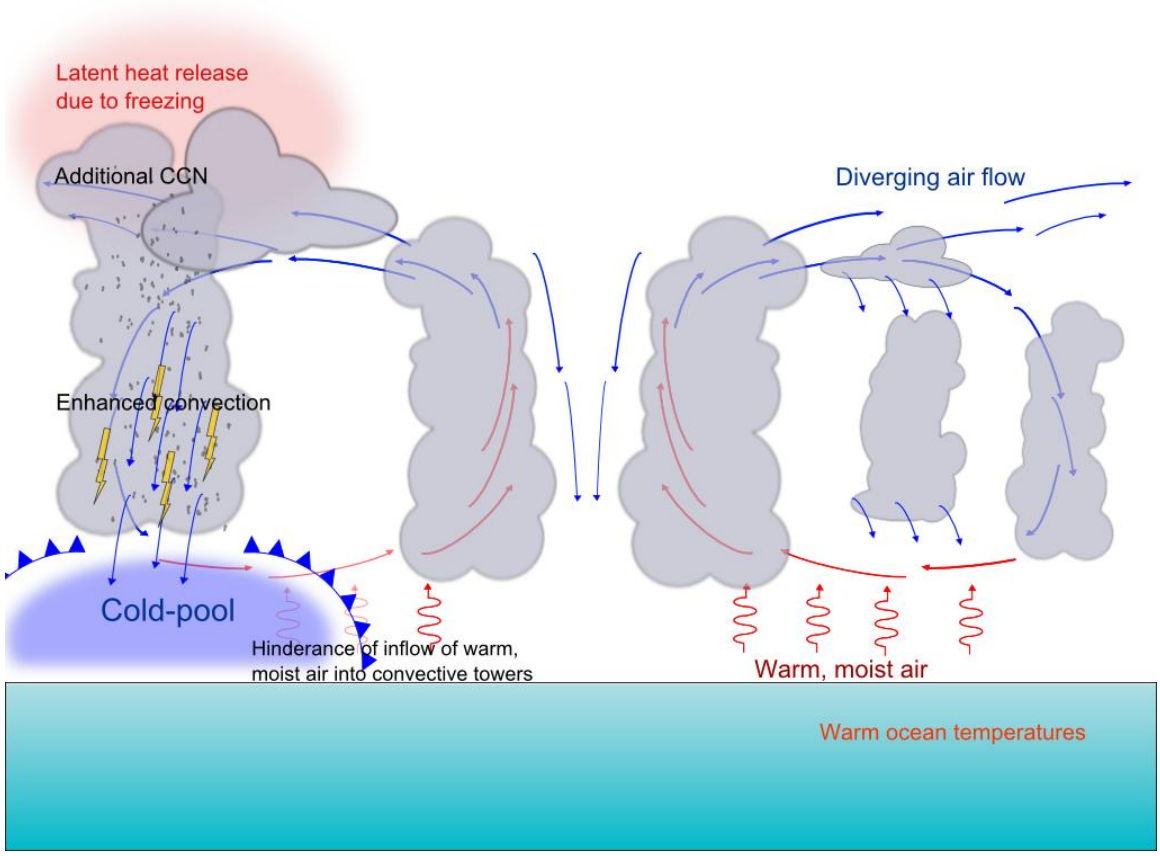

Figure 1.1: A schematic diagram showing the potential for CCN to hinder TC energetics. After initially suppressing precipitation in the outer rainbands, the additional CCN acts to reduce droplet size and increase amount of supercooled liquid water. As the supercooled liquid water freezes the enhanced latent heat release also enhances convection, which could in turn produce stronger downdrafts and cold-pools. The cold-pools may then work to suppress the warm, moist air entraining into the system.

CHAPTER 2 – THE RAMS MODEL

2.1: RAMS 4.3: the Microphysical Scheme

This study used the Regional Atmospheric Modeling System (RAMS). Being quite malleable in terms of regional modeling and containing an advanced microphysics scheme, the use of RAMS provides unique insight on aerosol interaction with various types of precipitation and cloud formation, even including convective storms and TSs.

Originally developed at Colorado State University (CSU), RAMS has undergone multiple updates and now exists in over 100 iterations throughout the world. It has been used to simulate a wide range of atmospheric situations, from large scale dynamics to boundary layer eddies and wind advecting around individual buildings to microscale wind tunnel simulations (Cotton et al. 2003). Primarily it is used to simulate atmospheric phenomena on the synoptic or mesoscale.

For this study version 4.3 of RAMS was used. It utilizes an Arakawa-C grid structure (Arakawa and Lamb, 1981; Randall, 1984) with the option for multiple two-way nested grids and the ability to add and subtract the nested grids within a simulation. The domain follows a rotated polar-stereographic transformation horizontally and a terrain-following coordinate system vertically. A

non-hydrostatic model, RAMS prognoses 14 variables: u, v, and, w wind components, ice-liquid water potential temperature, dry air density, total water mixing ratio and eight hydrometeor species. The radiation is calculated according to the Harrington (1997) long/shortwave model. The model includes a Kain-Fritsch convective parameterization. The boundary conditions allow for user-prescribed nudging time-scales. Much of the background information of RAMS can be found in Cotton et al. (2003). The remainder of this section will focus on the microphysical developments RAMS has undergone.

The inception of the RAMS model occurred in the early 1980's with a merger of three separate but related models: the sea breeze model as described by Mahrer and Pielke (1977), the CSU cloud model (Tripoli and Cotton 1980), and a hydrostatic version of the cloud model (Tremback 1990). The original "alpha"-version of RAMS had to be extremely constrained due to the limited computing resources at the time. Eventually as computing power increased, RAMS was released in 1988 as version 0a with the rewriting of much of the original RAMS code and the inclusion of parameterizations from the sea breeze model. Critical to the advancement of RAMS was its ability to take advantage of parallel computing thanks to the calculation of many of the variables locally, rather than globally. As such, the use of RAMS, widely distributed as version 2c in 1991, grew throughout the 1990's.

For this study, there is an inherent focus on microphysical and hydrometeorological processes. The first microphysics scheme, published in Cotton (1972a, b) was used for investigations into lake effect storms. The introduction of an ice crystal class of hydrometeors is described in Cotton (1982) and Cotton et al. (1986). Later, Verlinde et al. (1990) showed that solutions to the full stochastic collection equation can be obtained using approximations to the collection

efficiencies. The implementation of this allowance for prediction of mixing ratios of hydrometeors within RAMS is described in Walko et al. (1995). This was achieved by using a single-moment Gamma distribution of all hydrometeor species as the approximation. The solutions of the full stochastic equations were constructed into a set of look-up tables that allowed for fast and accurate implementation of the stochastic equations within RAMS. At this time the development of the RAMS ice nucleation scheme began to include homogeneous nucleation of ice from haze particles and cloud droplets. Meyers et al. (1997) extended this approach to include a second moment: mass concentration of the hydrometeor species. Feingold et al. (1998) advanced the use of the look-up tables by using realistic collection kernels and implementing a bin-emulating scheme by dividing the gamma distribution into discrete bins. The bin emulating approach also allowed for the sedimentation of hydrometeor species. Saleeby and Cotton (2004a, b) developed the inclusion of a large-mode for water droplets (40-80 microns). This effectively allowed for now eight hydrometeor species: small cloud droplets, large cloud droplets, rain, pristine ice, snow, aggregates, graupel, and hail.

The treatment and adjustment of CCN in RAMS will be the primary motivation of the sensitivity study of this research. The cloud droplet number is derived from a prognosed CCN field. The number of CCN that activate is a function of temperature, supersaturation, vertical velocity, and CCN concentration as determined by a series of look-up tables previously generated offline in a parcel model run (Saleeby and Cotton 2004) . Currently, activation according to chemistry is fixed (along with mean radius) for a given simulation, currently as ammonium sulfate. Recently, Ward et al. (2010) has investigated the inclusion of the kappa parameter as described in Petters and Kreidenweis (2007). Ward et al. (2010) demonstrated it can be included in RAMS simulations using an expanded look-up table. The CCN field is initially user-prescribed and may be advected,

consumed via activation, and/or diffused by the model.

2.2: ISAN (ISentropic ANalysis) Processing and the Barnes Scheme

For this research, a specific TS case study is utilized. We take advantage of the availability of both the model reanalysis data and specific dropsondes from the TC case study examined to assist in the initialization of the simulation. RAMS allows for both gridded data and irregularly spaced point data to be implemented in the initialization via ISAN processing and the Barnes Scheme. The ISAN processing is a routine that interpolates gridded data into the user-prescribed grid domain (Tremback 1990). The Barnes scheme (Barnes 1973) is an objective analysis routine that incorporates point data as well such as soundings from rawindsondes, dropsondes, etc., where available.

The Barnes scheme allows for the user to define the strength of the point data versus the gridded data processed by the ISAN routine. Typically the Barnes scheme is implemented with a point data weight of 10 to 1000 times stronger than the gridded data. The routine band-passes the data and applies a smoothing according to two user-prescribed parameters: the wavelength of the data on the isentropic and upper air surfaces and the fractional amplitude at which to retain that wavelength. Both the ISAN and Barnes routines construct fixed initialization grids and nudging varfiles according to the following recorded atmospheric parameters: u and v wind, temperature, geopotential height, and relative humidity.

2.3: Past RAMS-TC Experiments

RAMS has been used to simulate TCs in the past, albeit sparsely. Due to the high windspeeds, the

resolution required to sufficiently simulate a TC is rather fine such that a parcel of air may be advected over no more than a single grid space in a given time step, while the large scale meteorology must also be well represented. For this reason a nested grid scheme is ubiquitous in all RAMS-TC simulations.

Nicholls and Pielke (1995) used a nested grid scheme with a fine grid resolution of 4 km. A horizontally homogeneous Jordan (1958) sounding based on typical Atlantic hurricane conditions was used. The authors noted a realistic structure including spiral bands, a clear eye, and a radius of maximum wind that sloped with height. Upon spin-up, a maximum windspeed of 20 m/s was achieved 40 km from TC center. Eastman (1995) used RAMS to simulate hurricane Andrew via National Meteorological Center (NMC) gridded pressure data, upper air rawindsonde data observations, and a bogus vortex in gradient wind balance.

More recently Montgomery et al. (2006) investigated the role of vortical hot towers in idealized TC simulations with RAMS. This code utilized a balanced vortex initialization method and has been used extensively to investigate the dynamics of TCs. In particular Zhang (2007, 2009) investigated the impacts of African dust acting as CCN on Atlantic hurricanes in a series of idealized simulations. Those studies revealed a non-monotonic impact of CCN on TC intensity. While initial increases in CCN concentrations decreased the strength of the storm, higher concentrations had little impact, often even increasing the strength of the storm. The size of the storm was also affected, with the highest CCN concentrations yielding the most widespread storm.

Carrio and Cotton (2010) further investigated CCN impact on hurricanes by using RAMS to

simulate the seeding of a TC with extremely high concentrations of CCN within the outer rainbands of the storm. Those experiments yielded a smaller mean cloud droplet radius within the cloud bands leading to elevated levels of supercooled water and higher levels of latent heat released due to freezing. The resultant cold-pools were then stronger and more widespread under higher CCN concentrations. This acted to interfere with the inflow of moisture into the convective regions, acting to suppress the storm. The impact of very high CCN concentrations on riming on ice particles was also evident. Due to the extremely small hydrometeor size, very high CCN concentrations led to reduced riming and collision-coalescence and thus greater transport of pristine ice into the anvils of the storm rather than being precipitated to the surface.

Also potentially suppressing the strength of the storm is the act of initiating more disorganized convective fluxes, upward and downward, leading to greater asymmetrical heating as described in Nolan et al. (2007). An increase of shear indirectly caused by the ingestion of higher concentrations of CCN altering the latent heat profile and amplifying downdraft currents, would lead to the intrusion of low θ_e air into the convective towers near the eye and act to inhibit storm development (Reimer et al 2010).

In most RAMS simulations the Atlantic Jordan (1958) mean sounding has been used as the initial gridded wind and thermodynamic fields. The impacts of dust carried within the SAL have been investigated as the primary source of aerosol (Zhang et al. 2007, 2009). Among the features of the SAL, as indicated in Chapter 1, is a uniquely dry, stable layer, probably modulating a TC directly rather than taking microphysical effects into account.

To best understand the microphysical effects on TC development, a case study from the Western

Pacific (WP) was used. As discussed in Chapter 1, the aerosol-containing air from the WP is not dissimilar from a TC's large scale environment [need reference]. In the next chapter we describe the case study TC and field campaign used to guide and evaluate the RAMS model simulations. Chapter 4 contains a table summarizing many of the RAMS options available and those chosen for this experiment.

CHAPTER 3 - THE T-PARC CAMPAIGN AND TC NURI

3.1. The T-PARC Campaign

In 2008, an ambitious multi-national field campaign was conducted in the Western Pacific in part to better forecast high-impact weather events. THe Observing Research and Predictability EXperiment (THORPEX) Pacific Asian Regional Campaign (T-PARC) was a joint effort between the U.S. DoD-based Naval Research Laboratory, the National Science Foundation (NSF), the Japan Meteorological Agency, and several other institutions. The general scientific objectives were to better understand the route to tropical cyclogenesis and the implicit structure changes TCs undergo. In particular, there was an emphasis on parsing out the difference in synoptic versus mesoscale influences in the intensification and structure evolution of a TC.

To do this, T-PARC employed the use of several aircraft and ships from August 1 to September 30 collecting observational data in the form of dropsondes, ship-boarded radar, air-borne lidar, microwave radiometer, and satellite observations as well as the model forecasts from approximately seven weather centers.

3.2 Dropsonde Data

Witnessing several named typhoons, the T-PARC campaign had four aircraft at their disposal, each equipped with dropsonde drop capabilities. For the TC used for this case study the U.S. Air Force (AF) C-130 was the primary agent of dropsonde data. A total of 620 successful dropsondes were launched from the C-130 between August 15 and September 27. The TC used for this research was selected based on, in part, the wealth of dropsonde data provided by the AF C-130. A total of four flights during the lifespan of the selected TC were flown dropping over 60 dropsondes over the course of four days. The dropsonde data accumulated from the AF C-130 were incorporated into the model simulation initialization and internal nudging files according to the Barnes scheme, as described in Chapter 2. The locations of the release of the dropsondes during the lifespan of the studied TC are plotted in Figure 3.1.

3.3 TC NURI

On August16, 2008 at 18Z a mesoscale convective system (MCS) was developed into a TD. Observations and analyses show that the MCS became organized into a TD despite a relatively high level of shear (Raymond and Carillio 2010). Propagating westward, the TD was upgraded to a TS on August 17 at 12Z and declared a typhoon and given the name NURI on August 18 at 12Z. The disturbance began in the wake of an easterly wave but possibly had several other contributing factors (Montgomery 2009) such as interaction with a “monsoon gyre” as described by Chen et al. (2008) and the evidence of “bottom up” development (Montgomery and Enagonio 1998; Hendricks et al. 2004; Montgomery et al. 2006).

The system propagated westward for about four days averaging about 8 m/s zonally until it crossed over the Philippines and eventually made landfall on the Chinese coast where it subsequently dissipated. In addition to the wealth of data provided by the T-PARC campaign, this TC was selected as a case study due to the expectation of its interaction with pollution aerosols emanating from the Chinese coast. The interaction between TC NURI and Chinese aerosols as retrieved by MODIS is discussed more completely in Chapter 4. While it is currently impossible for satellites to accurately retrieve AOD within a cloud mass, with the large scale distribution of AOD, the seasonal climatology of AOD in the region, and the track of NURI, we can conclude that NURI interacted with the aerosols in some manner, even if only in the outer rainbands initially.

The track of typhoon NURI differed significantly from forecasts, moving more flatly than expected (Miyoshi et al. 2010). The path was more or less linear from southeast to west-northwest throughout its lifespan. Climatologically, typhoons typically move radially in a clockwise direction upon maturing, but NURI essentially stayed course upon developing into a TC. NURI is thought to have achieved a minimum sea-level pressure (SLP) of 955 mb with accompanying maximum gusts of about 35 m/s and sustained winds of 21 m/s according to the Japan Meteorological Agency (JMA), corresponding to a strong category 1 or weak category 2 TC. However, the T-PARC dropsondes show a maximum windspeed of 45 m/s. It is worth noting that the flights were isolated events and by nature are not expected to measure the TC consistently.

While there was clearly a pronounced axis of rotation, the visible satellite imagery shows no clearly defined eye upon nearing landfall (Figure 3.2). The National Aeronautics and Space

Administration (NASA) CloudSat satellite recorded cloud top heights of nearly 16 km and rainfall rates exceeded 30 mm/hr at times [CloudSat – visible eye?]. Upon nearing landfall, the evacuation of 250,000 people from coastal areas along the Chinese coast was ordered. NURI was implicated in the deaths of 20 people in the Philippines, Hong Kong, and China, along with over a hundred thousand acres of destroyed croplands, and millions of dollars in damage.

3.4: Chapter 3 Figures

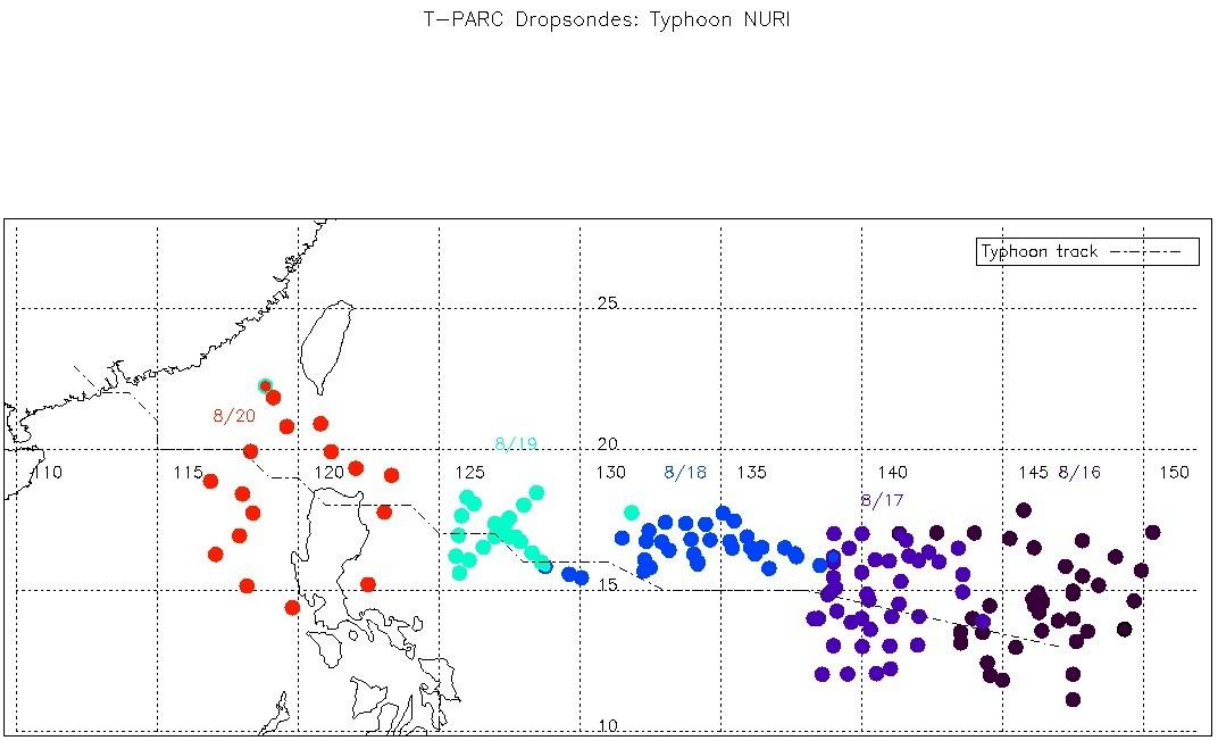

Figure 3.1: The locations of the successfully deployed dropsondes throughout the lifespan of typhoon NURI from 8/16/2008 to 8/20/2008, along with the track of the typhoon for clarity.

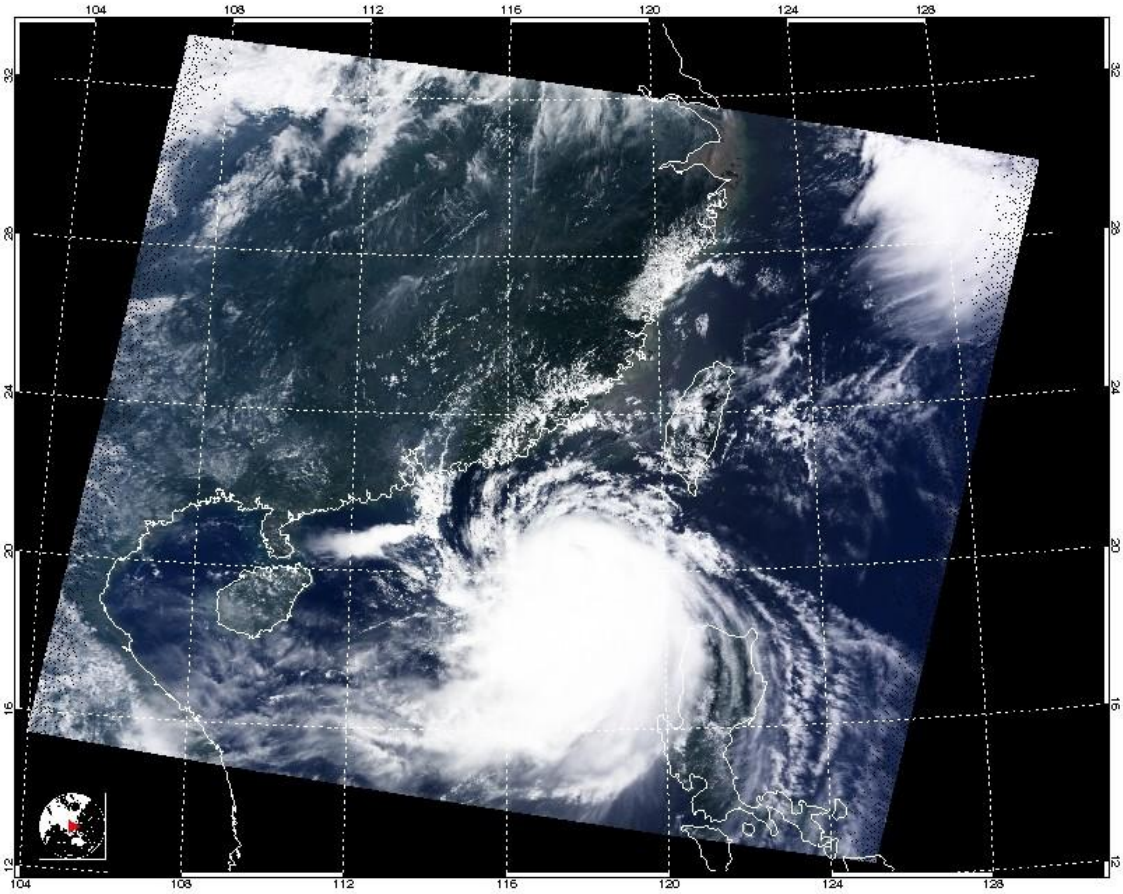

Figure 3.2: MODIS retrieved visible image of TC NURI as it approaches the Chinese coast. Eighty-six hours into the RAMS simulations corresponds to this image.

CHAPTER 4 - MODEL CONFIGURATION

4.1. Grid Configuration

To study the effect of added CCN on a TC case study, RAMS was used due to its sophisticated microphysical, convective, and turbulence schemes as well as the degree to which the model could be adapted to this case study. Ultimately two two-way interactive nested grids were used. However, during the initial model spin-up time, only one grid of 15 km was used. During the first 36 hours, this single grid was used to quickly allow the model to acclimate itself to the initialization and nudging data as well as allow for the synoptic environment to set up. At 36 hours, a second, finer grid of 3 km resolution was imposed to better represent the cloud-scale and convective elements of the storm. Also at this time, the balanced vortex routine (Montgomery et al. 2006) was implemented in the smaller grid. The addition of the routine aided with the generation of realistic convective fluxes that maintained the TC. Without the balanced vortex routine, similar windspeeds were achieved but a realistic thermodynamic structure of the storm was not achieved. Grid 1 consisted of 253 x 200 points horizontally while Grid 2 was 452 x 452 and centered at a latitude of 18.3N and a longitude of 130.1E. Vertically, both grids stretched from 120 m at the surface to a maximum of 1500 m consisting of 20 levels. The model top height was about 18 km.

In order to capture the entire lifespan of the TC from cyclogenesis to landfall the second grid had to be moved in order to keep the TC within its domain. Furthermore, the study's hypothesis was contingent upon resolving the middle and outer rainbands of the storm, where the additional CCN is expected to cause changes in cold-pool parameters. For this reason, Grid 2 was manually moved twice throughout the simulation. This is a similar approach to explicitly resolving convection and microphysical effects at cloud scale used by van den Heever et al. (2006) simulating convective sea-breeze storms. The first move occurred at 60 hours from the initial time of the simulation (24 hours after it was imposed). The grid was moved 375 km west and 225 km north. The second move occurred at 72 hours since simulation start (12 hours after the first move) and was moved another 300 km west and 75 km further north. The location of Grid 1 and the three positions of Grid 2 are shown in Figure 4.1. This allowed the convection to be explicitly resolved within the northwest rainbands of the TC. The entire simulation consisted of 96 hours, beginning on August 17, 2008, 00 GMT and finishing on August 21, 00 GMT.

Convection was parameterized on Grid 1 using a Kain-Fritsch (Kain 2004) cumulus parameterization scheme, but explicitly resolved for the finer grids. The time step for the larger grid was 30 seconds and 15 seconds for the smaller grid.

4.2. Model Initialization

The model initialization was constructed via the Barnes scheme, as discussed in Chapter 2, with both gridded and irregularly spaced point data. The gridded data utilized was the NCEP/NCAR Renalysis 1 global gridded data (Kalnay et al. 1996). The data are updated every six hours and have a horizontal resolution of 1.5 degrees and a vertical resolution involving 28 sigma levels

from the surface to 1 hPa. The horizontal and vertical components of wind, relative humidity and geopotential heights are processed via the RAMS ISAN routine. The point data were assimilated from the T-PARC dropsondes and incorporated into the gridded data as initialization conditions and nudging files. The internal nudging of the model occurred 900 seconds during the first 36 hours after which point, the internal nudging was switched off and only the boundary conditions were nudged every 450 seconds.

Reynolds weekly SSTs (Reynolds and Marsico 1993; Reynolds and Smith 1994) were used and not updated during the simulation (Figure 4.2). Reynolds weekly SST analysis has a one-degree resolution. The surface processes were parameterized using the Land Ecosystem-Atmosphere Feedback (LEAF-2; Walko et al. 2000). The Harrington (1997) parameterization was used for long/shortwave radiation and updated every 15 minutes and the Klemp and Wilhelmson (1978) boundary conditions were applied at the lateral boundaries.

4.3. Aerosol Prescription

TC NURI was chosen in part due to its path which took it near centers of large aerosol activity. As shown in Figure 4.3, the AOD in and near the TC path is significantly higher than the cleaner maritime environment in which the TC was birthed. Geography and geometry of the trend of AOD was taken into account when constructing this experiment. The MODerate Resolution Imaging Spectroradiometer (MODIS) retrievals show the aerosol concentration at elevated levels along the coast of China and extending to the northeast beneath the Japan. The elevated aerosol region provided by MODIS is further confirmed by the SPRINTARS three-dimensional aerosol model (Takemura et al. 2000) data for the dates of the TC which show aerosol plumes of sulfate (Figure 4.4) and dust (Figure 4.5) emanating from the Chinese and Indian coasts

advecting into the path of the TC. Both the MODIS satellite AOD retrievals and the SPRINTARS horizontal and vertical aerosol model data data gave rise to the aerosol prescription used for this study. The CCN prescription in the simulation follows the same middle to northeastern path through the model domain and is regenerated every six hours as sources of CCN to represent the continual influx of aerosol from the urban centers and the Gobi desert. As a result, the northwest rainbands of the simulated TC entered the regions of elevated concentrations of CCN first.

The vertical concentration of CCN was also constructed based on the SPRINTARS model. SPRINTARS calculates the transport of aerosols taking into account emission, advection, diffusion, wet deposition, dry deposition, and gravitational settling. The column aerosol concentration for Beijing for the duration of the lifespan of TC NURI is shown in Figure 4.6. There is a trend over the course of the TC lifespan of significantly elevated aerosol concentration of all species from the surface to 3000 meters. There is also a smaller, second local maximum of aerosol concentrations occurring near an elevation of 4000 meters. For the control simulation, a homogeneous field of 100 CCN per cubic cm was applied and replenished every six hours in the MODIS indicated domain. We use the Beijing SPRINTARS data (Fig. 4.6) as a guide to develop a vertical profile of CCN, assuming a positive correlation between aerosol mass and CCN number concentration. The vertical CCN prescriptions for the sensitivity studies are shown in Figure 4.7 and applied at each grid space within the geometric domain indicated by MODIS retrievals of elevated aerosol concentrations. The naming conventions used for the remainder of this text identifying each simulation are listed in Table 4.2.

Ice Nuclei and Giant CCN (GCCN) were not varied in this experiment and applied three-dimensionally homogeneously at low, background concentrations. Table 4.1 summarizes the model configuration and options for the TC NURI simulations.

4.4: Discussion of Control Simulation Results

This section will briefly introduce some of the results from the control simulation, or C100. Further discussion appears in Chapter 5, including comparisons with the sensitivity tests.

RAMS was able to produce a TC under low CCN concentrations. Despite not being an idealized simulation the vorticity yielded by the control simulation (Figure 4.8) is consistent with the described results of Montgomery et al. (2006). As indicated by Figure 4.8, the TC NURI has a westward tilt, consistent with the large scale meteorology of this case study and TCs in general. We also note the weak upper-level vorticity (Fig. 4.8d) as TC NURI was formed in an unusually high amount of shear (Raymond and Carillo 2010).

Grid-averaged maximum windspeed peaked at 54 hours into the simulation at about 30 m/s sustained winds, consistent with observations from the T-PARC dropsondes and ECMWF reanalysis data. The manually moved grid allowed for continued higher resolution in the northwest quadrant of the storm (see Figure 4.9), although this technique did yield a few modeling artifacts that must be considered. For instance, the rain rate was relatively constant throughout the storm except at the time where the nested grid was moved manually, at 60 and 72 hours. Figure 4.10 shows the rain rate dropping off to zero at both times. As the nested grid was moved, it took a brief amount of time for the nested grid to explicitly resolve convection

again. Still, explicit convection was achieved including a broad spectrum of hydrometeor species, similar to a real TC. Chapter 5 will further analyze the achieved results of the control run and the sensitivity tests.

4.5: Chapter 4 Tables and Figures

Table 4.1. RAMS model configuration and options.

Model Aspect	Setting
• **Grid**	• Arakawa C grid (Mesinger and Arakawa 1976) • Two grids • Grid 1: Δx=Δy =15 km; 253 x 200 • Grid 2: Δx=Δy=5 km; 452 x 452 • Manual moving of Grid 2, follows TC path • Vertical grid: Δz stretches from 120 m to 1500 m; 20 vertical levels
• **Initialization**	• Barnes objective analysis • NCAR/NCEP Reanalysis Data • T-PARC Dropsondes
• **Time Step**	• Grid 1: 30 s; Grid 2: 15 s
• **Simulation duration**	• 96 hours • 08/17/2008 to 08/21/2008
• **Microphysics scheme**	• Two-moment bin emulating microphysics (Meyers et al. 1997; Feingold et al. 1998; Saleeby and Cotton 2004)
• **Convective initiation**	• Kain-Fritsch parameterization (Kain 2004) for Grid 1; explicit convection on Grid 2
• **Radiation scheme**	• Harrington (1997)
• **Sea Surface Temperatures**	• Reynolds weekly SSTs (Reynolds and Smith 1994; Figure 4.2)
• **Aerosol Prescription**	• Horizontal domain based on MODIS AOD retrievals (Figure 4.3) • Varying vertical CCN profile (Figure 4.7) for sensitivity tests based on SPRINTARS (Figure 4.4) model output • Regenerated every 6 hours

Table 4.2: Naming convention used for this study of each sensitivity test simulation of TC NURI as well as the control run.

Simulation Identifier	CCN concentration of elevated aerosol field (per cubic centimeter)
C100 or "Control"	100
C400 or "Moderately clean"	400
C1000 or "Moderately polluted"	1000
C3000 or "High"	3000
C5000 or "Extreme"	5000

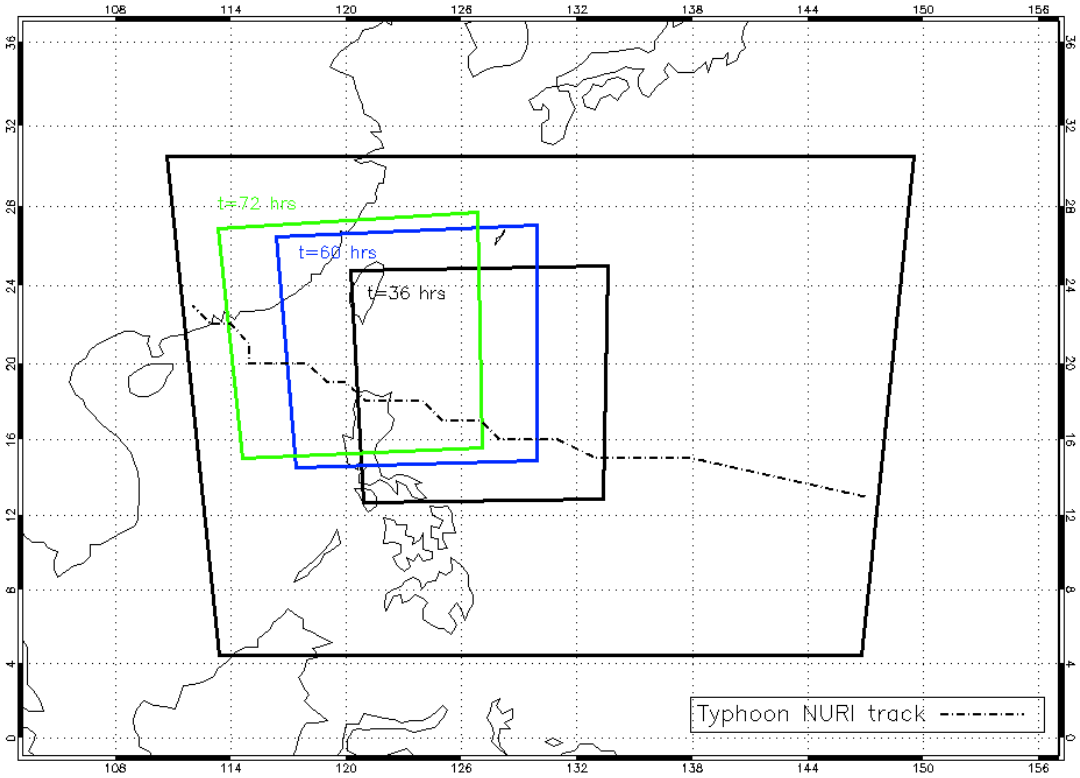

Figure 4.1: A map showing the location of Grid 1 and the three locations of the manually moved finer Grid 2 with the indicated time of implementation. The track of typhoon NURI according to the Japanese National Institute of Informatics (NII) is shown for clarity.

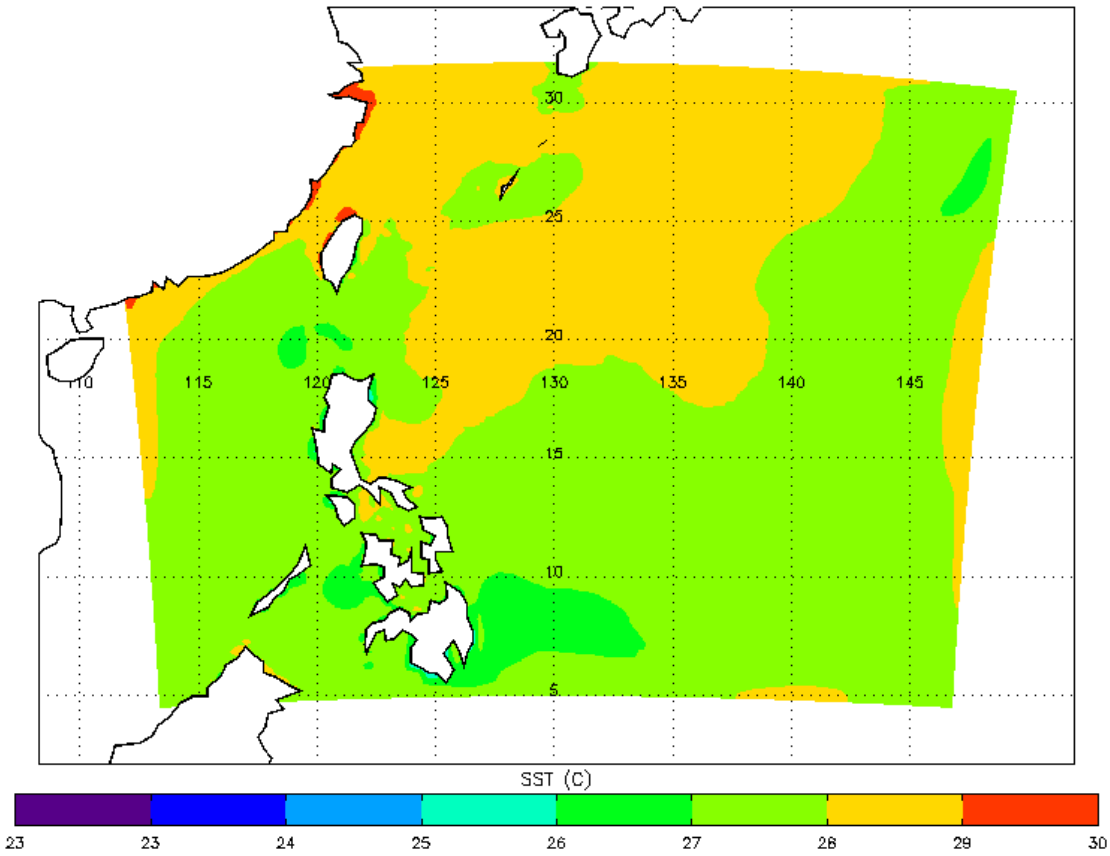

Figure 4.2: Mean SST for the duration of the simulation. Based on Reynolds weekly SST analysis.

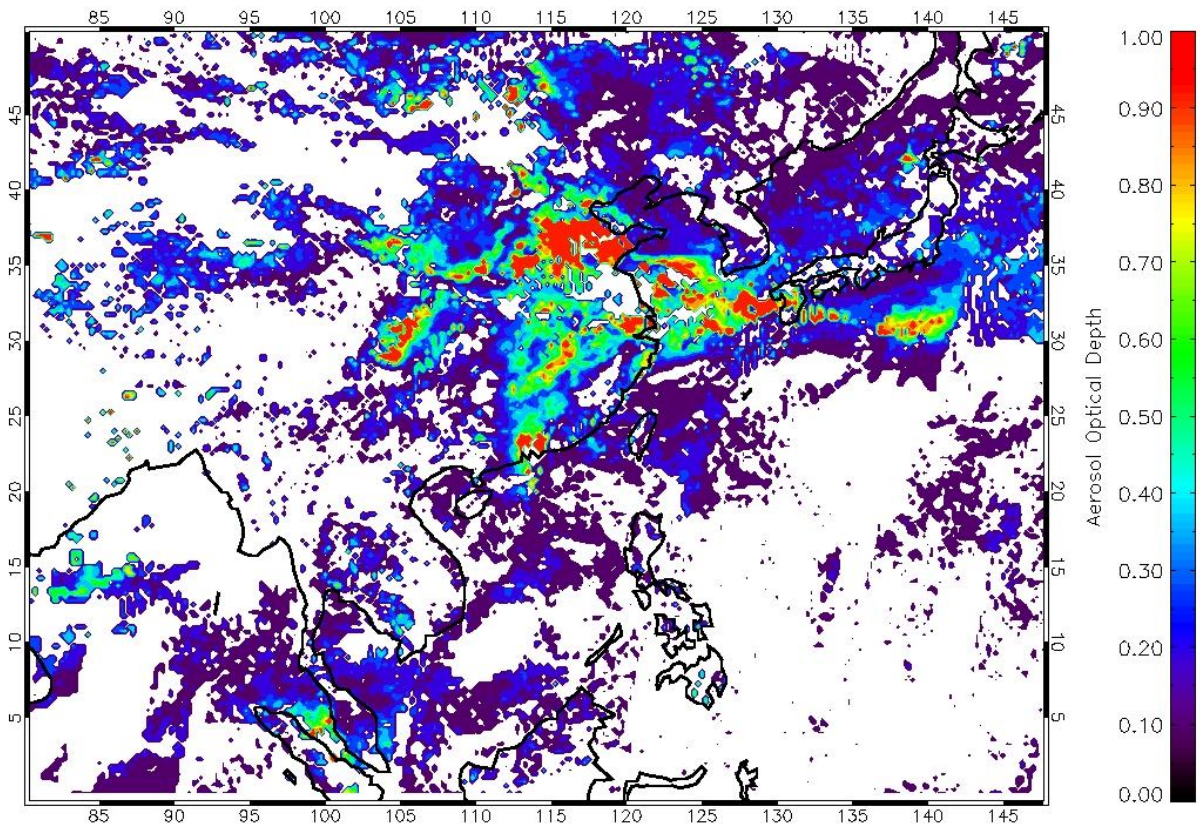

Figure 4.3: The AOD retrieved from MODIS averaged over the lifespan of TC NURI.

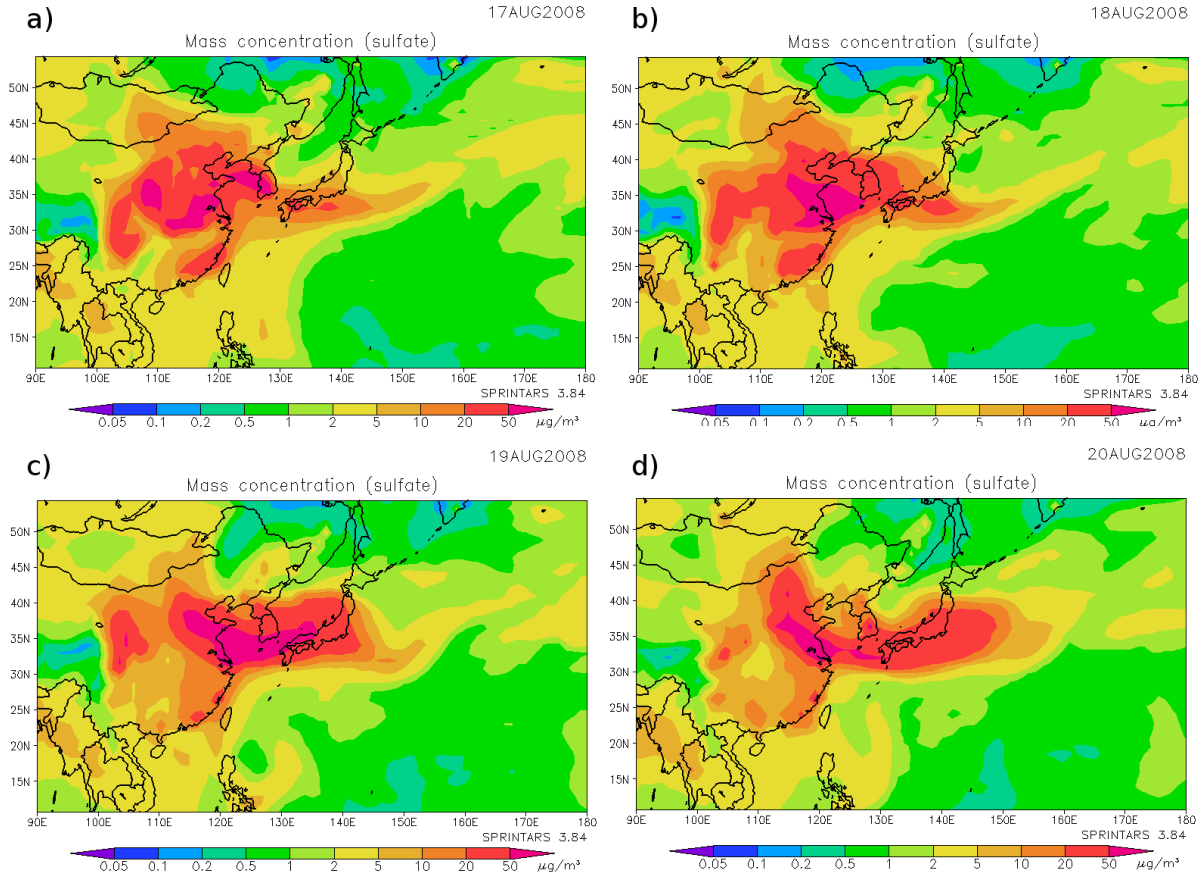

Figure 4.4: SPRINTARS East Asian model output of sulfate mass concentration for the four days used in this study.

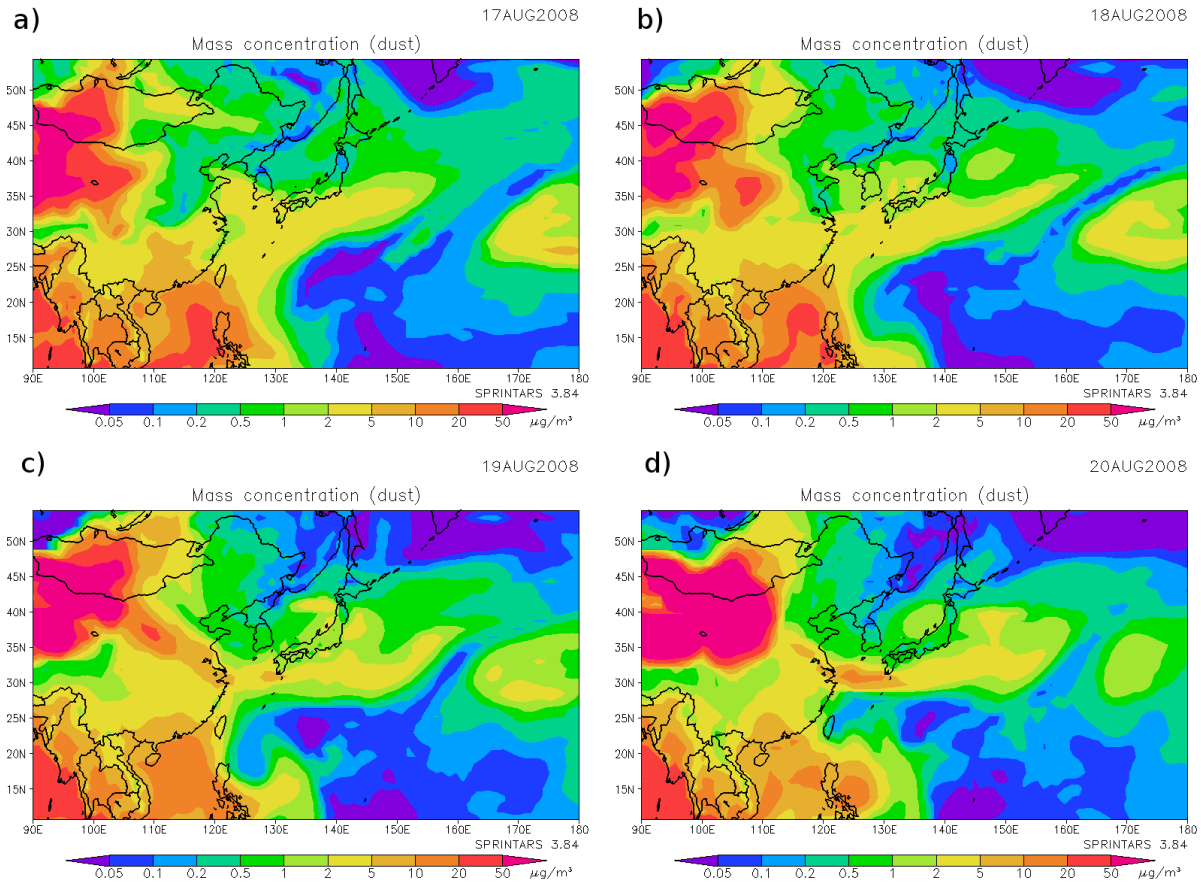

Figure 4.5: As Figure 4.3, but for dust mass concentration.

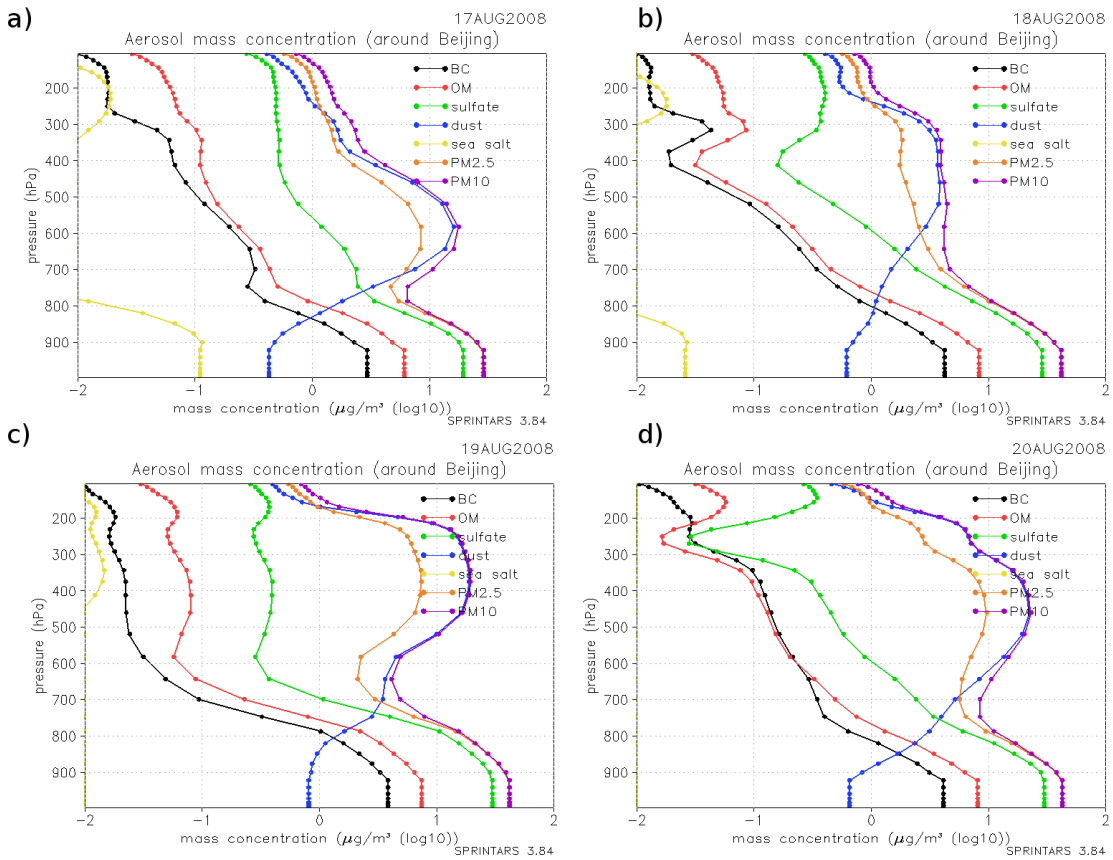

Figure 4.6: SPRINTARS model output of column aerosol over Beijing for the dates of the study averaged by day.

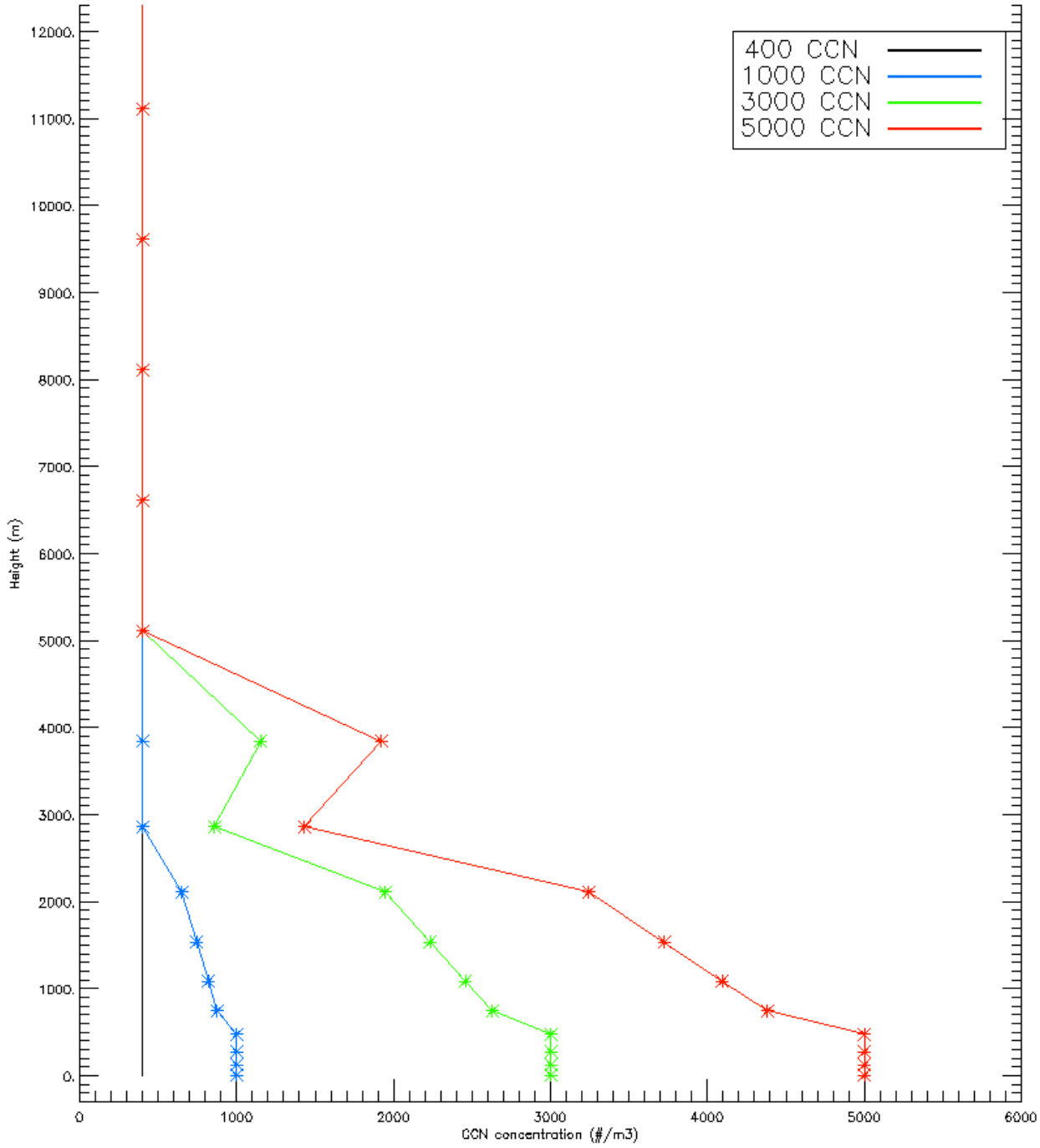

Figure 4.7: The prescribed vertical CCN profile for the four sensitivity experiments conducted.

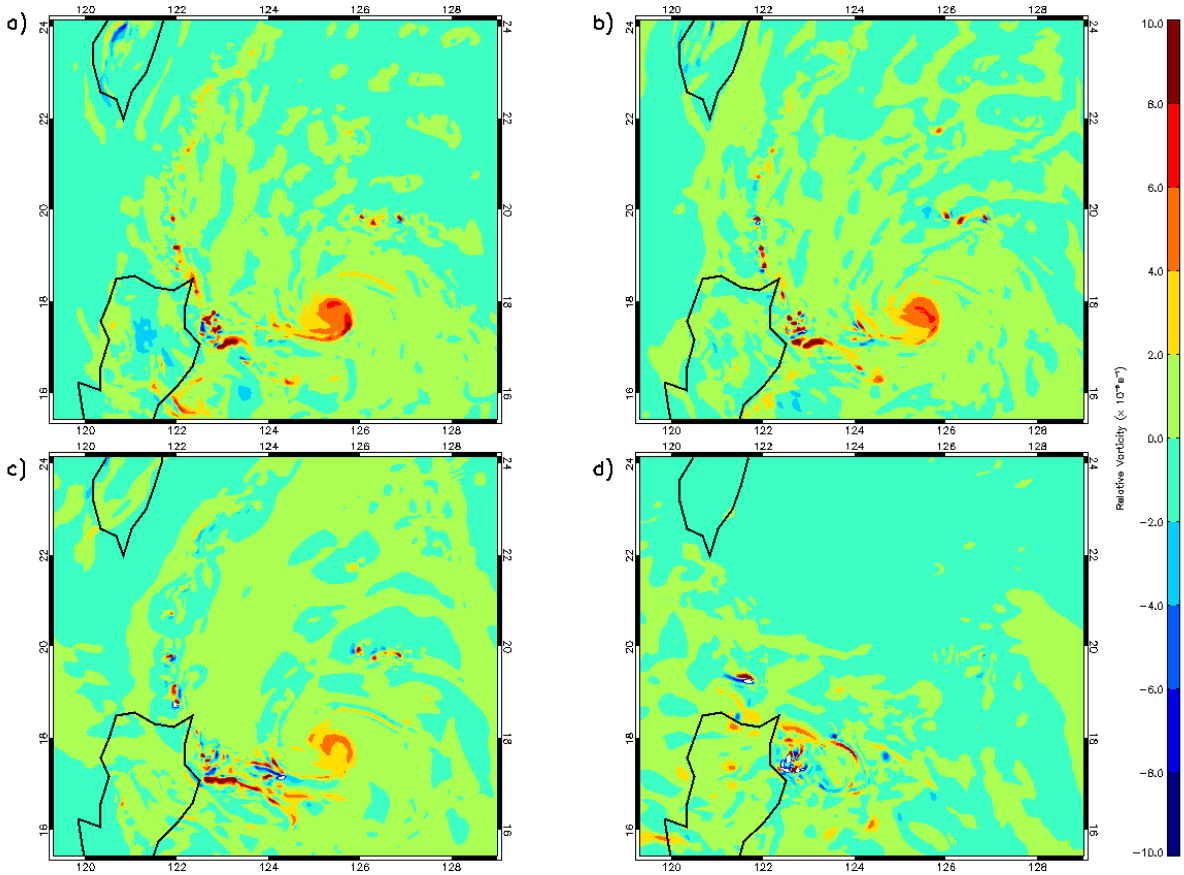

Figure 4.8: The relative vorticity of the C100 simulation at t=68 hours at the following vertical levels: a) 320m, b) 900m, c) 1800m, and d) 9000m.

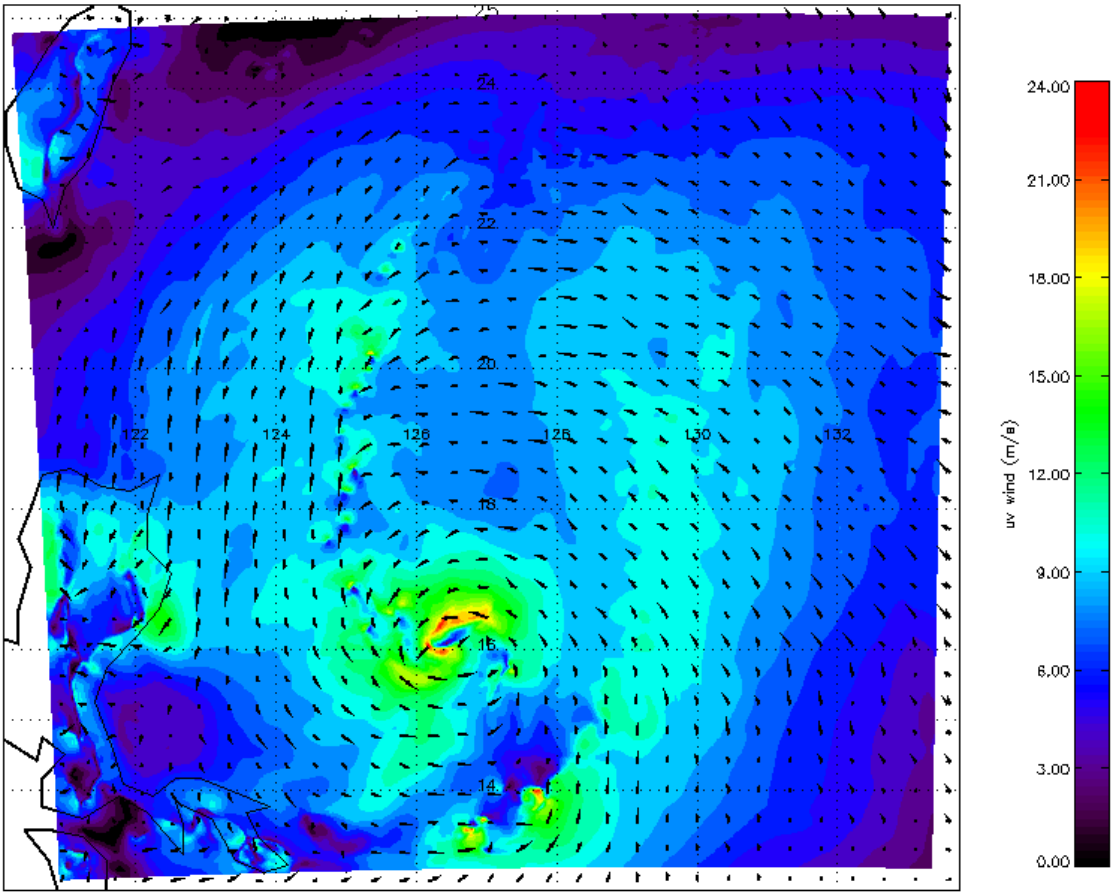

Figure 4.9: Entire nested grid domain showing near-surface windspeed (m/s) and wind vectors for C100 simulation at t=52 hrs.

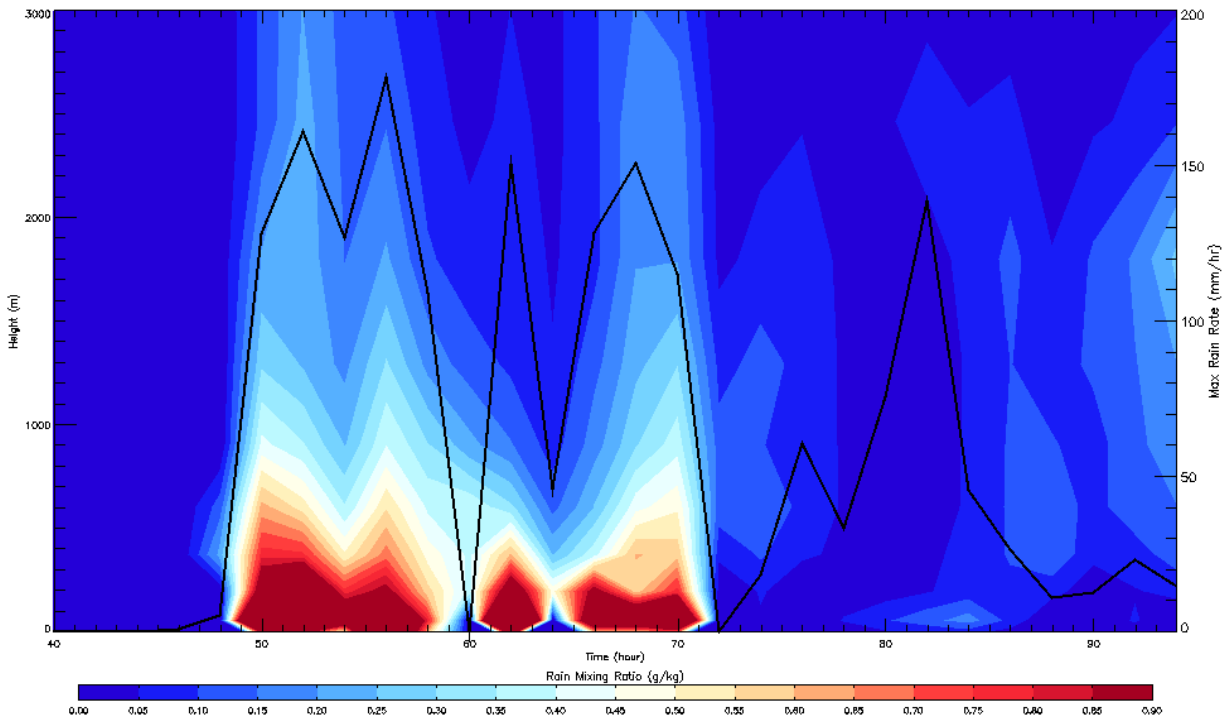

Figure 4.10: The rain mixing ratio within the downdrafts by height, along with the maximum rain rate. Note the precipitous drop in maximum rain rate at t=60 and t=72 hours. This is an artifact of the manually moving grid. However, the rain rate quickly became reinvigorated.

CHAPTER 5 – RESULTS

5.1: General Discussion

The RAMS model was able to successfully reproduce a WP storm of TC strength under all CCN experiments. The vortex as described in Montgomery et al. (2006) was implemented 36 hours into the simulations. From there, the typhoon developed into a strong Category 1 / weak Category 2 TC according to the Saffir-Simpson Hurricane Scale, exhibiting sustained winds topping 30 m/s, consistent with the observations yielded by the T-PARC dropsondes and the ECMWF Reanalysis data. The TC intensified similarly under all CCN experiments as the elevated CCN concentrations were constrained closer to the Chinese coastline, as indicated by MODIS retrievals and SPRINTARS model output. As such, the TC in each experiment intensified identically from 36 hours to 48 hours (Figure 5.1) according to maximum windspeed. The internal nudging of the model had been switched off at this point in the experiment. Therefore any future response of the TC can be attributed to the CCN differentiation.

The outer rainbands of the TC began to ingest the elevated levels of CCN around the 46 to 50 hour mark. At the same time the TC continued moving in a northwestern direction, ostensibly

advecting itself over the ingested and produced CCN (see Chapter 4 for description of CCN production). The TCs exhibit wildly different maximum windspeeds in the moderate CCN cases (C1000 and C3000 experiments) upon the ingestion of CCN into the TC rainbands. In particular the pattern of intensification from 56 to 64 hours differs under moderate CCN (C1000 experiment) and higher CCN (C3000) experiments. In C1000 the additional CCN produces a quick increase in maximum windspeed while the C3000 produces a similar peak, but about 6 hours later in the simulation. In both cases, the near 60-hour windspeed maxima far exceeds the clean (C400) and extreme (C5000) CCN experiments. The underlying reasons for these responses will be discussed later in this chapter.

Upon passing the near 60-hour maxima, the TC begins to dissipate somewhat into a tropical storm with maximum sustained winds between about 20 and 25 m/s. As the TC passes the Philippine coast and begins to cross slightly colder SSTs along the coastline, the storm maintains the northwest track and stabilizes as a TS until it makes landfall on the Chinese coast. However, in the C1000 there are two further peaks of sustained maximum windspeed at 74 and 82 hours that would reclassify the storm as a Category 1 TC. Even again as the storm is dissipating at the 88 hour mark the C1000 case again exhibits a slight peak while the other TC experiments continue to deintensify. As will be discussed in this chapter, the continual replenishment of CCN in these experiments has the effect of creating and recreating convective activity that acts to produce higher windspeeds due to downdrafts and cold-pool propagation than when CCN is kept at a minimum. While not producing the periodic convectively generated maximum windspeed peaks that the C1000 case does, the C3000 TC exhibits a general tendency to be a few meters per second stronger than the C400 case (Figure 5.2) throughout much of the storms

lifespan. Interestingly, the two most similar experiments are the clean, C400, and the extremely polluted, C5000, experiments, with the C5000 experiment showing a slight tendency to be damped between 1 and 3 m/s from experiment hours 76 onward.

The TC tracks for each experiment, along with the best track given by the Japanese National Institute of Informatics (NII) and the track of minimum geopotential height according to ECMWF model data are shown in Figure 5.3. RAMS produces a storm that maintains a track error of about 1.5 degrees rather consistently throughout the simulations. The model error yielded in RAMS was similar to that of the forecasted track of the storm (Miyoshi et al. 2010). While the C5000 exhibits the highest amount of drift in the TC track, the amount it differs in track is negligible. In the dissipation phase of the storm the RAMS simulated track, the center of the TC, as indicated by minimum perturbation pressure, turns southward bringing it more in line with the NII and ECMWF indicated tracks.

5.2: Precipitation Modulation and Convective Activity

Additional CCN has been shown to alter precipitation in continental convective storms (van den Heever et al. 2006, Seifert and Beheng 2006, Storer et al. 2010). This largely occurs due to an alteration of the latent heat release resulting from the perturbation of the amount, location, and timing of the freezing of cloud drops. As the CCN increases, the droplet concentration increases and the size of droplets decrease. This results in less sedimentation, fallout, reduced collision efficiency, and scavenging for the smaller droplets, as well as the tendency for the droplets to freeze at lower sub-zero temperatures. The TC NURI experiments confirm there is also a precipitation modulation due to additional CCN in the case of TCs. Figure 5.4 shows the

modeled reflectivity 74 hours into the simulation, or about 14 hours after initial contact with the elevated CCN field. By this time the TC has advected over the location of initial CCN ingestion, as indicated by the surface perturbation pressure contours. The convective activity takes on a different form in terms of strength and distribution for each of the modeled experiments. At this time C3000 shows the most vigorous convective activity at the southwest corner of the TC center, while both the C1000 and C3000 show a significant secondary convective mode along the northwest corner of the TC center. When comparing to the C400 case, we note that this secondary convective mode is either absent or broken up into less vigorous convective cells. The C5000 shows significantly damped convective activity at both convective locations. Similarly the rain rate at this time (Figure 5.5) is greatly increased for C1000 and C3000 and significantly damped for C5000. In all cases at this time, the locations of higher rain rates are located within the elevated CCN field. Six hours later, C5000 does begin to show convective activity (Figure 5.6). Spatially, however, the reflectivity shows a distinct contour around the TC center. Also, it is worth noting the high reflectivity over the Philippine Islands in the C5000, absent in the other three cases. The additional CCN appears to have “locked in” some of the atmospheric condensate until a time in which it may be condensed and precipitated out.

Due to the smaller droplet size, the condensed water is more susceptible to updrafts and transported into the upper atmosphere. This is evident in Figure 5.7, which shows the average condensate mass within the updrafts from the time of initial CCN ingestion (t=60 hrs). The amount of condensate being uplifted away from the mid-troposphere in the C5000 case dwarfs the other three experiments; twice as much condensate mass over the course of the model run. Conversely, the opposite CCN-moisture flux association is true when we examine the

condensate in the downdrafts of the model runs. Figure 5.8 shows the average rain mixing ratio within the downdrafts of the storm. In this instance, the C5000 case shows an enhanced rain mixing ratio within the downdrafts below 1500 meters. Between 1500 meters and 4000 meters, the C5000 case shows lower rain mixing ratios, evidence of a drier mid-troposphere, when considered along with the condensate within the updrafts above 6000 meters (Fig. 5.7). The convective trend continues at 86 hours into the simulations (Figure 5.9), with enhanced modeled reflectivity in the C3000 case and almost none in the C5000 simulation.

Regarding the modulation of latent heat release, we now examine the presence of supercooled liquid water (SCLW) for all simulations; that is, the mass of moisture above freezing level still in liquid form. The time evolution of the amount of SCLW within the outer domain of the TC, as defined as 250 km from TC center, is shown in Figure 5.10. The low to high CCN concentration simulations (C400, C1000, and C3000) all show a time delay of maxima of SCLW compared to the C100 case. These simulations reach their maxima two hours later than in the control run. The C3000 simulation shows the greatest increase in SCLW, exceeding the control simulation by 1000 kg (or, 212%). This is by far the greatest amplitude change, however, each simulation shows a distinct variance in peak SCLW, with the most polluted case, C5000, showing the latest peak in SCLW.

When we examine the time-averaged amount of SCLW according to height (Figure 5.11) over the course of the simulations we see a monotonic increase in SCLW just above the freezing level except for the C5000 case, which shows a steep decrease in SCLW. The potential causes for C5000's decrease will be discussed later in this chapter. As for the other cases, the C3000 shows

a ubiquitous increase in SCLW at all height levels. C1000 shows an increase in SCLW compared with C100 just above freezing level, a slight decrease in the mid-troposphere (around 9000 meters), and reverses trend again with C100, containing a higher SCLW at 10500 meters). By altering the profile of SCLW, it stands to reason the profile of latent heat release would show a similar alteration with increased CCN. In the next section, the impact of the variances in hydrometeor activity will be examined alongside convective fluxes.

5.3: Downward Flux

Downward flux (DFX) is defined in (Riemer et al. 2009. Eq. 23) as

$$DFX = \theta_e{}'_w, \qquad \text{(Eq. 5.1)}$$

where $\theta_e{}'$ is the deviation of equivalent potential temperature from the azimuthal mean and $_w$ is the vertical velocity. This parameter yields an indication as to both the upward and downward motion and the thermodynamics of the air being transported vertically. Essentially, in a period of high convection and precipitation, the net downward flux will be strongly positive due to the downdrafts and air associated with the downdrafts. Conversely, the DFX parameter will also be positive for a strong upward flux of relatively high θ_e air. As suggested in Riemer et al. (2009), DFX is calculated for the model height corresponding to about 1500 m to best represent the inflow from the BL. The closest model height available for this study was 1300 m, so all DFX calculations occur at that level. The time evolution of net DFX throughout the simulation is shown in Figure 5.12. Here we see a pattern similar to some of the maximum windspeed patterns (Fig. 5.1): invigorated DFX followed by a reduction in DFX. All simulations generally follow the same trend of DFX: each local maximum is generally located at the same model hour (t=68, 78hours) All sensitivity tests show an initial damping of positive DFX compared to the

control simulation until 68 hours. At this point all simulations except C5000 quickly show an amplified DFX. The C3000 simulation shows a dramatic increase in DFX at this point in the simulation, jumping to nearly 10000 K m/s. The C3000 case also shows a reinvigoration of DFX six hours later that is absent in the other simulations. Cold-pool activity has been linked to invigoration of MCSs; it is possible the abnormally strong cold-pool generated in the C3000 simulation had the effect of invigorating further convection. It is critical to remember too that a strong positive DFX signal could either be indicative of strong downward flux of low θ_e or strong upward flux of high θ_e. Once the second DFX maxima is reached, for the rest of the simulation the C3000 case remains one of the more damped cases of DFX.

Once again, the C5000 base shows the most damped DFX, consistent with the reduced convection described in the previous section. We also note that the C5000 case deviates comparatively little in magnitude with the C100 case after the 60 hour mark: the DFX minima and maxima are not as strong as in the other cases, generally staying within 2000 to 4000 K m/s.

One of the primary hypotheses of this study is that the imposition of higher CCN concentrations will cause a variance in SCLW aloft, resulting in differences in convective and cold-pool activity in a TC. The link between SCLW and convective activity can readily be seen in Figure 5.13. Here the amount of SCLW is lag-correlated with DFX by two hours, with the linear correlation coefficients (r) also shown. The strong r values for the C400, C1000, and C3000 indicate a linear relationship between a high presence of SCLW and the DFX of a system two hours later. The composite r value for all five simulations is 0.57. And if we exclude the extremely polluted case, where the advection of SCLW away from the system is more of a factor (discussed in detail in section 5.5),

the correlation coefficient is 0.63: a clear sign of positive linear correlation. The generation of large amounts of SCLW results in an eventual generation of large amounts of DFX.

We now examine the time evolution of DFX regionally compared to the TC center (Figure 5.14). As we are largely concerned with the activity of precipitation within the outer rainbands, we observe that the DFX response is stronger in the C1000 and C3000 cases when looking past 60 hours and 50 to 150 km from TC center. In the C1000 simulation starting at 78 hours, we can evidently see the movement of strong DFX towards the center of the TC, an artifact of the movement of the TC. A similar inward-tendency of strong DFX is evident in the C3000 simulation; however, as the additional CCN damps the DFX initially, the strongest period of DFX is stronger and closer to the TC center. The C5000 simulation shows the most neutral DFX response over the entire simulation. The maximum tangential windspeed is concurrently shown in Figure 5.14, exhibiting a fluctuating response akin to the DFX strength.

The spatial distribution of DFX relative to TC center along with the wind vectors, indicating the direction of the inflow of DFX in the BL are shown for the C100 and C3000 cases at 76 hours in Figure 5.15. When examining the individual wind vectors, we note that the wind vectors propagating from regions near strong DFX are pointed more outward than tangential to the TC center. These wind vectors are pointed out in Figure 5.15. Even without considering CCN concentration, we see a clear linkage between enhanced positive DFX and a disruption in the storm dynamics from the strong downdrafts. In the C3000 case the region of strongest DFX is closer to the TC center: 100 km west of the TC center for the C100 case, while only 50 km west

for the C3000 case. In this instance, it is possible the low θ_e air is more likely to be entrained in the convective towers near the TC eye.

As discussed earlier, the C3000 case shows a strong reinvigoration of DFX near the 80 hour mark, shown spatially along with the C100 case in Figure 5.16. Here the region of DFX is more widespread. However, there are also pockets of negative DFX within the inflow layer. Recall from the definition of DFX (Eq. 5.1), a region of negative DFX could be indicative of either an upward flux of low θ_e air and/or a downward flux of high θ_e air. Another possibility is that this is an artifact of the azimuthal averaging when calculating θ_e' as given in the definition. Adjacent to extremely low θ_e, the pockets of negative DFX could simply be more damped regions comparatively, but not necessarily exhibiting overly high or low raw θ_e values. Regardless, the increase in both positive and negative DFX is indicative of strong convective activity at the BL inflow layer. Rain mixing ratio within the downdrafts may also be examined over time and according to height to obtain a better working knowledge of the convective activity of the storm. As shown in Figure 5.17, the downdraft rain mixing ratios are altered according to the CCN concentration field. From 64 hours to 74 hours, the simulations differ in terms of the rain mixing ratio and how it is distributed vertically. The enhanced CCN cases all show levels of enhanced downdraft rain mixing ratio existing higher in the atmosphere than in the cleanest case. The clean, C400 case shows a maxima of downdraft rain mixing ratio at 68 hours, extending no higher than 1500m above the surface. The C1000 delays that maxima by a few hours and extends it vertically to nearly 3000m. The C3000 and C5000 each show two local maxima of downdraft rain mixing ratio at 66 and 70 hours, which are also concurrent with periods of maximum rain rate. Again, the extent of the relative maxima extends vertically to 2500m, suggesting a lifting of the level of precipitation compared to the C1000 case. In the next

section the relation of these parameters to cold-pool activity and their impact on the dynamics of the storm will be discussed.

5.4: Cold-pool Parameters

It hypothesized that the cold-pool activity due to enhanced CCN may act to modulate TC strength (Carrio and Cotton, 2010). This section will examine the response of various cold-pool parameters to each elevated CCN experiment. Cold-pools can form readily from convective precipitation. With higher concentrations of CCN, more water droplets will ascend past the freezing point in the atmosphere and eventually freeze. The associated latent heat release can cause the upper atmosphere to become relatively heated. Along with the latent heat release in the high atmosphere due to the freezing of liquid water will come a cold downdraft that propagates outward upon reaching the surface [need reference]. The mathematical definition of a cold-pool can differ from study to study. For this study, we will define a cold-pool explicitly as any grid cell at or near the surface that is more than 5K colder than the horizontal mean, or,

$$T - \bar{T} < -5. \qquad \text{(Eq. 5.2)}$$

With that definition in hand, we can evaluate the time evolution of the number of cold-pool grid cells throughout each simulation and determine how they differ from the cleanest case (Figure 5.18). We see in conjunction with the periods of enhanced DFX, periods of greater swaths of cold-pools. Similarly, for the C5000 case, which has been established to have dampened convective activity, the spatial extent of cold-pools is damped as well. For the moderately elevated CCN cases, there is a near-uniform increase in cold-pool extent from 82 hours and beyond. Hovering at around an additional 200 grid cells at 3km x 3km in the nested grid, the

moderately elevated CCN cases translate to a roughly 1800 square km increase at each time step.

Upon analyzing the cold-pool activity, we must also take the location of the cold-pools into account. Based on the mean meteorology of the WP, a TC will advect in a westward direction, which acts to advect itself over locations of elevated anthropogenic aerosols. In this sense, it differs from Atlantic TCs that interact with African dust from the SAL. In the case of the SAL, the dust is transported into the outer rainbands of a TC from the rear, while this and other WP TCs ingest aerosol, then drift over the location where aerosol was ingested. This results in a different dynamical response and gives rise to a different set of working hypotheses.

In that context, buoyancy is examined. As defined in Emmanuel (1994), buoyancy is given as

$$B = \frac{g(\theta_p - \overline{\theta_p})}{\overline{\theta_p}} \qquad \text{(Eq. 5.3)}$$

where g is the acceleration due to gravity and θ_p is the density potential temperature,

$$\theta_p = \theta(1 + 0.608q_v - q_{cl} - q_r) \qquad \text{(Eq. 5.4)}$$

and θ is the potential temperature and q_v, q_{cl}, and q_r are the mixing ratios for vapor, cloud condensate and rain, respectively.

As suggested in Tompkins (2001), buoyancy may act as a proxy for cold-pools. We compare the evolution of a buoyancy-pool (Figure 5.19) for the C400 and C3000 cases, along with the location of the TC center. Each frame is separated by two hours of model time. We note in both

cases how the storm center passes through the generated cold-pool, beginning at 76 hours. By this time, roughly 16 hours have passed since the storm initially came into contact with the elevated CCN field. At 74 hours, the shape of the cold pools differ in that the C400 shows a radial patch of negative buoyancy while the C3000 shows a more “squall-like” cold pool, curving around the center of the storm. At 76 hours, the storm has drifted over the cold pool. However, the mid-to-outer extent of the TC differs in buoyancy. In the C400 cases there are two patches of positive buoyancy, one just south of the TC center and the other about two degrees east of the TC center, both of which are non-existent in the C3000 case. By this time the enhanced CCN field has sufficiently wrapped around the storm (see Fig. 5.5), so the additional CCN has caused a much greater extent in negatively buoyant air throughout the TC’s storm outer band region. There is even a small second cold pool at this time in the C3000 case, not present in the cleaner case, east and slightly north of TC center. As at 74 hours, the C3000 cold-pool is non-uniform in shape and scope.

In fact, the non-uniformity of the cold pool can be observed when we examine the relative vorticity at an elevation 1300m (Figure 5.20). While in the C400 case we observe organized bands of generally positive relative vorticity, in the C3000 case we see tiny patches of negative vorticity. These patches are assumed to be caused by small eddies emanating from the negatively buoyant cold-pools occurring at the same time at the surface (Fig. 5.19). In theory, this could act to break up the storm, however, it is not evident when we compare the response to the overall maximum windspeed (Fig. 5.2).

In the other elevated CCN cases (C1000, C5000; Figure 5.21) we see a similar absence of positive buoyancy that we observed in the C400 case (Fig. 5.19c). We also see a similar lack of uniformity

in cold-pool shape. The C5000 case for instance shows an enclosed region of less negatively buoyant air just near the TC center (Fig. 5.21e).

The buoyancy parameter, which is a function of θ_e, effectively measures the tendency of air to be able to ascend or descend at a given point. The cold-pools have been shown to penetrate the inner core of the storm. If we examine the equivalent potential temperature directly, we can see the potential additional aerosol may have to disrupt the storm. Figure 5.22 shows the azimuthal average around the storm of θ_e at 84 hours into the simulations. In the clean, C400 case, we see a classic example of a warm-core TC with regions of high θ_e near storm-center. In the enhanced CCN cases we see a suppression of the convectively generated "hot towers" with lower θ_e air near the storm-center at or above 1500m. Moreover, the C1000 and C3000 show a tendency for low θ_e air to dip to near-BL levels and impinge into the middle of the TC. The C5000 case, with its damped convection, shows a much more horizontal gradient of θ_e indicating limited downdraft and convective fluxes.

Two hours later (Figure 5.23) we see the TC in one of its convectively active periods, as indicated by the prevalence of influx of low θ_e air. This time, the C1000 case shows a near complete suppression of the convective "hot towers" near the center of the storm. The downdrafts present are strongest near the TC center at this point in the C1000 case. The C3000 case shows the existence of another patch of low θ_e 170 km away from TC-center, potentially ready to advect into the center of the storm.

5.5: Response of Hydrometeors

The imposition of elevated aerosol concentrations has been theorized and simulated to affect the number concentration, size, and type of hydrometeors in the atmosphere. As discussed in Chapter 2, the RAMS model allows for eight classes of hydrometeors. For this section, we will focus on five: cloud droplets, rain droplets, pristine ice, snow, and aggregates. Hail and graupel were excluded from the hydrometeor plots for clarity. Examining the aerosol impact on hydrometeors will aid in the explanation of the varying convective activity throughout the life of the TC.

A cross section of the storm at 64 hours showing the different mixing ratios for the five hydrometeors in question, plotted in Figure 5.24, for the C400 and C3000 case is instructive as to the significant effect of additional CCN on convective fluxes and precipitation regimes. The C400 case at this time exhibits strong precipitation, as indicated by the elevated rain mixing ratio to the west of the storm reaching the surface while the C3000 shows reduced rain mixing ratio. There is however, the presence of an elevated pristine ice mixing ratio above 10000m. In this case, much of the condensate has remained in the atmosphere as a result of the additional CCN's ability to initially suppress rainfall. Figure 5.25 shows the same information 6 hours later. Here, we see the C3000 is now the storm with heaviest precipitation. Also at this time we note the heaviest precipitation is east of the storm. The cloud mixing ratio appears to be of similar concentration and vertical distribution while the snow and aggregates mixing ratios are more substantial in the cleaner case. At both times, the C400 case has a more uniform distribution of all five hydrometeor types suggesting a more balanced distribution of hydrometeor species, more akin to the control simulation. Meanwhile the more polluted cases appear to favor the

production of pristine ice while suppressing snow. The additional pristine ice provided by the additional CCN can then be advected away from the storm at high elevation, failing to precipitate back to the surface. This is evident when examining the extreme case of high CCN (the C5000 case; Figure 5.26). Here we see even the C3000 case precipitating substantially and transitioning from ice to snow at about 10000m, then finally as cloud and rain mixing ratios below 5000m. For the C5000 case, now at 68 hours into the simulation, all these five hydrometeor species are present, but in differing mixing ratio concentration. Here, the vertical distribution of ice in the C5000 case stretches well past 15000m while the C3000 case appears capped. The mixing ratio of aggregates is substantially higher in the C5000 case. Presumably the size of the cloud droplets in the less polluted case are larger and are less subject to updrafts as well as being easier to fall out by precipitation, sedimentation, or scavenging. Much of the moisture is in the form of aggregates at this time in the C5000 case.

This size difference of hydrometeors under different CCN concentrations is evidence of indirect effects of aerosol ingestion into clouds. As the atmosphere ingests more and more CCN similar amounts of condensed water will result in smaller nucleated droplets. As these droplets are caught in updrafts, the smaller particles will be thrust further up in the atmosphere until they are carried away by the inevitable divergence of the wind, presuming the particles are small enough and the updrafts are vigorous enough.

As we look at the time evolution of droplet number for all four sensitivity tests we can readily see the indirect effects of increased aerosol concentration on number concentration of the five hydrometeor species. At 62 hours (Figure 5.27) the outer rainbands have just come into contact

with the elevated CCN field. Immediately, we see a near monotonic decrease in snow (a moderately rimed ice species in RAMS) and an increase in the number concentration pristine ice, particularly in the two more extreme pollution regimes. At this time, the C1000 and C3000 cases are the more highly precipitating regimes. Twelve hours later (Figure 5.28), the C3000 case shows evidence of the pristine ice being carried away in the upper atmosphere, above 10000m due to the diverging winds. This is also one of the more convectively active periods of the storm and the C3000 exhibits high precipitation near the storm center while the other three cases show increased rain concentration about 100 km away from the TC center. Again, we see the suppression of snow distribution with increasing concentration of CCN. Six hours later, now at 80 hours into the simulation, and about 20 hours after the storm has come in contact with the elevated aerosol levels, the C1000 and C3000 cases are very connectively active (Figure 5.29). Interestingly in the C3000 case there are multiple columns of high rain number concentration and an increased drizzle regime about 500 km away from storm center. The number concentration of pristine ice stretches well above the freezing level at this point in the more polluted cases, capping out well past 15000 meters above the surface. As at previous time steps, the C5000 case appears to be vertically advecting condensate in the form of pristine ice aloft. As this ice is lofted and advected away, it loses the ability to be re-entrained in the storm, removing it as a potential source of energy to help maintain or intensify the storm. We see a similar dynamic occurring 6 hours after that (Figure 5.30): the highly polluted C3000 case is producing significant precipitation while the extremely polluted case is producing almost none. This phenomenon suggests a point of maximum aerosol impact as far as convection goes. After a certain CCN threshold, the additional CCN does not invigorate convective activity, but rather condensate transport in the anvils is enhanced by reducing the riming of ice particles aloft. In theory, both of these phenomena could act to weaken a TC. Invigorated convection in the outer

rainbands could potentially lead to enhanced cold-pool activity, cutting off the energetics of the system with low θ_e air, or water substance could be removed directly by the vertical advection away of tiny pristine ice crystals. Recall Figures 5.7 and 5.8, showing the removal of water substance in the mid-troposphere in the C5000, and in particular the mass condensate contained within the updrafts (Figure 5.8).

The hypothesis relating extreme concentrations of CCN and droplet size are confirmed in Figure 5.31. In the most highly polluted case the mean cloud droplet diameter is smaller throughout the simulation. Being smaller, these droplets are less likely to fall out and will also have a lower sub-zero freezing temperature. The remaining three CCN sensitivity tests' time-distance evolution of mean cloud droplet size mimics the aforementioned convective pattern of invigoration and subsidence. It is worth noting that the cleanest case shows the most "medium-sized" drops (between 9 and 18 microns in diameter) whereas the C1000 and C3000 cases have more extreme mean droplet diameters, both large and small. For rain droplet size the sensitivity tests show an increase in diameter during convective periods for increasing CCN, excepting C5000 (Figure 5.32). With more vigorous convective updrafts, a droplet is able to grow larger due to its longer residency within the cloud mass, despite the initially smaller size as a cloud droplet. This also suggests more available moisture aloft, confirmed by the relatively high presence of aggregates in the cross section diagrams (e.g. Fig. 5.29) for the C3000 simulation. The effect of rain drop size on cold-pool area via evaporative cooling may also be extrapolated. At 74 hours, the rain drop size of the C3000 is much higher than in the other simulations (Fig 5.32), however, the cold-pool area two hours later is smaller than that of the C400 and C1000 simulations (Fig. 5.19). This suggests another added layer of complexity to the system in which a

larger droplet size regime may result in less evaporative cooling at the surface, hindering cold-pool development. Still, while the feedback is negative, it's counterbalanced by an increase in convection overall.

As discussed previously, the C3000 cold-pool shape is more "squall-like" (Figure 5.14). The presence of these squalls could work to produce further convection as suggested by Simpson (1980). This appears to be what is happening in Figure 5.25. The precipitation has generated a cold-pool which is in turn generating other regions of convection. This is also hinted at in the diagram of relative vorticity (Figure 5.15) showing tiny anti-cyclonic patches. It is worth noting that at this time (86 hours) the gross maximum windspeeds of all the simulations are not dissimilar (Figure 5.1). In fact, the C3000 case contains the strongest maximum windspeed, presumably due to the convective activity. However, these cold-pool results are instructive and point to the ability of additional CCN to modulate cold-pools (Carrio and Cotton 2010).In a stronger TC, it is possible the windspeeds will not be increased by the convective activity itself, but could be subject to additional convective fluxes and low θ_e air.

5.6: Chapter 5 Figures

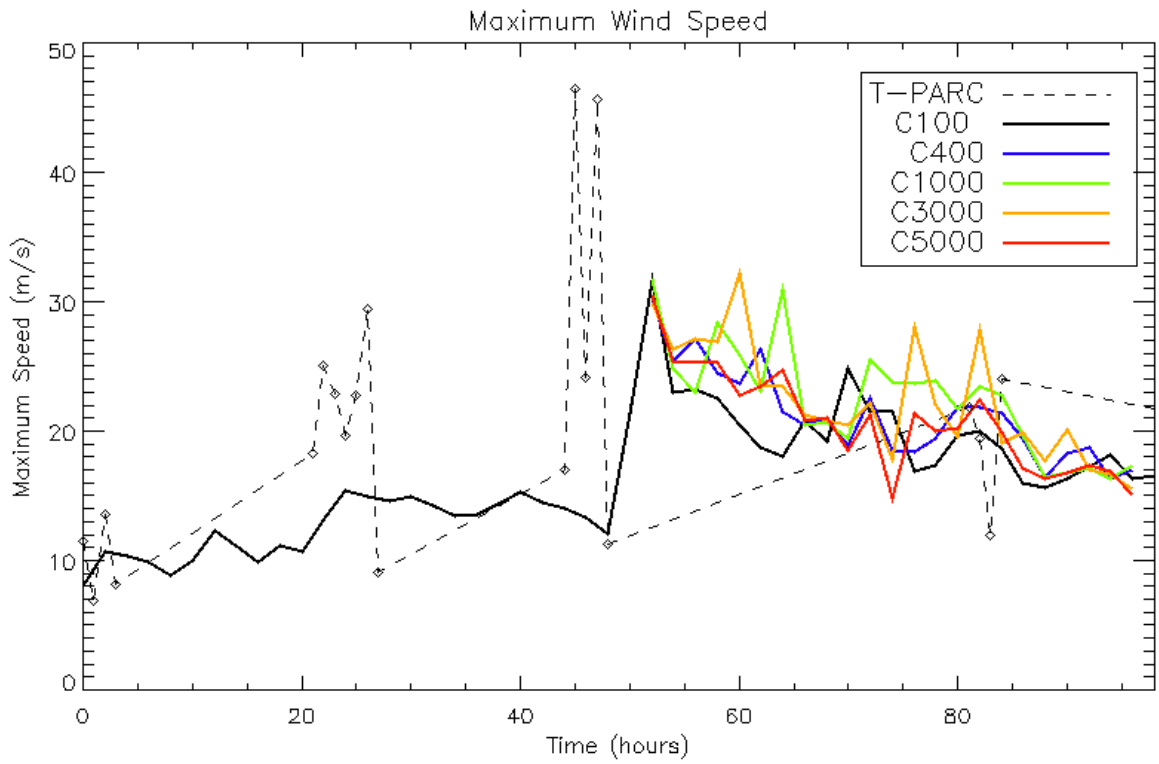

Figure 5.1: The maximum sustained near surface windspeed for the control simulation and each of the sensitivity tests and the recorded maximum near surface windspeed from the T-PARC dropsondes.

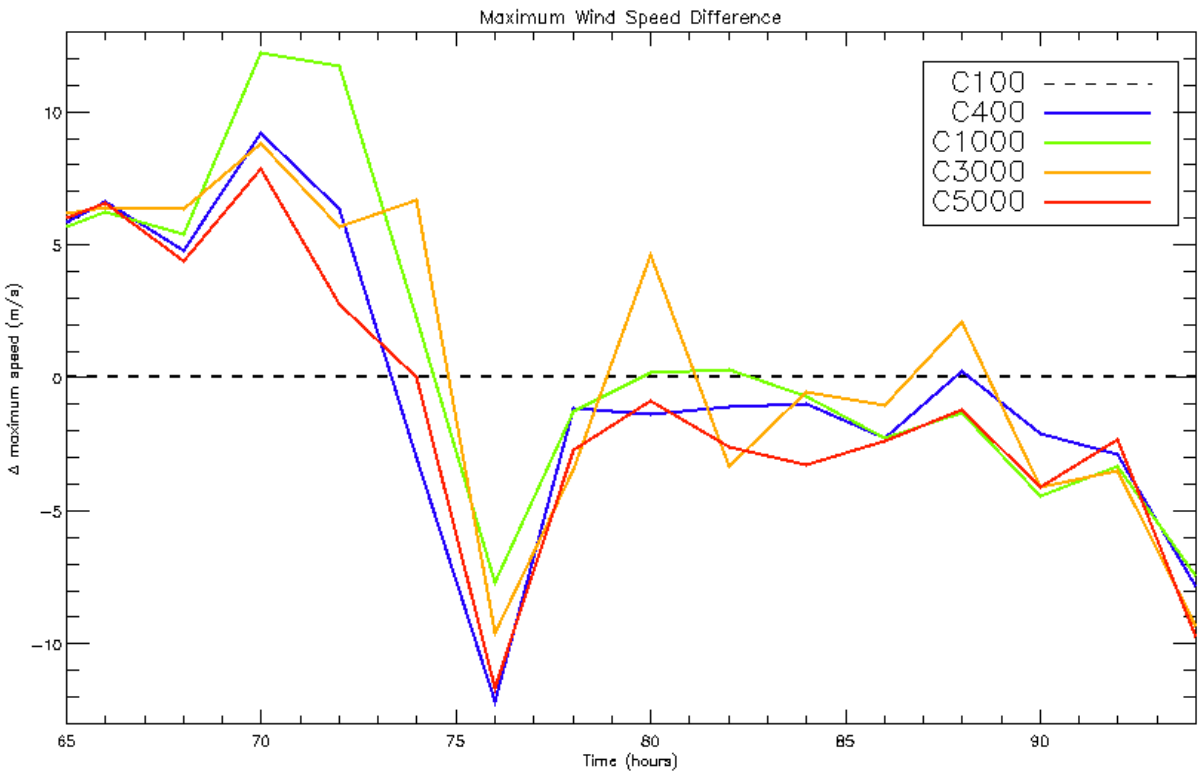

Figure 5.2: Difference of near surface maximum windspeeds from the C100 case for each sensitivity tests.

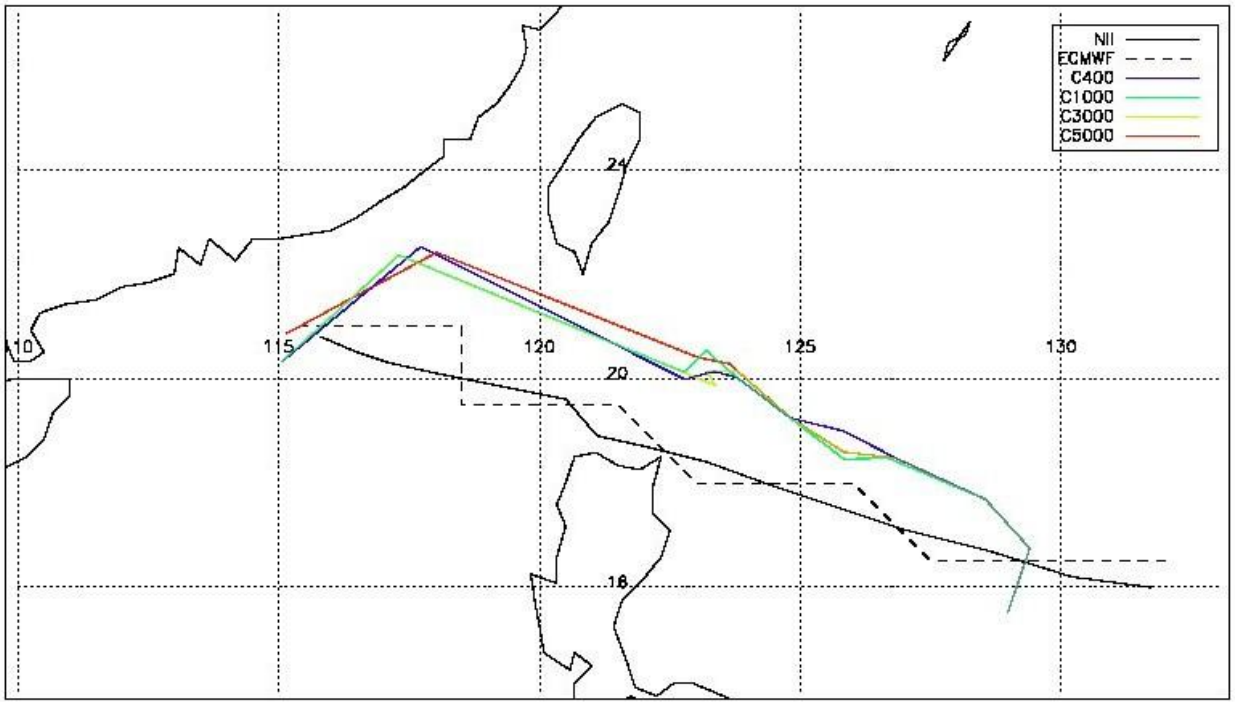

Figure 5.3: The track of TC from each sensitivity test as determined by perturbation pressure and NII best track and ECMWF Reanalysis Data as given by geopotential height.

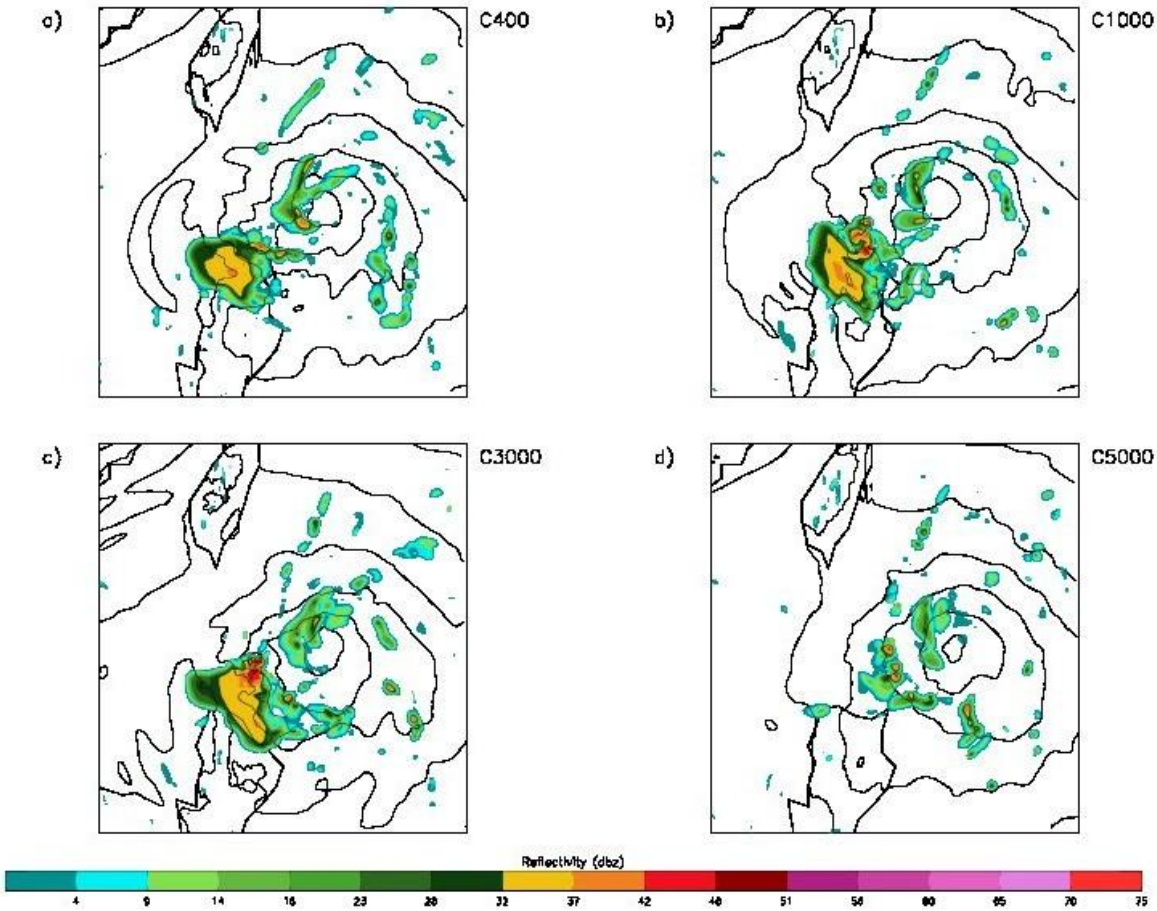

Figure 5.4: The surface modeled reflectivity (dbz) at t=74 hrs with perturbation pressure contours of 1 mb for each sensitivity test.

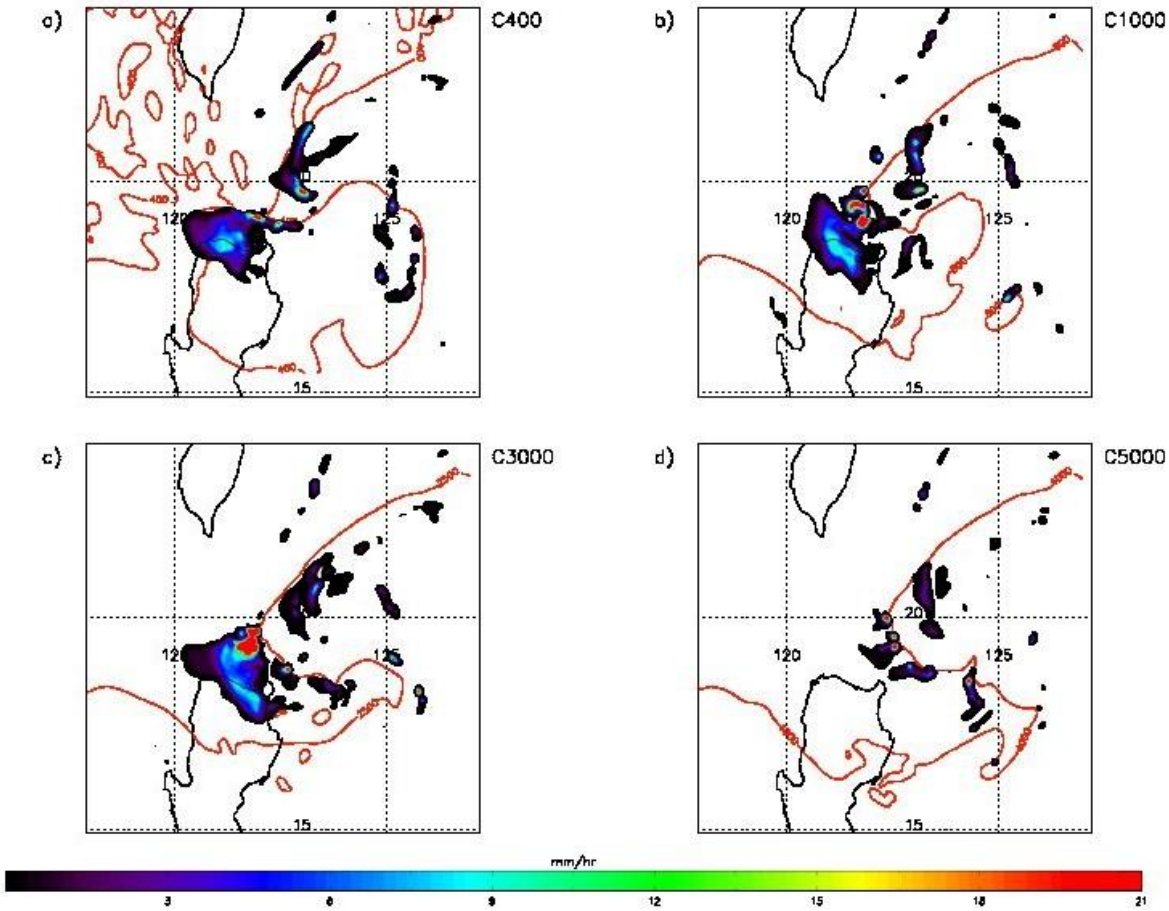

Figure 5.5: Rain rate (mm/hr) at t=74 hrs for each sensitivity test. Selected contours of CCN concentration are shown to demonstrate the entrainment of the CCN into the storm.

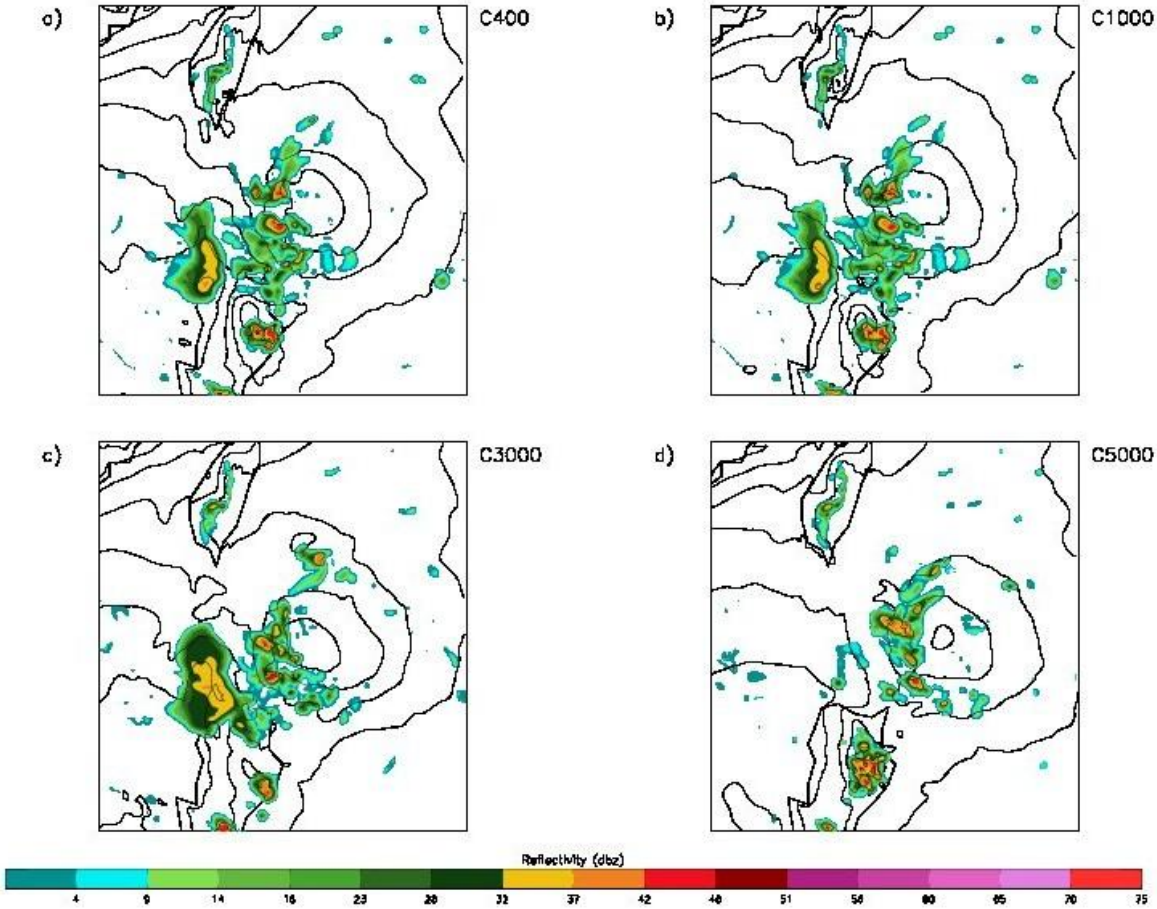

Figure 5.6: As Figure 5.4, but at t=80 hrs.

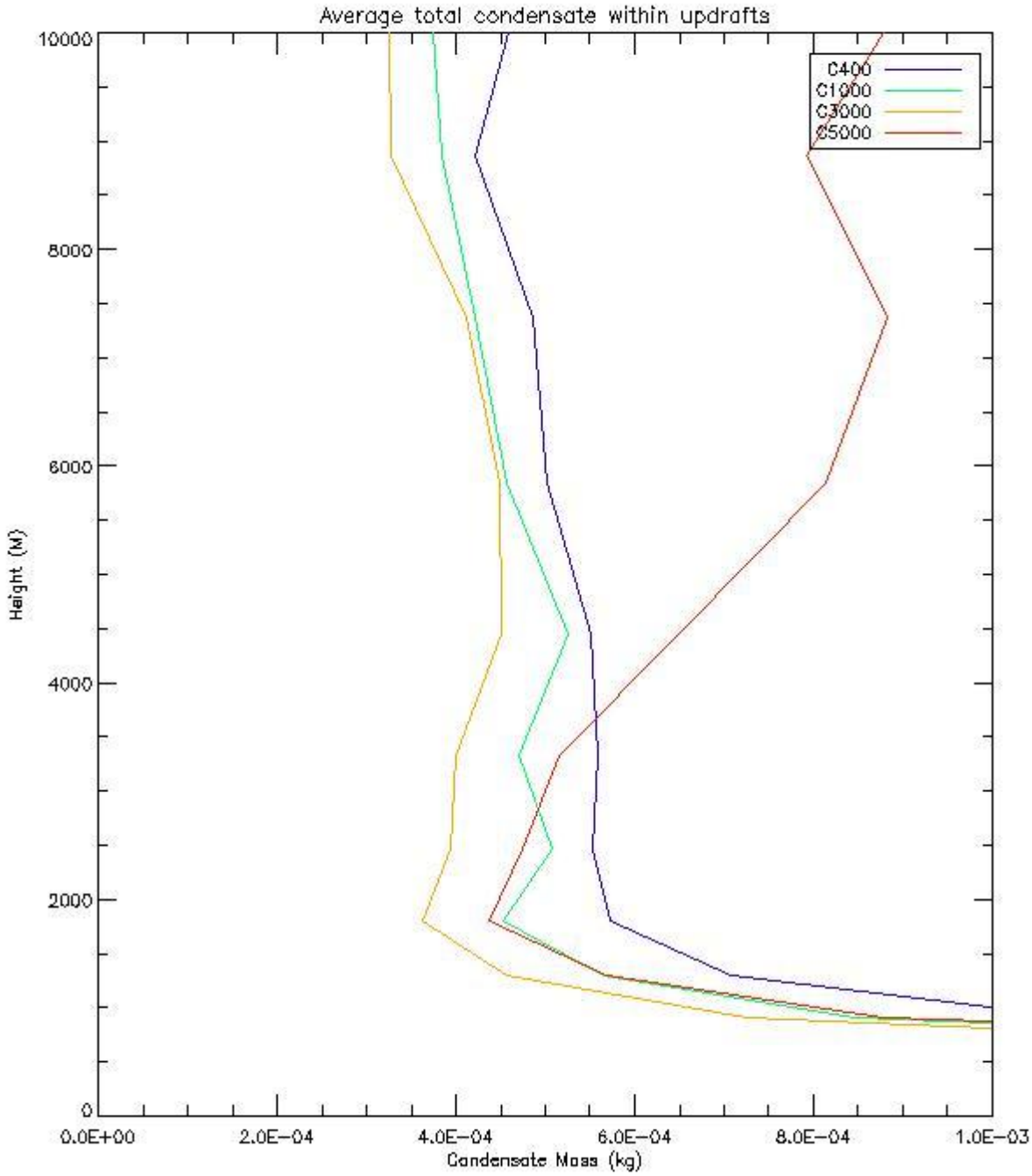

Figure 5.7: Average total condensate mass within updrafts of 1.0 m/s or greater from 60 to 96 hours according to height for each sensitivity test.

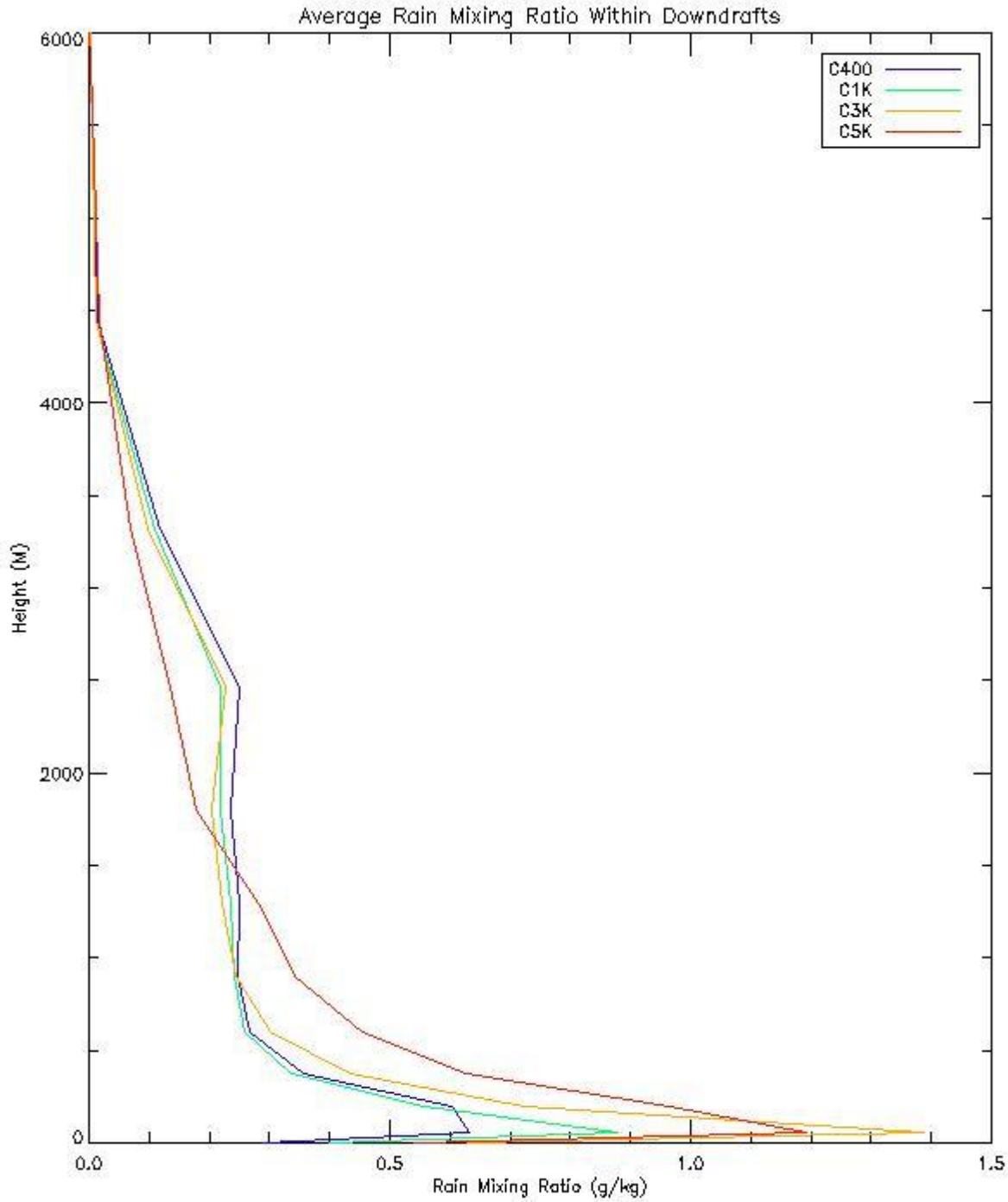

Figure 5.8: Average rain mixing ratio within downdrafts greater than -0.25 m/s from 60 to 96 hours according to height for each sensitivity test.

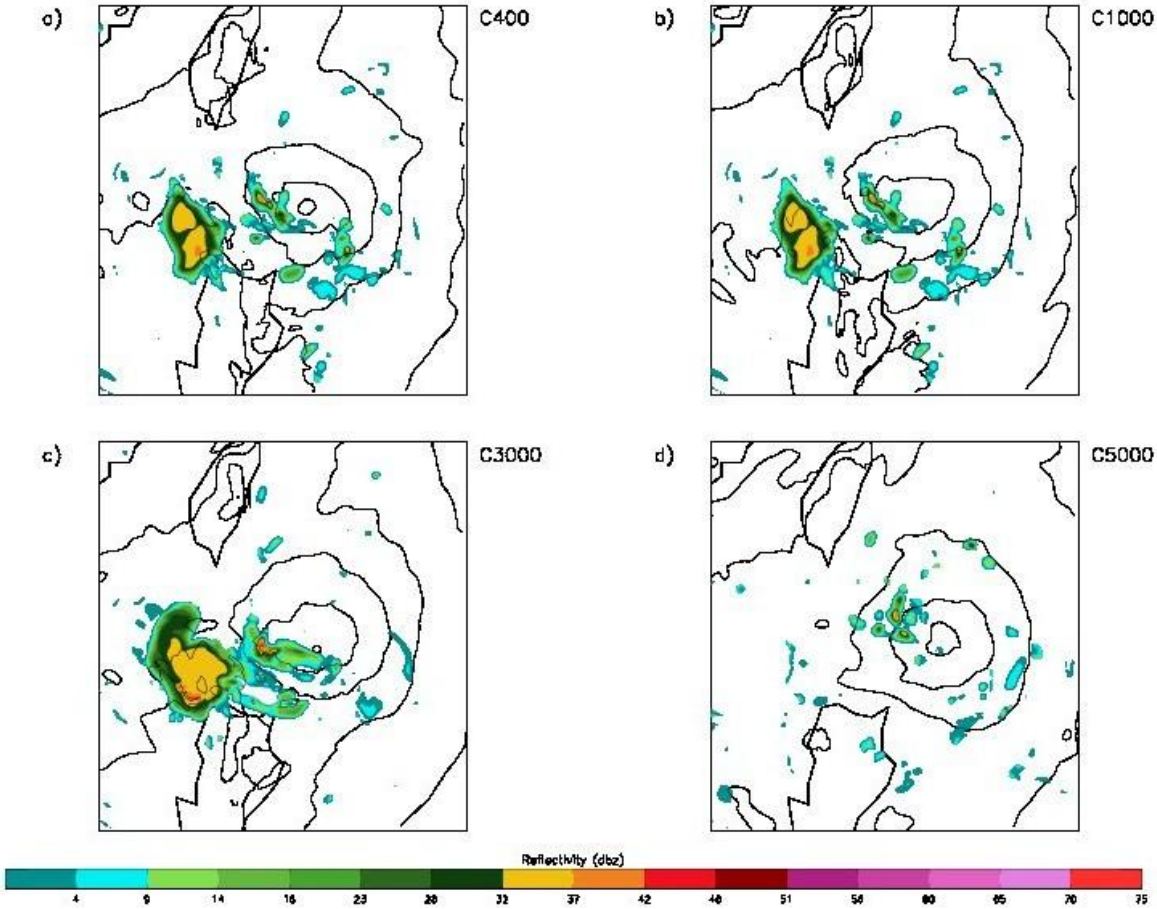

Figure 5.9: As Figure 5.4, but at t=86 hrs.

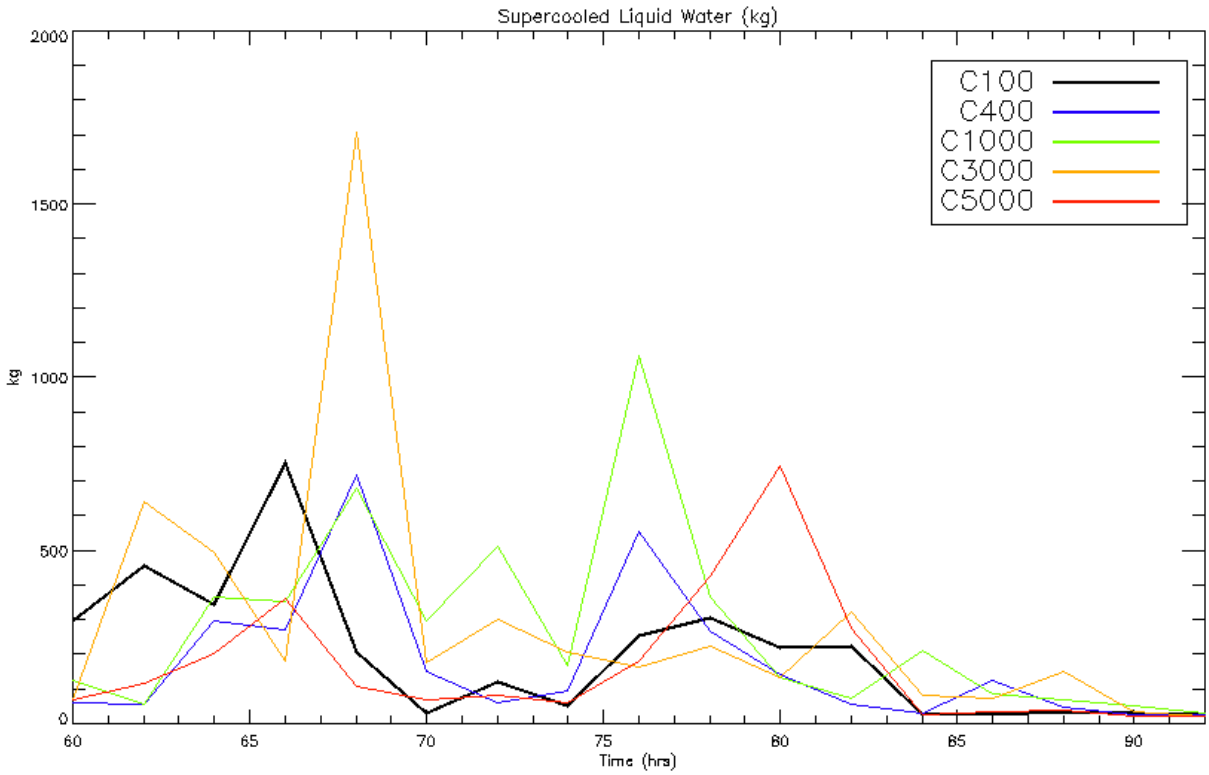

Figure 5.10: The total amount of SCLW (kg) within the TC domain by time for each simulation.

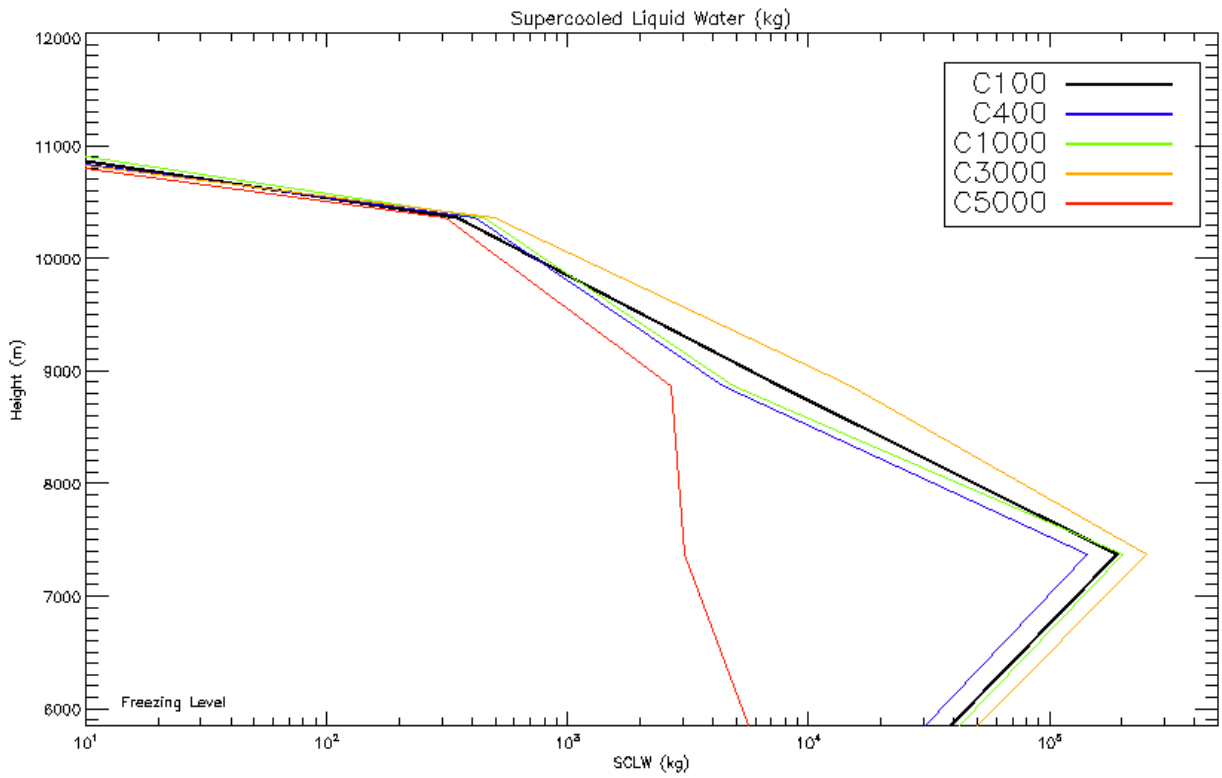

Figure 5.11: Grid cell average of SCLW mass (kg) by height over the course of each simulation.

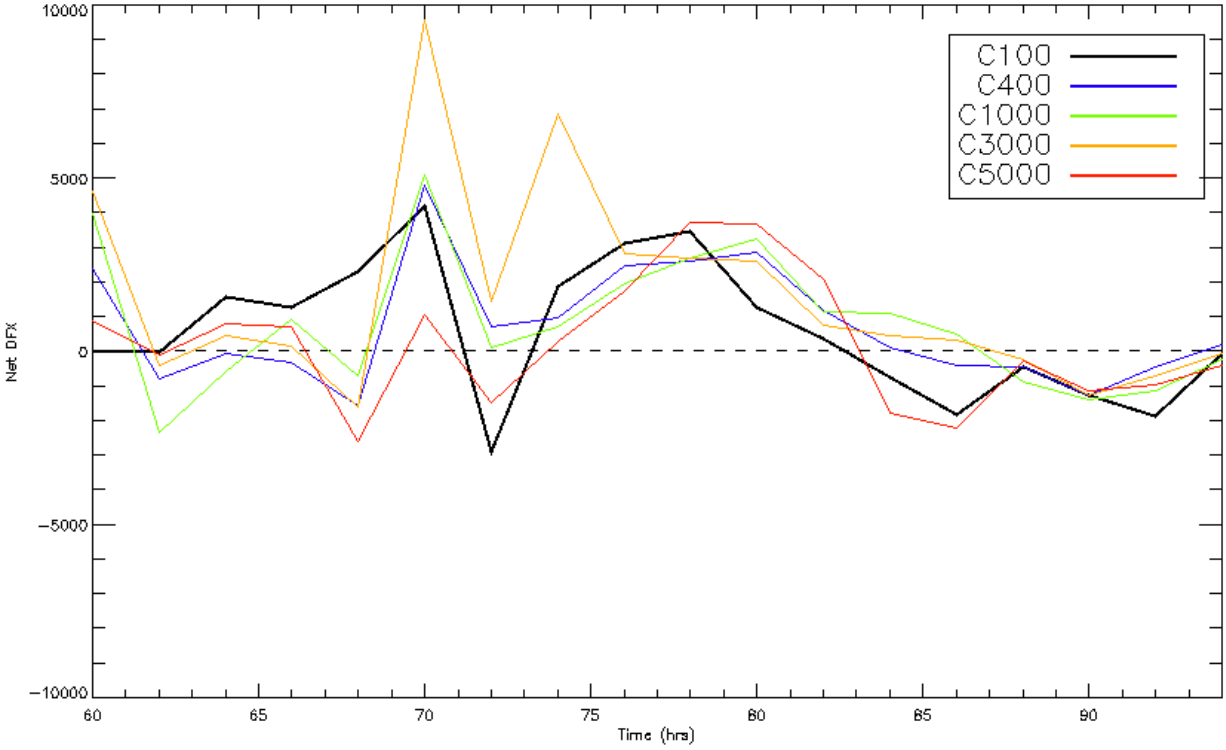

Figure 5.12: Net DFX over the inner grid domain at 200m height at over the course of each simulation for control simulation and all sensitivity tests.

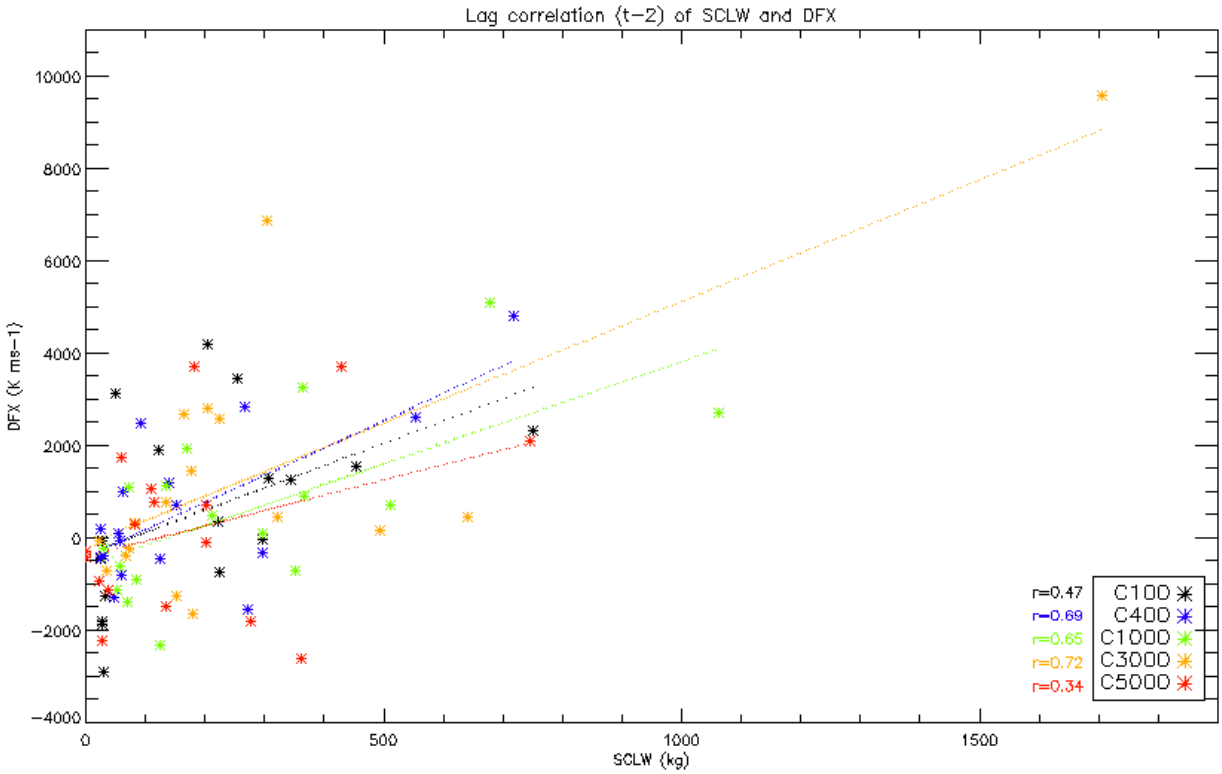

Figure 5.13: Scatterplot of SCLW and DFX (lagged two hours) for all simulations. Linear correlation coefficients (r) for each simulation are shown. The composite r value is 0.57.

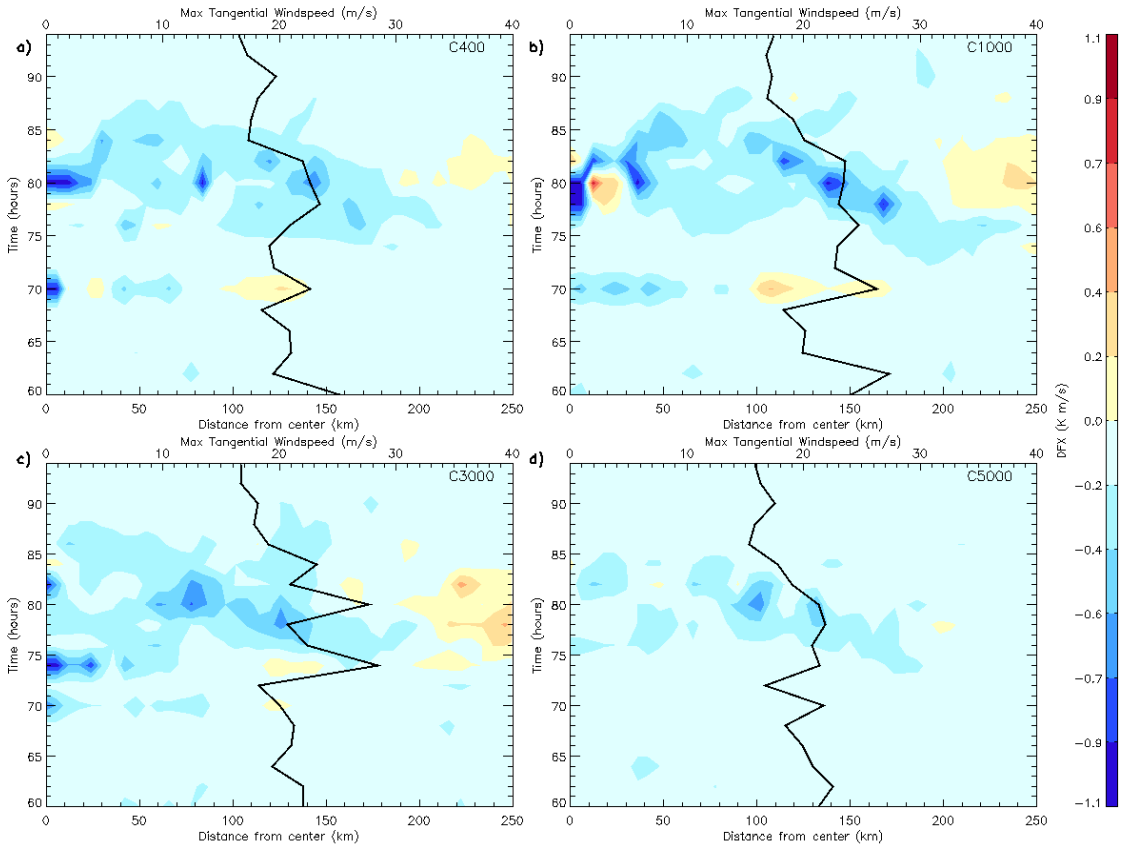

Figure 5.14: Azimuthal average of DFX by time for each sensitivity test plotted along with the maximum tangential windspeed.

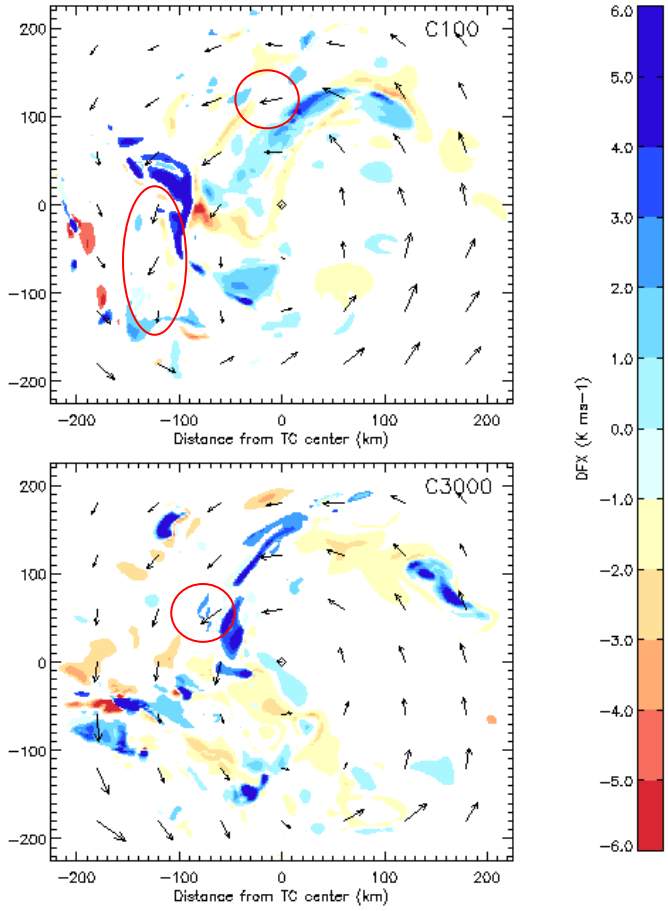

Figure 5.15: DFX and wind vectors at t=76 hours for C100 (top) and C3000 (bottom) simulations. Circles indicated wind vectors that have been affected by propagating cold-pools.

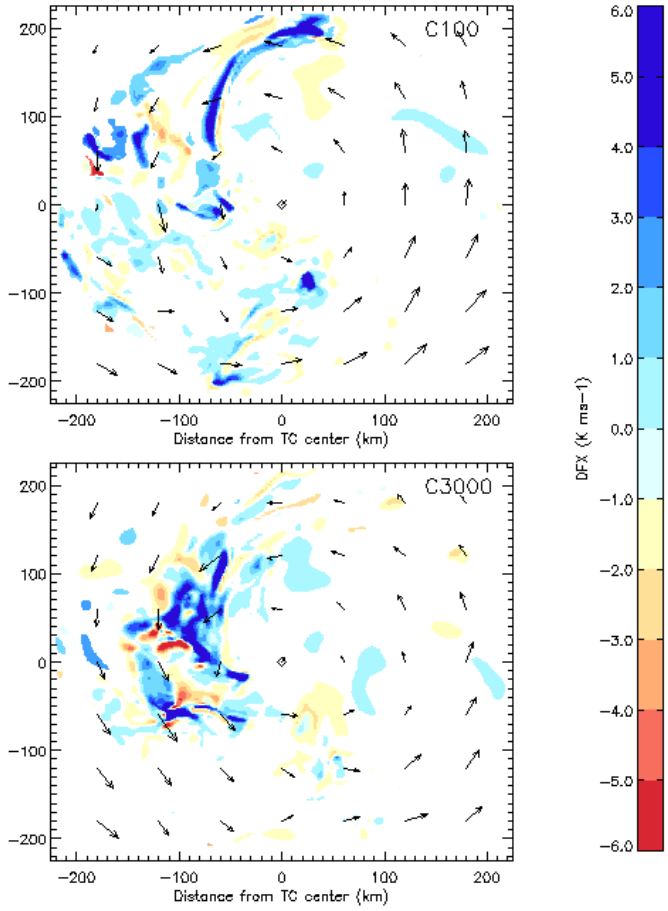

Figure 5.16: As Figure 5.15 but for t=80 hours.

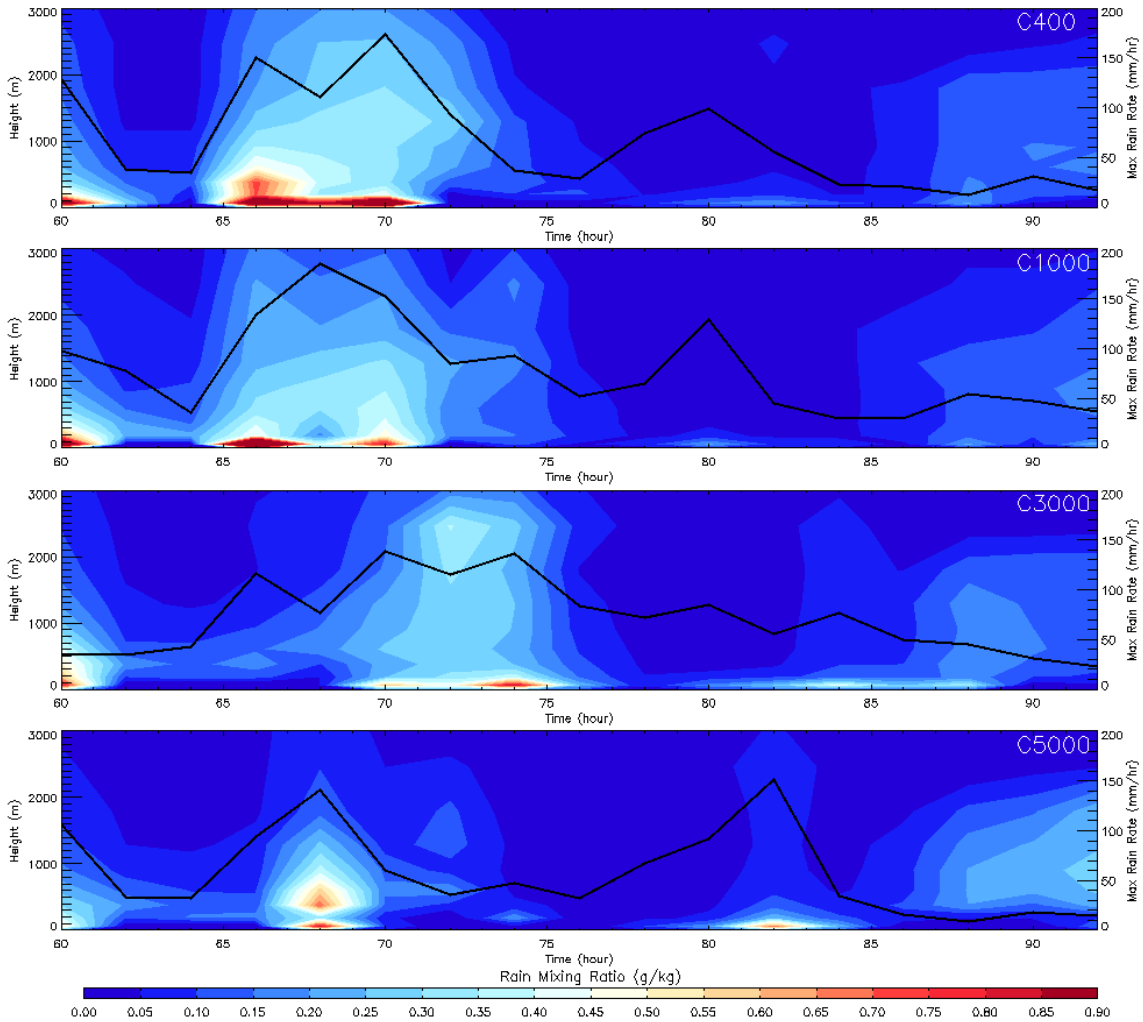

Figure 5.17: Average rain mixing ratio (g/kg) within downdrafts by time according to height. Maximum rain rate is plotted according to simulation time.

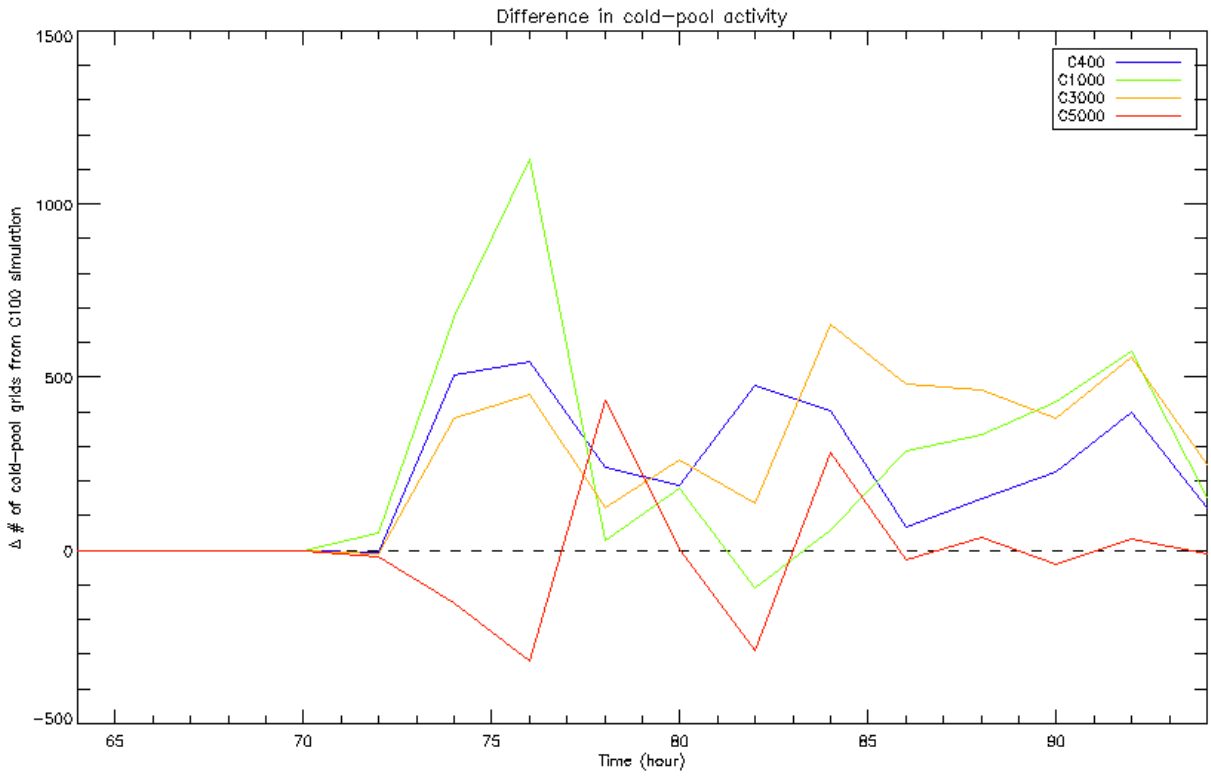

Figure 5.18: Change in the number of cold-pool grid cells (see text for definition) for nested grid from C100 simulation over time.

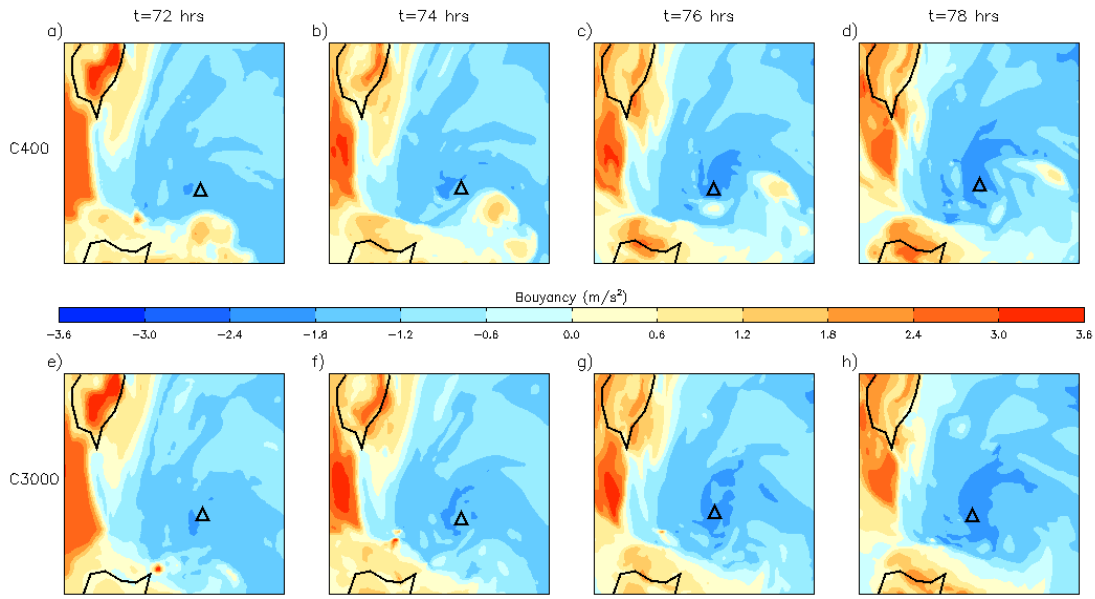

Figure 5.19: Buoyancy (m/s^2) at 200m elevation plotted in time intervals of 2 hours beginning at t=72 hrs for C400 case (a through d) and C3000 case (e through h).

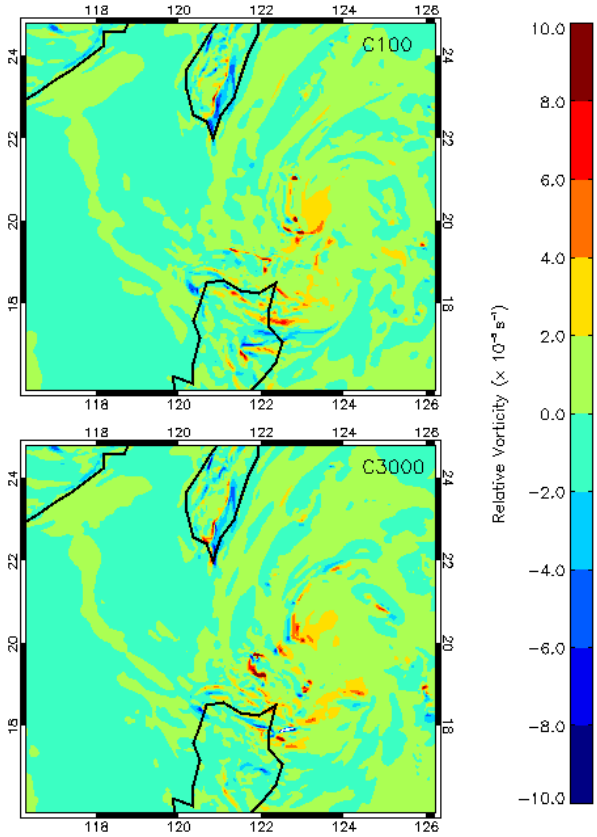

Figure 5.20: Relative vorticity at t=76 hrs and height 1300m for C400 and C3000 cases.

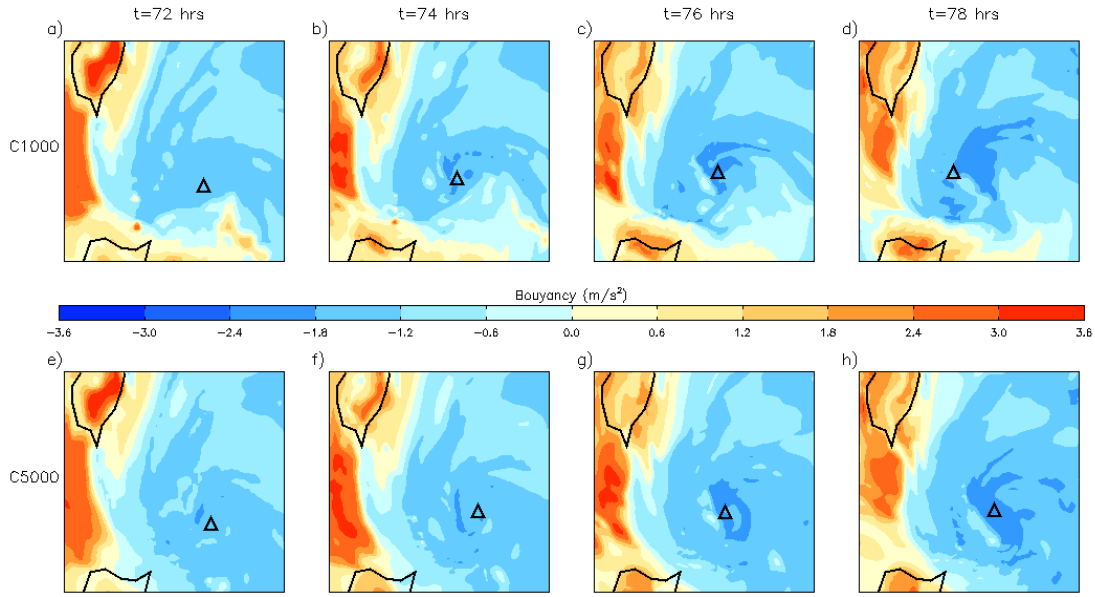

Figure 5.21: As Figure 5.14, but for C1000 (a through d) and C5000 (e through h) cases.

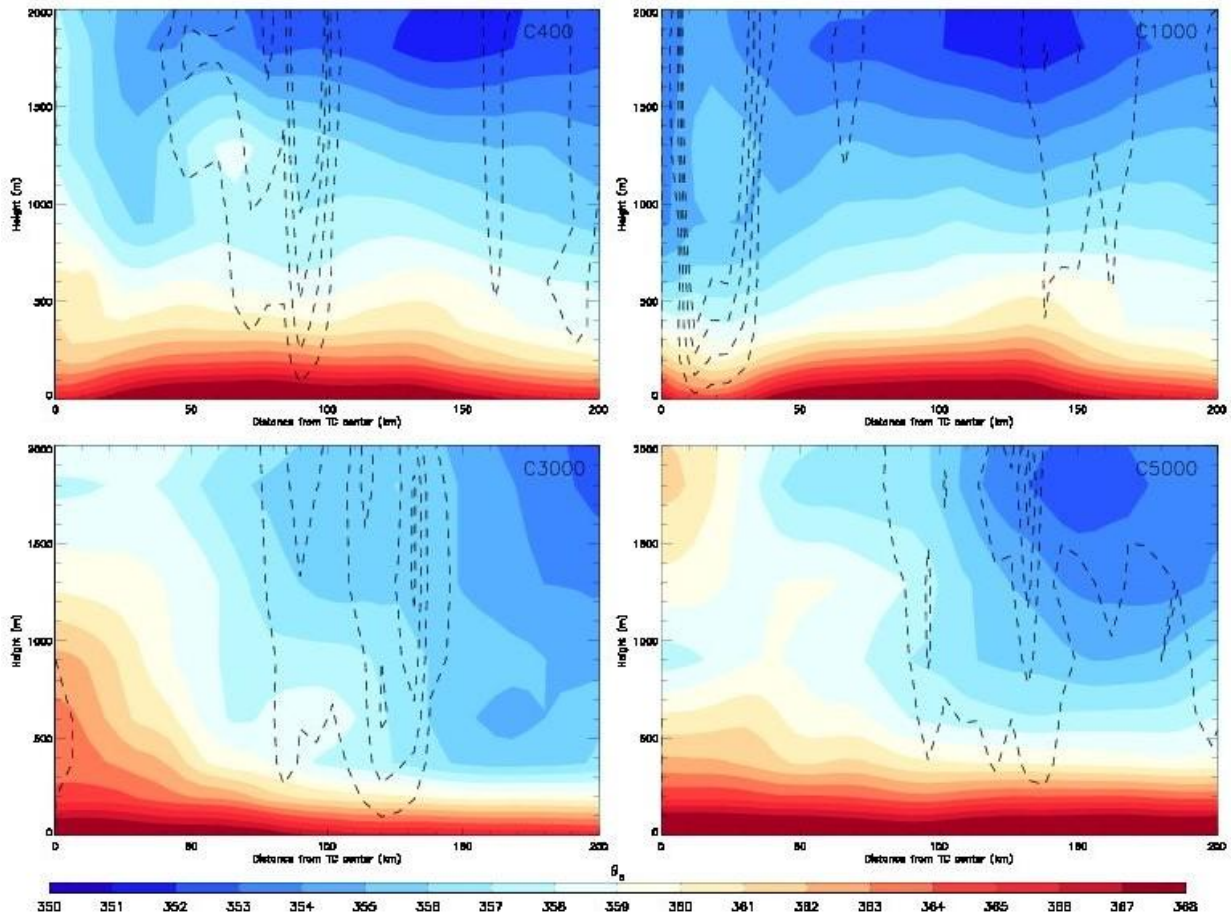

Figure 5.22: Azimuthal average of θ_e according to height at t=80 hrs. Azimuthal average of downdraft contours of -0.5 m/s are also plotted (dashed lines).

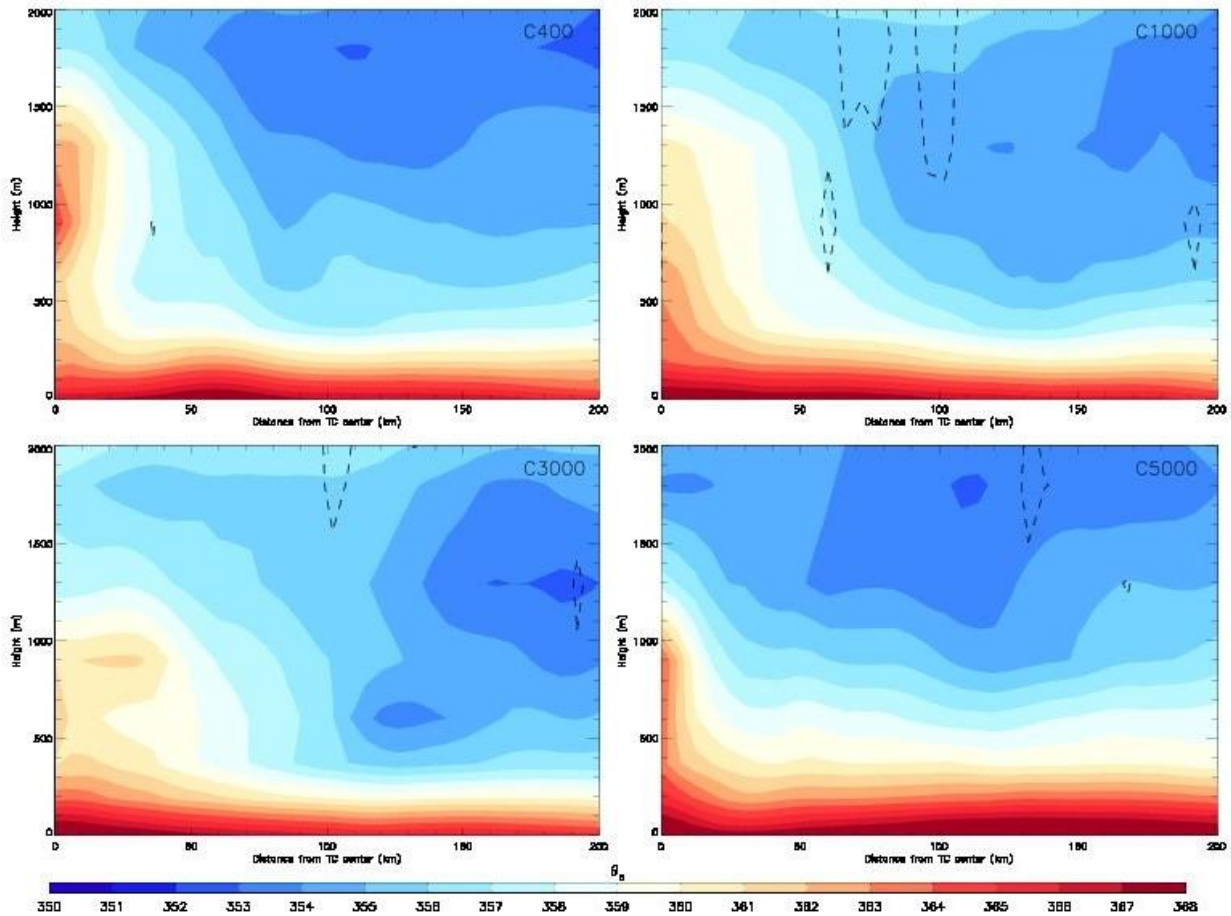

Figure 5.23: As Figure 5.17, but for t=84 hrs.

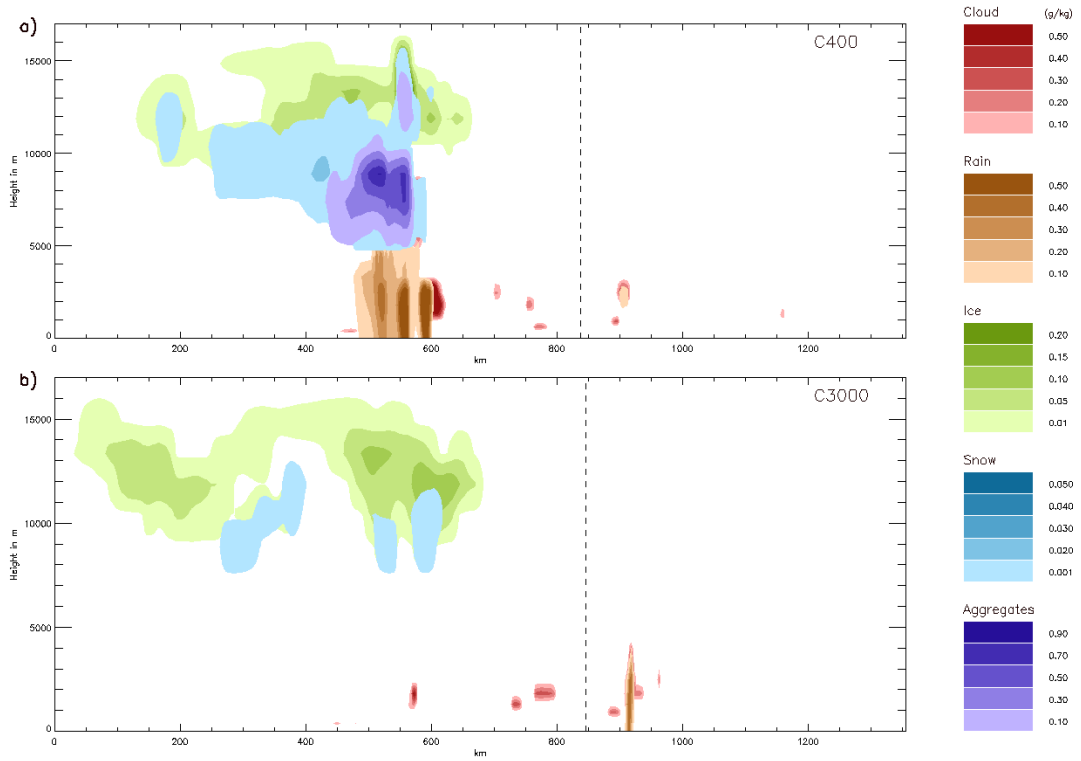

Figure 5.24: Cross section of storm at t=64 hrs showing mixing ratios for five selected hydrometeor species for C400 (a) and C3000 cases (b). Center of the TC according to minimum sea level pressure is also plotted (dashed line).

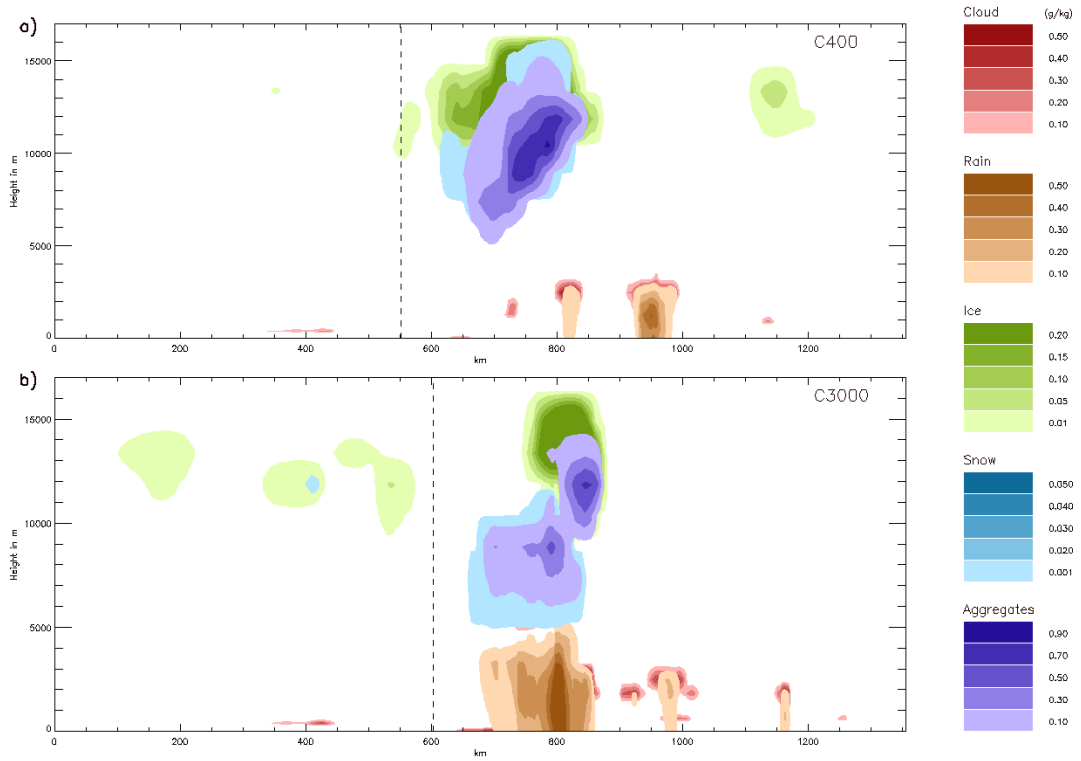

Figure 5.25: As Figure 5.19, but for t=70 hrs.

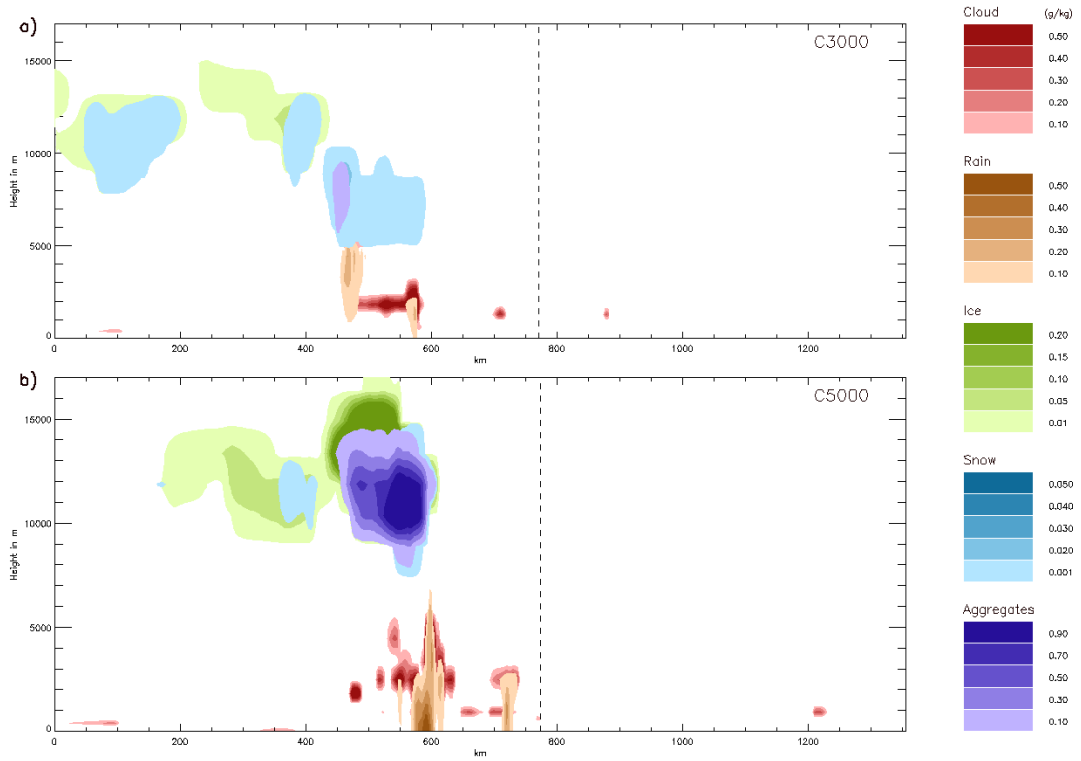

Figure 5.26: As Figure 5.19, but for C3000 (a) and C5000 (b) cases and t=68 hrs.

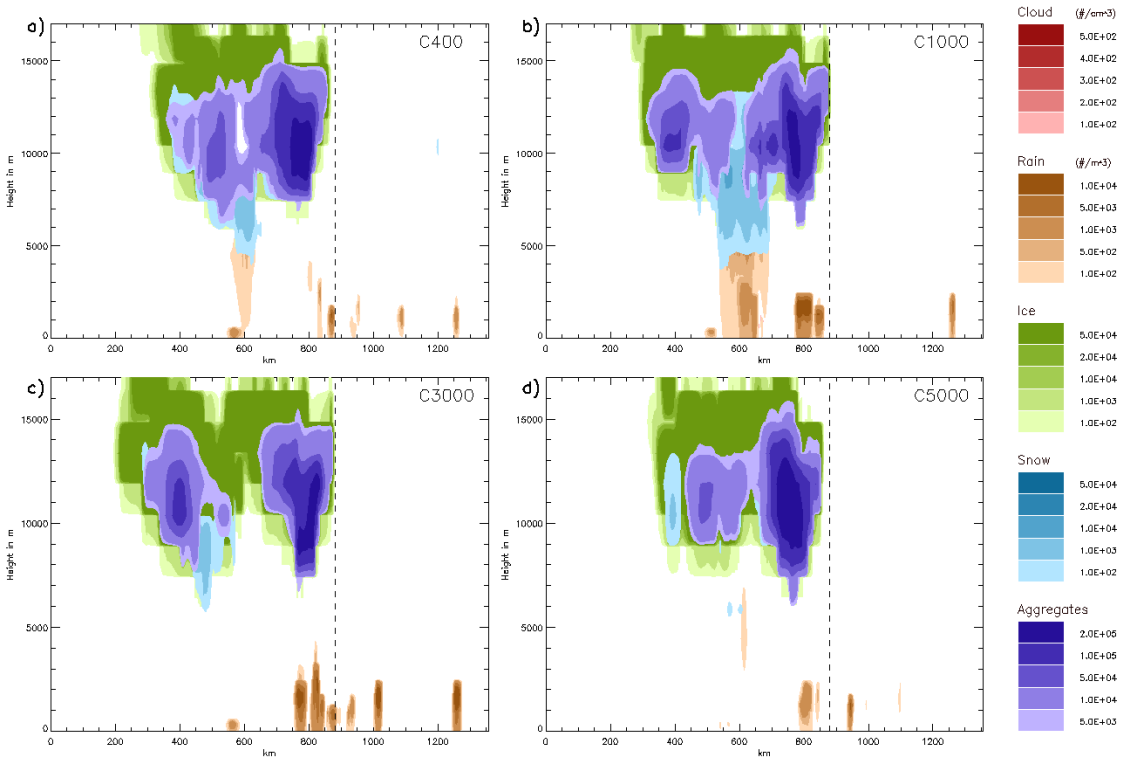

Figure 5.27: As Figure 5.19, but for number concentration of five selected hydrometeor species, all sensitivity tests (a: C400; b: C1000; c: C3000; d: C5000), at t=62 hrs. Cloud droplet concentration is in units of cm^{-3}; all others are in units of m^{-3}.

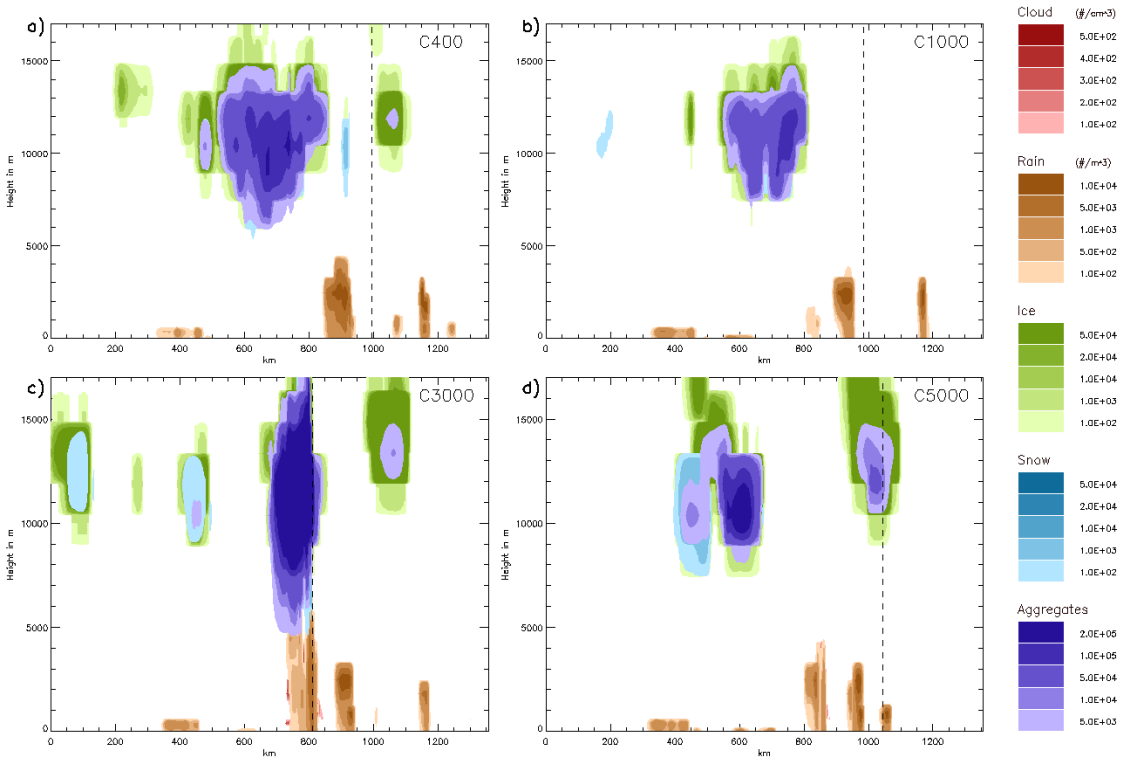

Figure 5.28: As Figure 5.22, but for t=74 hrs.

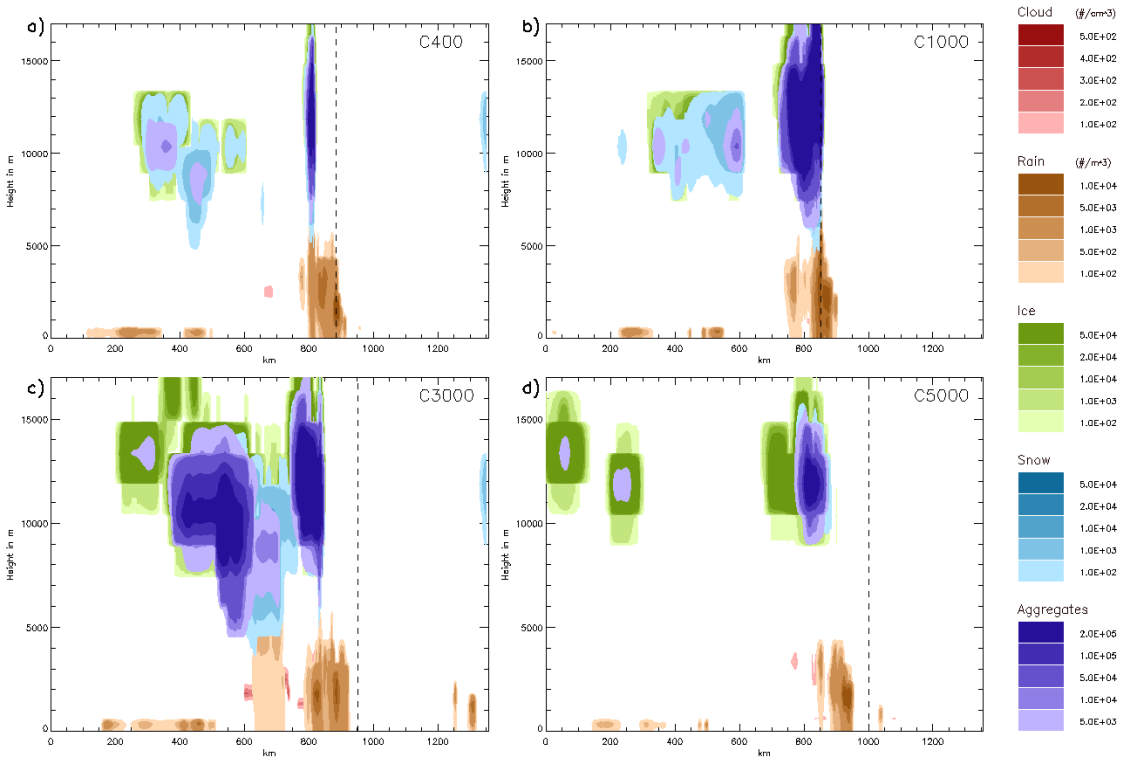

Figure 5.29: As Figure 5.22, but for t=80 hrs.

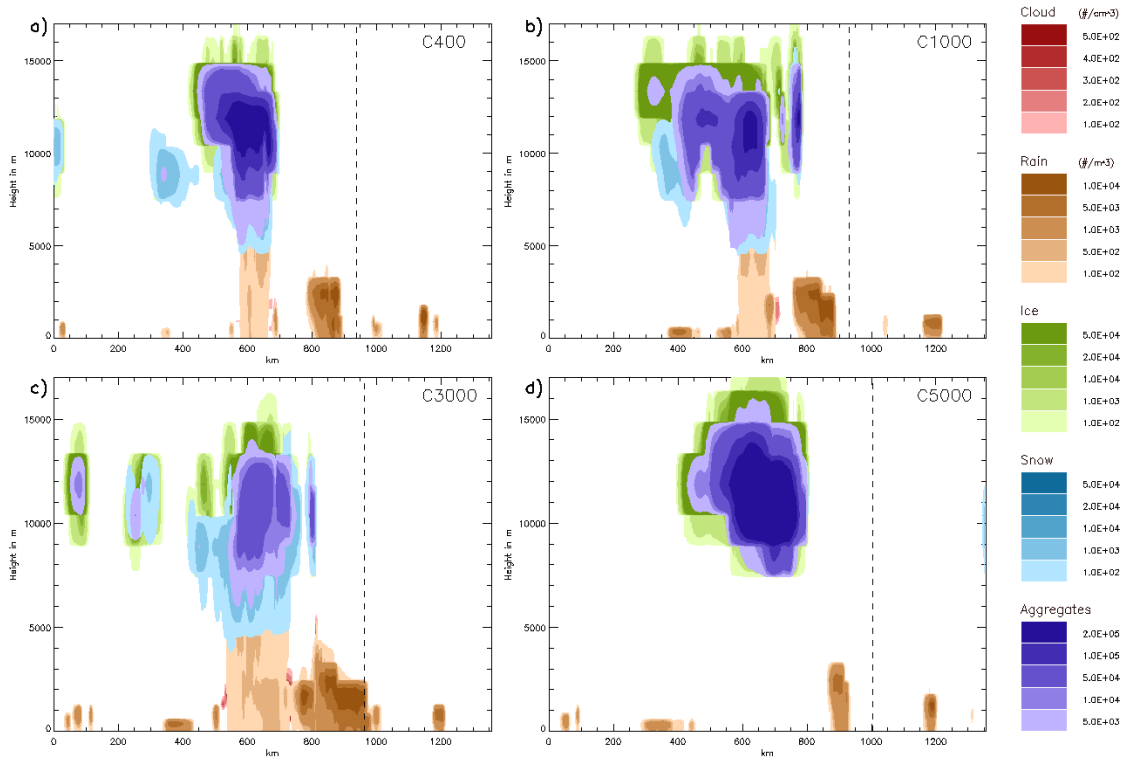

Figure 5.30: As Figure 5.22, but for t=86 hrs.

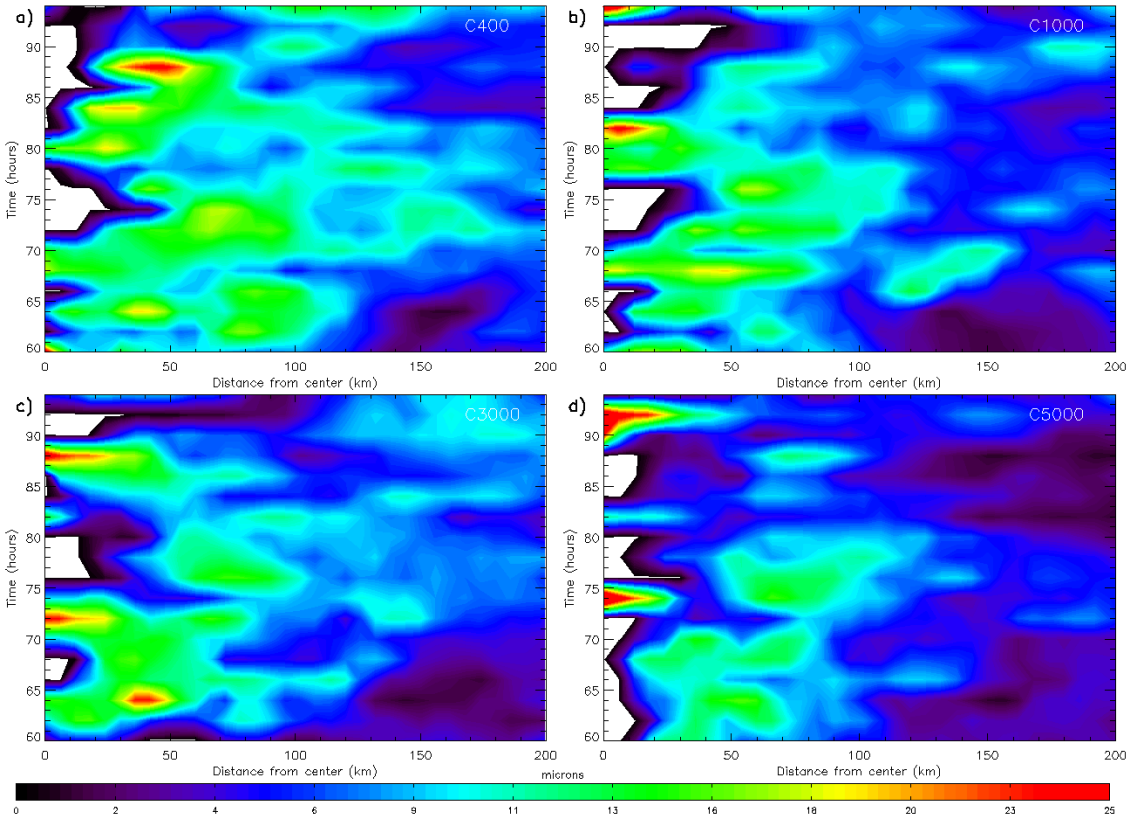

Figure 5.31: Azimuthally averaged cloud droplet diameter (microns) according to distance from TC center by time for all sensitivity tests (a: C400; b: C1000; c: C3000; d: C5000).

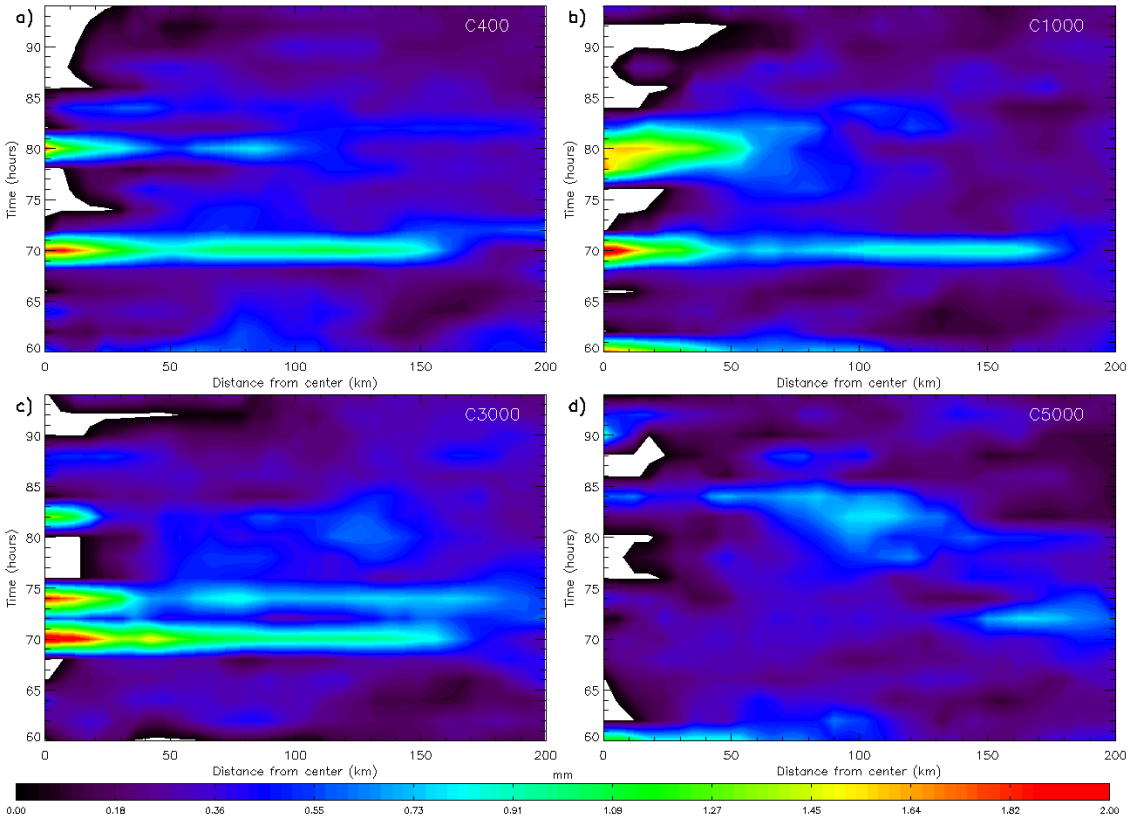

Figure 5.32: As Fig. 5.31, but for rain droplet diameter (mm).

CHAPTER 6 – CONCLUSIONS

6.1: Summary of Study

The RAMS regional model with two-moment bin emulating microphysics was used to simulate a 2008 typhoon entering fields of elevated CCN concentrations. The model was initialized with both gridded reanalysis data and irregularly spaced and timed dropsonde data obtained from the T-PARC campaign. The CCN domain and vertical profile were derived from both MODIS satellite retrievals and SPRINTARS aerosol model output. The simulations utilized a manually-moved nested grid in order to best represent the microphysical activity beginning in the northwest rainbands where the elevated CCN first became ingested into the storm. The simulations ran for 96 hours with internal nudging switched off after 36 hours, allowing the storm to develop from the model equations only. In all, five simulations differing only by CCN concentration were run: a control run of 100 CCN per cubic centimeter applied homogeneously over the model domainand four sensitivity tests of elevated CCN fields with concentrations of 400, 1000, 3000, and 5000 per cubic centimeter. The TC began to enter the elevated CCN fields and ingest the CCN at the 56 hour mark.

6.2: TC Speed and Track

The maximum windspeeds and track of the simulated TC are consistent with the ECMWF reanalysis and T-PARC dropsonde data after the internal nudging was switched off. After an initial amplification of windspeed, the invigorated convection and other dynamical aspects potentially resulting from the elevated CCN reduced the windspeed after the 74 hour mark (Fig. 5.2), with only brief periods of amplified windspeed. The most polluted case (C5000) showed the most consistent damping of windspeed compared to the control simulation and all other sensitivity tests. However, it is difficult to immediately assign additional CCN as a TC intensity damping agent, without first considering its more direct links to changes in other parameters.

6.3: Droplet size, SCLW, and Convective Fluxes

The ingestion of increased CCN concentrations resulted in a smaller cloud droplet size (Fig 5.31), particularly in the mid to outer rainbands of the TC (50 km to 100 km from TC center). Smaller liquid droplets result in three immediate effects:

1. **An initial reduction in precipitation.** The cloud droplets are less likely to be coalesced or scavenged in precipitating regimes. However, this does not imply an overall reduction in precipitation. Due to other effects of the smaller droplet sizes, the convectively produced precipitation can possibly be increased later in the storm, similar to the results in Seifert and Beheng (2006).
2. **The droplets will be more subject to updrafts.** In addition to having a smaller mass and being more susceptible to updrafts, the fall-speed of the smaller particles is reduced, causing the system to retain more condensate at higher levels.

3. **A lower sub-zero freezing level.** The reduction in collision-coalesence processes brought on by smaller hydrometeors reduces the possibility the moisture may be removed from the system via precipitation, sedimentation or scavenging. This results in smaller droplets existing at temperature levels closer to the temperature at which homogenous freezing occurs (-40 C). Therefore the lifted mass of freezing water can alter the vertical heating profile of a system due to the vertical perturbations in latent heat release.

These three immediate effects of the elevated CCN were evident in the sensitivity tests in the form of more SCLW (Fig. 5.10). The increase in SCLW led to a direct increase in convectively-produced downdrafts, as given by DFX. Net DFX lag-correlated strongly with SCLW (Fig. 5.13), particularly in the moderate CCN simulations.

6.4: Cold-pool Modulation

The increase in convective activity resulted in appreciable cold-pool modulation. As defined by raw temperature change (Eq. 5.2, Fig 5.18), buoyancy (Eq. 5.3, Figs. 5.19, 5.21), and θ_e(Figs. 5.22, 5.23), the cold-pool activity differed significantly under different CCN conditions. The C3000 simulation in particular showed evidence of low $\theta_e$air intruding into the inflow of the TC (Figs. 5.22c, 5.23c). Interestingly, Reimer et al. (2009) showed a similar cold-pool response using increasing shear instead of CCN. The shape of the cold-pools also differed under elevated CCN levels. The C3000 case for example, developed a negative-buoyancy pool (Fig. 5.19) that was more “squall-like” in shape which eventually drifted beneath the TC eye. While it is difficult to directly attribute the cold-pool’s presence, strength, and domain to TC deintensification, the

addition of dry, cool air would act to disrupt the energy source of a TC requiring large amount of moist, warm air, as proposed by Wang (2002).

6.5: Two Potential Routes of CCN to Weaken a Storm

While noting the difficulty in directly and explicitly linking additional CCN to TC deintensification, this study provides two routes for this potential phenomenon.

1. **Increased convective activity leading to a decrease a TC's energy source: warm, moist air.** After the initial damping of precipitation, the moderately polluted simulations (C1000 and C3000), showed a dramatic increase in the downward flux of low θ_e air. Upon reaching the BL the low θ_e air swept out and eventually into the TC eye. Presuming the "bottom-up" development of TCs (Montgomery and Enagonio, 1998; Hendricks et al, 2004; Montgomery et al, 2006), an influx of cold-pool air could weaken a storm or at least hinder a TC's intensification.
2. **The removal of moisture from the system in the form of pristine ice.** The highest CCN simulation (C5000) showed the least amount of convective downdrafts in the form of net DFX (Fig. 5.12) and cold-pool area increase (Fig. 5.18). However, the system did show a perturbation in windspeed compared with the control run. Upon noting the smallest droplet size yielded by the C5000 simulation (Fig. 5.31d), we hypothesize that the droplets are sufficiently small to be frozen or rimed heavily and advected away from the system as pristine ice, rather than precipitating to the surface. Evidence of this rests in the form of elevated mixing ratios of ice aloft exiting the storm center (e.g. Fig. 5.26b) as well as the drying out of the mid-troposphere throughout the simulation through vertical moisture advection (Figs. 5.7 and 5.8). It is worth noting that C3000 also showed some evidence of the enhanced vertical transport and advection away of pristine ice

(Fig. 5.26b), yet was still able to produce sufficient convection and precipitation. This result is consistent with Carrio and Cotton (2010) which showed a similar response under extreme CCN conditions. This study and that of Cotton and Carrio (2010) suggest a “tipping-point” of sorts where additional CCN will switch from a “convection-creating” regime to a “moisture-removing” regime. A schematic diagram of the potential for extreme amounts of CCN to suppress TC strength via ice advection aloft is shown in Figure 6.1.

6.6: A Comment on the Importance of Microphysics in TC Forecasting and Predicting

The inclusion of advanced microphysics into TC forecast and prediction models could prove both instructive and strategic. As evidenced by this study, varying only a single moisture nucleation species (CCN) yielded significantly different dynamical results. Giant cloud condensation nuclei (GCCN) and IN were not varied for this study, but could also potentially affect the dynamics of a TC. However, it is difficult to conclusively prescribe aerosol concentration and species given the lack of observational platforms. The sources of the aerosols in question complicate matters further: the chemistry of anthropogenic Chinese aerosol is notoriously complex and at this point there are still open questions as to the nature of the aerosols produced – are they hydroscopic, hydrophobic, or neutral? How does the chemistry of the aerosol change throughout its lifetime? Are the aerosols radiatively active? This study did not include the direct radiative effect of aerosol.

Explicit resolution of convection and nucleation of CCN in the nested grid necessitates the use of a fine grid on the scale of 3 to 7 km resolution. Initial simulations using 10 km grid spacing

damped the response of the additional CCN, particularly the convective fluxes. The inclusion of microphysics into TC forecasting models and testing the results is an endeavor worth undertaking. As computing power continues to increase, the meshing of advanced microphysics into TC forecasting and predictions will become less expensive computationally. And as the practice becomes more widespread, it will become easier to compare and evaluate the microphysical schemes implemented. Still, while TC forecasting models lag behind mesoscale models in resolution, it is unlikely that an advanced microphysics scheme will practically be able to be implemented into real-time forecasts.

6.7: Recommendations for Future Work

As described in the previous section, the ability of aerosols to become active nucleation sites for water or ice is still not well understood. Moreover, even the concentrations of the different species of aerosols are not well known. While aerosol transport models improve, sampling and observational campaigns of aerosols are still scant in their deployment. Any verification of a model's ability to well represent microphysical impacts on a TC would begin with better aerosol data.

The resultant change of TC intensity yielded by this study is instructive, but not conclusive. Still, the impact of CCN on SCLW and convective downdrafts is evident. Further cold-pool analyses could prove insightful as this study noted a strong cold-pool signal on the TC dynamics. In particular, the mapping of cold-pools, and the TC's response to their strength, shape, size, and timing would provide further evidence on the susceptibility of a TC to be affected at the BL

inflow region and perhaps the eventual damping of storm intensity. The addition of CCN is only one potential route to cold-pool enhancement. Cold-pools may also be modulated by shear and moisture content.

Coupled Ocean-Atmosphere mesoscale model simulations would provide an enhanced understanding of the effect of CCN on incoming shortwave radiation and the potential for cooling off the surface of the ocean, which could also modulate TC strength.

This study, as all TC-aerosol studies, is by no means comprehensive. The simulations conducted were especially regime specific, consisting of a particular CCN domain, TC intensity, meteorological background, aerosol species, etc., all of which could alter the impact of aerosols on the development of a TC. These and other variables could be explored with different regional and/or TC forecasting models. The “alpha-testing” of an advanced microphysics scheme into a real-time TC forecasting model could provide the most immediate and significant test case scenario of TC-aerosol interaction to date.

6.8: Chapter 6 Figures

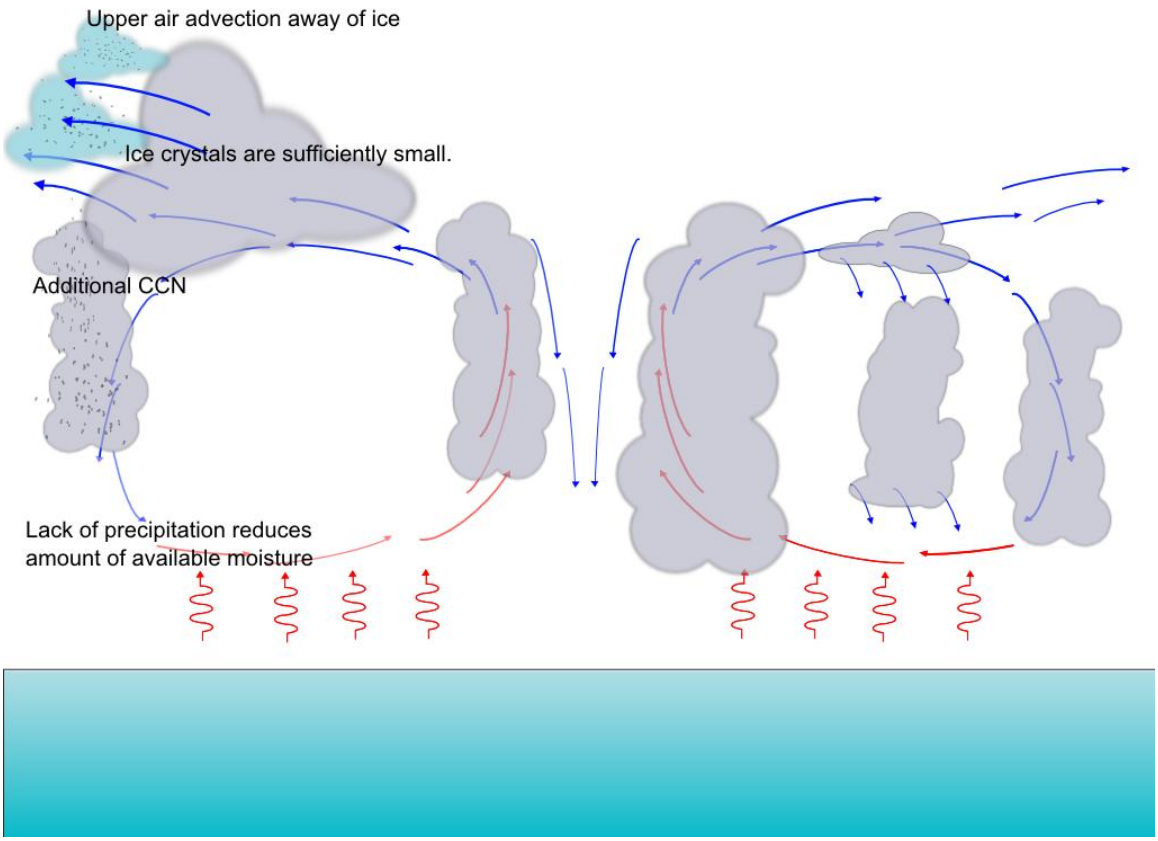

Figure 6.1: A schematic showing the potential of extreme amounts of CCN to suppress TC strength via the removal of moisture from the system in the form of ice aloft. The additional CCN works to reduce hydrometeor size such that collision-coalescence and riming are greatly reduced. The ice crystals may then be advected away from the system due to their inability to precipitate back to the surface.

REFERENCES

Albrecht, Bruce A. “Aerosols, Cloud Microphysics, and Fractional Cloudiness.” *Science* 245.4923 (1989): 1227-1230.

Anderson, Suzanne P. et al. “Integrated hydrologic and hydrochemical observations of Hidden Creek Lake jökulhlaups, Kennicott Glacier, Alaska.” *J. Geophys. Res.* 108.F1 (2003): 6003.

Arakawa, Akio, and Vivian R Lamb. “A Potential Enstrophy and Energy Conserving Scheme for the Shallow Water Equations.” *Monthly Weather Review* 109.1 (1981): 18-36.

Bahreini, Roya et al. “Aircraft-based aerosol size and composition measurements during ACE-Asia using an Aerodyne aerosol mass spectrometer.” *J. Geophys. Res.* 108.D23 (2003): 8645.

Barnes, S. L., 1973: Mesoscale objective analysis using weighted time-series observations. *NOAA Tech Memo*. ERL NSSL-62, National Severe Storms Laboratory, Norman, OK 73069, 60 pp. [NTIS-COM-73-10781].

Bender, Morris A. et al. “Modeled Impact of Anthropogenic Warming on the Frequency of Intense Atlantic Hurricanes.” *Science* 327.5964 (2010): 454-458.

Berglen, Tore F. et al. “A global model of the coupled sulfur/oxidant chemistry in the troposphere: The sulfur cycle.” *J. Geophys. Res.* 109.D19 (2004): D19310.

Braun, Scott A, and Wei-Kuo Tao. “Sensitivity of High-Resolution Simulations of Hurricane Bob (1991) to Planetary Boundary Layer Parameterizations.” *Monthly Weather Review* 128.12 (2000): 3941-3961.

Carmichael, Gregory R. et al. “Changing Trends in Sulfur Emissions in Asia: Implications for Acid Deposition, Air Pollution, and Climate.” *Environmental Science & Technology* 36.22 (2002): 4707-4713.

Carrio, G. G., Cotton, W. R., 2010: Investigations of aerosol impacts on hurricanes: Virtual seeding flights. (In process of submission). *Atmos Phys Chem.*

---. 2010: Study of the feasibility of the mitigation of the intensity of tropical cyclones by CCN seeding in the outer rainband region: A HAMP Project, 29th Conference on Hurricanes and Tropical Meteorology.May 10-14, 2010, Tucson, AZ

Charlson, R. J. et al. "Climate Forcing by Anthropogenic Aerosols." *Science* 255.5043 (1992): 423-430.

Charney, J., Eliassen, A., 1964: On the growth of the hurricane depression. *J. Atmos. Sci.*,**21**, 68-75.

Chen, Tsing-Chang et al. "Role of the Monsoon Gyre in the Interannual Variation of Tropical Cyclone Formation over the Western North Pacific." *Weather and Forecasting* 19.4 (2004): 776-785.

Chin, Mian et al. "A global aerosol model forecast for the ACE-Asia field experiment." *J. Geophys. Res.* 108.D23 (2003): 8654.

Clarke, A. et al. "Sea-Salt Size Distributions from Breaking Waves: Implications for Marine Aerosol Production and Optical Extinction Measurements during SEAS*." *Journal of Atmospheric and Oceanic Technology* 20.10 (2003): 1362-1374.

Cotton, William R. "Numerical Simulation of Precipitation Development in Supercooled Cumuli—Part I." *Monthly Weather Review* 100.11 (1972): 757-763.

---. "Numerical Simulation of Precipitation Development in Supercooled Cumuli—Part II." *Monthly Weather Review* 100.11 (1972): 764-784.

---. "Modification of Precipitation from Warm Clouds—A Review." *Bulletin of the American Meteorological Society* 63.2 (1982): 146-160.

Cotton, William R et al. "Numerical Simulation of the Effects of Varying Ice Crystal Nucleation Rates and Aggregation Processes on Orographic Snowfall." *Journal of Climate and Applied Meteorology* 25.11 (1986): 1658-1680.

Cotton, W.R., R.A. Pielke, Sr., R.L. Walko, G.E. Liston, C.J. Tremback, H. Jiang, R.L. McAnelly, J.Y. Harrington, M.E. Nicholls, G.G. Carrió, J.P. McFadden, 2003: "RAMS 2001: Current status and future directions." *Meteor. Atmos Physics*, 82, 5-29.

Craig, George C., and Suzanne L. Gray. "CISK or WISHE as the Mechanism for Tropical Cyclone Intensification." *Journal of the Atmospheric Sciences* 53.23 (1996): 3528-3540.

DeMott, P.J., K. Sassen, M. Poellot, D. Baumgardner, .D.C. Rogers, S.Brooks, A.J. Prenni, S. M. Kreidenweis. "African dust aerosols as atmospheric ice nuclei." *Geophysical Research Letters* (2003) 30(14)1732.

Dentener, F., J. Drevet, J. F. Lamarque, I. Bey, B. Eickhout, A. M. Fiore, D. Hauglustaine, L. W. Horowitz, M. Krol, U. C. Kulshrestha, M. Lawrence, C. Galy-Lacaux, S. Rast, D. Shindell, D. Stevenson, T. Van Noije, C. Atherton, N. Bell, D. Bergman, T. Butler, J. Cofala, B. Collins, R. Doherty, K. Ellingsen, J. Galloway, M. Gauss, V. Montanaro, J. F. Müller, et al. "Nitrogen and sulfur deposition on regional and global scales: A multimodel evaluation." *Global Biogeochem. Cycles* 20.4 (2006): GB4003.

Dunion, Jason P, and Christopher S Velden. "The Impact of the Saharan Air Layer on Atlantic Tropical Cyclone Activity." *Bulletin of the American Meteorological Society* 85.3 (2004): 353-365.

Dusek, U. et al. "Size Matters More Than Chemistry for Cloud-Nucleating Ability of Aerosol Particles." *Science* 312.5778 (2006): 1375-1378.

Eastman JL (1995) "Numerical simulation of hurricane Andrew – Rapid intensification." 21st Conf. on Hurricanes and Tropical Meteorology, Miami, Florida.

Emanuel, Kerry A. "An Air-Sea Interaction Theory for Tropical Cyclones. Part I: Steady-State Maintenance." *Journal of the Atmospheric Sciences* 43.6 (1986): 585-605.

---. "The Maximum Intensity of Hurricanes." *Journal of the Atmospheric Sciences* 45.7 (1988): 1143-1155.

---., 1994: *Atmospheric Convection.* New York, Oxford Univ. Press, 580 pp.

Emanuel, Kerry A., J. David Neelin, and Christopher S. Bretherton. "On large-scale circulations in convecting atmospheres." *Quarterly Journal of the Royal Meteorological Society* 120.519 (1994): 1111-1143.

Evan, Amato T. et al. "New evidence for a relationship between Atlantic tropical cyclone activity and African dust outbreaks." *Geophysical Research Letters* 33.19 (2006): L19813.

Feingold, Graham et al. "Simulations of marine stratocumulus using a new microphysical parameterization scheme." *Atmospheric Research* 47-48 (1998): 505-528.

Formenti, P. et al. "Chemical composition of mineral dust aerosol during the Saharan Dust Experiment (SHADE) airborne campaign in the Cape Verde region, September 2000." *J. Geophys. Res.* 108.D18 (2003): 8576.

Fovell, Robert G, Kristen L Corbosiero, and Hung-Chi Kuo. "Cloud Microphysics Impact on Hurricane Track as Revealed in Idealized Experiments." *Journal of the Atmospheric Sciences* 66.6 (2009): 1764-1778.

Gentry, R. Cecil. "Genesis of Tornadoes Associated with Hurricanes." *Monthly Weather Review* 111.9 (1983): 1793-1805.

Granier, Claire, Paulo Eduardo Artaxo Netto, and Claire E. Reeves. *Emissions of atmospheric trace compounds*. Springer, 2004.

van den Heever, Susan C et al. "Impacts of Nucleating Aerosol on Florida Storms. Part I: Mesoscale Simulations." *Journal of the Atmospheric Sciences* 63.7 (2006): 1752-1775.

van den Heever, Susan C., and William R. Cotton. "Urban Aerosol Impacts on Downwind Convective Storms." *Journal of Applied Meteorology and Climatology* 46.6 (2007): 828-850.

---. "Urban Aerosol Impacts on Downwind Convective Storms." *Journal of Applied Meteorology and Climatology* 46.6 (2007): 828-850.

Hendricks, Eric A, Michael T Montgomery, and Christopher A Davis. "The Role of "Vortical" Hot Towers in the Formation of Tropical Cyclone Diana (1984)." *Journal of the Atmospheric Sciences* 61.11 (2004): 1209-1232.

Harrington, J. Y., 1997: The effects of radiative and microphysical processes on simulated warm and transition season Arctic. Acknowledgments. During the completion of this stratus. Dept. Of Atmospheric Science Bluebook 637, Colorado State University, Fort Collins, CO, 289 pp.

Jensen, Jørgen B, and Sunhee Lee. "Giant Sea-Salt Aerosols and Warm Rain Formation in Marine Stratocumulus." *Journal of the Atmospheric Sciences* 65.12 (2008): 3678-3694.

Jordan, C. L. "MEAN SOUNDINGS FOR THE WEST INDIES AREA." *Journal of Meteorology* 15.1 (1958): 91-97.

Kain, John S. "The Kain–Fritsch Convective Parameterization: An Update." *Journal of Applied Meteorology* 43.1 (2004): 170-181.

Kalnay, E. et al. "The NCEP/NCAR 40-Year Reanalysis Project." *Bulletin of the American Meteorological Society* 77.3 (1996): 437-471.

Khain, A., B. Lynn, and J. Dudhia. "Aerosol Effects on Intensity of Landfalling Hurricanes as Seen from Simulations with the WRF Model with Spectral Bin Microphysics." *Journal of the Atmospheric Sciences* 67.2 (2010): 365-384.

Klemp, Joseph B, and Robert B Wilhelmson. "The Simulation of Three-Dimensional Convective Storm Dynamics." *Journal of the Atmospheric Sciences* 35.6 (1978): 1070-1096.

Kohler, H., 1926: Zur Thermodynamik der Kondensation an hygroskopischen Kernen und Bemerkungen uber das Zusammenfliessen der Tropfen. *Medd. Met. Hydr. Anst. Stockholm* 3:8**.**

Laktionov, A. G., and O. A. Volkovitsky. “Investigation of the initial condensation stage of cloud formation in the chamber.” *Pure and Applied Geophysics* 77.1 (1969): 78-88.

Lavoie, R.L., Cotton, W.R. and Hovermale, J.B., 1970. “Investigations of Lake Effect Storms.” Final Rep. Environ. Sci. Serv. Administration, Boulder, CO, Contract No. E22- 103-68(N), January 1970, 127 pp.

LeMone, Margaret A, Edward J Zipser, and Stanley B Trier. “The Role of Environmental Shear and Thermodynamic Conditions in Determining the Structure and Evolution of Mesoscale Convective Systems during TOGA COARE.” *Journal of the Atmospheric Sciences* 55.23 (1998): 3493-3518.

Lyons, Walter A, and Cecil S Keen. “Observations of Lightning in Convective Supercells within Tropical Storms and Hurricanes.” *Monthly Weather Review* 122.8 (1994): 1897-1916.

Mahrer, Ytzuaq, and Roger A Pielke. “The Effects of Topography on Sea and Land Breezes in a Two-Dimensional Numerical Model.” *Monthly Weather Review* 105.9 (1977): 1151-1162.

Mapes, Brian E. “Convective Inhibition, Subgrid-Scale Triggering Energy, and Stratiform Instability in a Toy Tropical Wave Model.” *Journal of the Atmospheric Sciences* 57.10 (2000): 1515-1535.

---. “Gregarious Tropical Convection.” *Journal of the Atmospheric Sciences* 50.13 (1993): 2026-2037.

Massie, Steven T., Omar Torres, and Steven J. Smith. “Total Ozone Mapping Spectrometer (TOMS) observations of increases in Asian aerosol in winter from 1979 to 2000.” *J. Geophys. Res.* 109.D18 (2004): D18211.

McCaul, Eugene W. “Buoyancy and Shear Characteristics of Hurricane-Tornado Environments.” *Monthly Weather Review* 119.8 (1991): 1954-1978.

McFarquhar, Greg M, and Robert A Black. “Observations of Particle Size and Phase in Tropical Cyclones: Implications for Mesoscale Modeling of Microphysical Processes.” *Journal of the Atmospheric Sciences* 61.4 (2004): 422-439.

Meyers, Michael P. et al. “New RAMS cloud microphysics parameterization. Part II: The two-moment scheme.” *Atmospheric Research* 45.1 (1997): 3-39.

Miyoshi, Takemasa et al. “Impact of Resolution Degradation of the Initial Condition on Typhoon Track Forecasts.” *Weather and Forecasting* (2010): 100804092600065.

Molinari, John, Paul Moore, and Vincent Idone. “Convective Structure of Hurricanes as Revealed by Lightning Locations.” *Monthly Weather Review* 127.4 (1999): 520-534.

Montgomery, M. T., L. L. Lussier III, et al. “The genesis of Typhoon Nuri as observed during the Tropical Cyclone Structure 2008 (TCS-08) field experiment – Part 1: The role of the easterly wave critical layer.” *Atmospheric Chemistry and Physics Discussions* 9.5 (2009): 19159-19203.

Montgomery, M. T., M. E. Nicholls, et al. “A Vortical Hot Tower Route to Tropical Cyclogenesis.” *Journal of the Atmospheric Sciences* 63.1 (2006): 355-386.

Montgomery, Michael T, and Janice Enagonio. “Tropical Cyclogenesis via Convectively Forced Vortex Rossby Waves in a Three-Dimensional Quasigeostrophic Model.” *Journal of the Atmospheric Sciences* 55.20 (1998): 3176-3207.

Nicholls, M.E., and R.A. Pielke, 1995: “A numerical investigation of the effect of vertical wind shear on tropical cyclone intensification.” 21st Conference on Hurricanes and Tropical Meteorology, AMS, Boston, April 24-28, Miami, Florida, 339-341.

Nolan, David S, Yumin Moon, and Daniel P Stern. “Tropical Cyclone Intensification from Asymmetric Convection: Energetics and Efficiency.” *Journal of the Atmospheric Sciences* 64.10 (2007): 3377-3405.

Novlan, David J, and William M Gray. “Hurricane-Spawned Tornadoes.” *Monthly Weather Review* 102.7 (1974): 476-488.

Ooyama, K., 1964: A dynamical model for the study of tropical cyclone development. *Geofis. Intern.*,**4**, 187-198.

Orville, R.E., and J.M. Coyne, 1999: Cloud-to-ground lightning in tropical cyclones (1986-1996). Preprints, 23-rd Conf. on Hurricanes and tropical meteorology, *Dallas, Amer. Meteor. Soc*., 194pp.

Petters, M. D., and S. M. Kreidenweis. “A single parameter representation of hygroscopic growth and cloud condensation nucleus activity.” *Atmos. Chem. Phys.* 7.8 (2007): 1961-1971.

Powell, Mark D. “Boundary Layer Structure and Dynamics in Outer Hurricane Rainbands. Part I: Mesoscale Rainfall and Kinematic Structure.” *Monthly Weather Review* 118.4 (1990): 891-917.

---. “Boundary Layer Structure and Dynamics in Outer Hurricane Rainbands. Part II: Downdraft Modification and Mixed Layer Recovery.” *Monthly Weather Review* 118.4 (1990): 918-938.

Price, Colin, Mustafa Asfur, and Yoav Yair. “Maximum hurricane intensity preceded by increase in lightning frequency.” *Nature Geosci* 2.5 (2009): 329-332.

Ramanathan, V. and A. M. Vogelmann, 1997: “Greenhouse Effect, Atmospheric Solar Absorption and the Earth’s Radiation Budget: From the Arrhenius-Langley Era to the 1990s,” in The

Legacy of Svante Arrhenius Understanding the Greenhouse Effect. H. Rodhe and R. Charlson, Eds. (Royal Swedish Academy of Sciences, Stockholm University, 1997), pp. 85-103.

Randall, David A. "Buoyant Production and Consumption of Turbulence Kinetic Energy in Cloud-Topped Mixed Layers." *Journal of the Atmospheric Sciences* 41.3 (1984): 402-413.

Raymond, D. J., and C. López Carrillo. "The vorticity budget of developing Typhoon Nuri (2008)." *Atmospheric Chemistry and Physics Discussions* 10.7 (2010): 16589-16635.

Redemann, J. et al. "Clear-column closure studies of aerosols and water vapor aboard the NCAR C-130 during ACE-Asia, 2001." *J. Geophys. Res.* 108.D23 (2003): 8655.

Riehl, H. and Malkus, J. S.: On the heat balance in the equatorial trough zone, *Geophysica*, 6,503–538, 1958. 3537, 3538, 3539, 3541, 3543, 3544, 3545, 3549

Reynolds, Carolyn A. et al. "Naval Research Laboratory Multiscale Targeting Guidance for T-PARC and TCS-08." *Weather and Forecasting* 25.2 (2010): 526-544.

Reynolds, Richard W, and Thomas M Smith. "Improved Global Sea Surface Temperature Analyses Using Optimum Interpolation." *Journal of Climate* 7.6 (1994): 929-948.

Riemer, M., M. T. Montgomery, and M. E. Nicholls. "A new paradigm for intensity modification of tropical cyclones: thermodynamic impact of vertical wind shear on the inflow layer." *Atmospheric Chemistry and Physics Discussions* 9.3 (2009): 10711-10775.

Rogers, Robert F et al. "An Evaluation of Microphysics Fields from Mesoscale Model Simulations of Tropical Cyclones. Part I: Comparisons with Observations." *Journal of the Atmospheric Sciences* 64.6 (2007): 1811-1834.

Rotunno, Richard, Joseph B Klemp, and Morris L Weisman. "A Theory for Strong, Long-Lived Squall Lines." *Journal of the Atmospheric Sciences* 45.3 (1988): 463-485.

Saleeby, Stephen M., and William R. Cotton. "A Large-Droplet Mode and Prognostic Number Concentration of Cloud Droplets in the Colorado State University Regional Atmospheric Modeling System (RAMS). Part I: Module Descriptions and Supercell Test Simulations." *Journal of Applied Meteorology* 43.1 (2004): 182-195.

---. "A Large-Droplet Mode and Prognostic Number Concentration of Cloud Droplets in the Colorado State University Regional Atmospheric Modeling System (RAMS). Part II: Sensitivity to a Colorado Winter Snowfall Event." *Journal of Applied Meteorology* 44.12 (2005): 1912-1929.

Saxena, Pradeep, and Christian Seigneur. "On the oxidation of SO2 to sulfate in atmospheric aerosols." *Atmospheric Environment (1967)* 21.4 (1987): 807-812.

Seifert, A., and K. D. Beheng. “A two-moment cloud microphysics parameterization for mixed-phase clouds. Part 1: Model description.” *Meteorology and Atmospheric Physics* 92.1-2 (2005): 45-66.

---. “A two-moment cloud microphysics parameterization for mixed-phase clouds. Part 2: Maritime vs. continental deep convective storms.” *Meteorology and Atmospheric Physics* 92.1-2 (2005): 67-82.

Shapiro, Lloyd J, and James L Franklin. “Potential Vorticity Asymmetries and Tropical Cyclone Motion.” *Monthly Weather Review* 127.1 (1999): 124-131.

Shao, X.M., et al., 2005: “Katrina and Rita were lit up with lightning.” Eos, 86 (42), 398.

Simpson, Joanne. “Downdrafts as Linkages in Dynamic Cumulus Seeding Effects.” *Journal of Applied Meteorology* 19.4 (1980): 477-487.

Smith, M.A., 2007: Evaluation of mesoscale simulations of dust sources, sinks and transport over the Middle East. Master’s Thesis, Department of Atmospheric Science, Colorado State University, Fort Collins, CO.

Stokowski, D.M., 2005: Addition of aerosol direct effect to the Colorado State University Regional Atmospheric Modeling System (CSU-RAMS). Master’s Thesis, Department of Atmospheric Science, Colorado State University, Fort Collins, CO.

Storer, Rachel L., Susan C. van den Heever, and Graeme L. Stephens. “MODELING AEROSOL IMPACTS ON CONVECTIVE STORMS IN DIFFERENT ENVIRONMENTS.” *Journal of the Atmospheric Sciences* (2010): 100903135953021.

Streets, D. G. et al. “An inventory of gaseous and primary aerosol emissions in Asia in the year 2000.” *J. Geophys. Res.* 108.D21 (2003): 8809.

Streets, D.G., Waldhoff, S.T., 2000. Present and future emissions of air pollutants in China: SO_2, NO_x, and CO. *Atmos. Environ*. 34, 363-374.

Takemura, Toshihiko et al. “Global three-dimensional simulation of aerosol optical thickness distribution of various origins.” *J. Geophys. Res.* 105.D14 (2000): 17853-17873.

Tegen, Ina. “Modeling the mineral dust aerosol cycle in the climate system.” *Quaternary Science Reviews* 22.18-19 (2003): 1821-1834.

Thorpe, A. J., Miller, M. J., and Moncrieff, M. W.: “Two-dimensional convection in non-constant shear: a model of mid-latitude squall lines.” *Q. J. Roy. Met. Soc*., 108, 739–762, 1982.

Tompkins, Adrian M. “Organization of Tropical Convection in Low Vertical Wind Shears: The Role of Cold Pools.” *Journal of the Atmospheric Sciences* 58.13 (2001): 1650-1672.

Tremback, C. J., 1990: Numerical simulation of a mesoscale convective complex: Model development and numerical results. Ph.D. dissertation, Department of Atmospheric Science, Colorado State University, Fort Collins, CO, 247 pp. [Available from Department of Atmospheric Science, Colorado State University, Fort Collins, CO 80523.].

Tripoli, Gregory J, and William R Cotton. "A Numerical Investigation of Several Factors Contributing to the Observed Variable Intensity of Deep Convection over South Florida." *Journal of Applied Meteorology* 19.9 (1980): 1037-1063.

Twomey, S. "Aerosols, clouds and radiation." *Atmospheric Environment. Part A. General Topics* 25.11 (1991): 2435-2442.

Twomey, S. and Squires, P. (1959). "The Influence of Cloud Nucleus Population on the Microstructure and Stability of Convective Clouds." *Tellus*, 11: 408–411.

Verlinde, Johannes, Piotr J Flatau, and William R Cotton. "Analytical Solutions to the Collection Growth Equation: Comparison with Approximate Methods and Application to Cloud Microphysics Parameterization Schemes." *Journal of the Atmospheric Sciences* 47.24 (1990): 2871-2880.

Walko, Robert L., Larry E. Band, et al. "Coupled Atmosphere–Biophysics–Hydrology Models for Environmental Modeling." *Journal of Applied Meteorology* 39.6 (2000): 931-944.

Walko, Robert L., Craig J. Tremback, et al. "An Interactive Nesting Algorithm for Stretched Grids and Variable Nesting Ratios." *Journal of Applied Meteorology* 34.4 (1995): 994-999.

Wang, Yuqing. "An Explicit Simulation of Tropical Cyclones with a Triply Nested Movable Mesh Primitive Equation Model: TCM3. Part II: Model Refinements and Sensitivity to Cloud Microphysics Parameterization*." *Monthly Weather Review* 130.12 (2002): 3022-3036.

---. "How Do Outer Spiral Rainbands Affect Tropical Cyclone Structure and Intensity?*." *Journal of the Atmospheric Sciences* 66.5 (2009): 1250-1273.

---. "Vortex Rossby Waves in a Numerically Simulated Tropical Cyclone. Part I: Overall Structure, Potential Vorticity, and Kinetic Energy Budgets*." *Journal of the Atmospheric Sciences* 59.7 (2002): 1213-1238.

Ward, D. S., Eidhammer, T., Cotton, W. R., and Kreidenweis, S. M.: The role of the particle size distribution in assessing aerosol composition effects on simulated droplet activation, *Atmos. Chem. Phys*., 10, 5435-5447, doi:10.5194/acp-10-5435-2010,

Weisman, M. L, and J. B Klemp. "The Dependence of Numerically Simulated Convective Storms on Vertical Wind Shear and Buoyancy." *Monthly Weather Review* 110.6 (1982): 504-520.

Willoughby, H. E. "Gradient Balance in Tropical Cyclones." *Journal of the Atmospheric Sciences* 47.2 (1990): 265-274.

---. “Tropical Cyclone Eye Thermodynamics.” *Monthly Weather Review* 126.12 (1998): 3053-3067.

Willoughby, H. E, J. A Clos, and M. G Shoreibah. “Concentric Eye Walls, Secondary Wind Maxima, and The Evolution of the Hurricane vortex.” *Journal of the Atmospheric Sciences* 39.2 (1982): 395-411.

Zender, C. S., R. L. Miller, and I. Tegen (2004). “Quantifying mineral dust mass budgets: Systematic terminology, constraints, and current estimates”. *Eos Trans. AGU*, *85*(48), 509.

Zhang, Henian et al. “Direct and indirect impacts of Saharan dust acting as cloud condensation nuclei on tropical cyclone eyewall development.” *Geophys. Res. Lett.* 36.6 (2009): L06802.

Zhang, Henian, Greg M. McFarquhar, Stephen M. Saleeby, et al. “Impacts of Saharan dust as CCN on the evolution of an idealized tropical cyclone.” *Geophys. Res. Lett.* 34.14 (2007): L14812.

Zhu, Hongyan, and Roger K Smith. “The Importance of Three Physical Processes in a Minimal Three-Dimensional Tropical Cyclone Model.” *Journal of the Atmospheric Sciences* 59.11 (2002): 1825-1840.

Zhu, Tong, and Da-Lin Zhang. “Numerical Simulation of Hurricane Bonnie (1998). Part II: Sensitivity to Varying Cloud Microphysical Processes.” *Journal of the Atmospheric Sciences* 63.1 (2006): 109-126.

Zipser, E. J. “Mesoscale and Convective–Scale Downdrafts as Distinct Components of Squall-Line Structure.” *Monthly Weather Review* 105.12 (1977): 1568-1589.